12-19-2008

Study of Magnetization Switching in Coupled Magnetic Nanostructured Systems

Cosmin Radu
University of New Orleans

Study of Magnetization Switching in Coupled Magnetic Nanostructured Systems

A Dissertation

Submitted to the Graduate Faculty of the
University of New Orleans
in partial fulfillment of the
requirements for the degree of

Doctor of Philosophy
in
Engineering and Applied Science
Physics

by

Cosmin Radu

B.S. Al. I. Cuza University of Iasi, Romania, 2000
M.S. Al. I. Cuza University of Iasi, Romania, 2002

December, 2008

Aknowledgement

I would like to thank my advisor, Professor Leonard Spinu, for his encouragement, guidance, and patience. Working with professor Spinu, I have learned that the passion and the pursuance are essential for the success in experimental work. It has been a pleasure to be his student.

I would like to thank my supervisory committee members for their insightful suggestions, their help and guidance in my studies: Professor Leonard Spinu, the committee chair, Professor Leszek Malkinski from Department of Physics at University of New Orleans, Professor Dimitrios Charalampidis from Department of Engineering at University of New Orleans, Professor Carl Ventrice from Department of Physics at Texas State University and Professor Jinke Tang from Department of Physics & Astronomy at University of Wyoming.

I am deeply grateful to my colleagues, Dr. Dorin Cimpoesu and Huy Pham for their support and valuable opinions. My work wouldn't have been possible without their continuous help.

I would like to thank to Professor Ashok Puri and to Professor Kevin Stokes from Department of Physics at University of New Orleans for their help in my studies and research work.

I am very thankful for the synthetic antiferromagnet thin film samples received from Seagate Technologies that were prepared by Dr. Ganping Ju and Dr. Erol Girt.

I would like to thank to Dr. Ganping Ju and Dr. Julius Hohlfeld for their guidance and support during my half year internship with Seagate Technologies in Pittsburgh, PA, especially in the period following hurricane Katrina. Their help was essential for the continuation of my research through those difficult times.

I want to express my deepest gratitude for the continuous support from the Advanced Materials Research Institute at University of New Orleans that offered me a Graduate Research Assistant position for all the duration of my studies.

Table of Contents

List of Figures

List of Tables

Abstract

A study of magnetization dynamics experiments in nanostructured materials using the rf susceptibility tunnel diode oscillator (TDO) method is presented along with a extensive theoretical analysis. An original, computer controlled experimental setup that measures the change in susceptibility with the variation in external magnetic field and sample temperature was constructed. The TDO-based experiment design and construction is explained in detail, showing all the elements of originality.

This experimental technique has proven reliable for characterizing samples with uncoupled magnetic structure and various magnetic anisotropies like: CrO_2 , FeCo/IrMn and Co/SiO_2 thin films. The TDO was subsequently used to explore the magnetization switching in coupled magnetic systems, like synthetic antiferromagnet (SAF) structures.

Magnetoresistive random access memory (MRAM) is an important example of devices where the use of SAF structure is essential. To support the understanding of the SAF magnetic behavior, its configuration and application are reviewed and more details are provided in an appendix. Current problems in increasing the scalability and decreasing the error rate of MRAM devices are closely connected to the switching properties of the SAF structures.

Several theoretical studies that were devoted to the understanding of the concepts of SAF critical curve are reviewed. As one can notice, there was no experimental determination of SAF critical curve, due to the difficulties in characterizing a magnetic coupled structure.

Depending of the coupling strength between the two ferromagnetic layers, on the SAF critical curve one distinguishes several new features, inexistent in the case of uncoupled systems. Knowing the configuration of the SAF critical curve is of great importance in order to control its switching characteristics.

For the first time a method of experimentally recording the critical curve for SAF is proposed in this work. In order to overcome technological limitations, a new way of recording the critical curve by using an additional magnetic bias field was explored.

Keywords: *magnetization dynamics, magnetic susceptibility, tunnel diode oscillator, critical curve, synthetic antiferromagnet, coupled magnetic structures, MRAM.*

Introduction

The technological advancement in all its aspects, from the field of complex digital communication and data storage systems to the field of daily-use commodities, relies on the scientific research in electromagnetism and materials science. Our topic of research is at the crossing of these two fields of interest and deals predominantly with the study of magnetization switching in coupled magnetic nanostructured materials. These materials are used in a multitude of electronic devices, ranging from handheld computers to the space exploration industry.

The term of "magnetic nanostructures" is used to summarize all the magnetic structures of which at least one out of three dimensions is reduced to a nanometer length scale, such as layers, wires, and dots. It was already recognized in the 1950's from theoretical considerations that reduced dimensions and the presence of interfaces should alter the magnetic properties of these structures, such as magnetic anisotropy and domain structure, for example, which could be useful for applications. However, at that time it was not possible to produce high quality nanostructures yet because of the lack of technology, especially high vacuum deposition systems, and successful verification of most of these predictions was delayed until recently.

Magnetization dynamics is one of the central issues in the physics of mesoscopic magnetic systems [1, 2] and its understanding is important not only for its evident fundamental interest but also due to the big impact on magnetic information storage technologies.

The dynamics of nanoscale magnetic structures are of both fundamental interest and primary importance for the development of new high-speed electronic devices that incorporate nanomagnets. Magnetic random access memory (MRAM), for example, could enable "instant-on" computers that would not require booting each time the power is cycled. There are many unresolved questions, however, concerning how the interactions within a nanostructure affect the magnetization switching. A clear understanding of this mechanism is essential, since this is the process by which information (in the form of bits) is written on the magnetic recording materials used in computer data storage.

Magnetic recording is rapidly approaching the nanometer scale as storage densities are increasing toward a terabit per square inch. High volume of data requires higher data transfer rates. These aspects present new challenges and opportunities in nanometer scale materials engineering and in understanding the magnetic properties of nanometer scale magnetic materials.

Among the critical issues is the manner and speed which the magnetization direction can be reversed from one stable configuration to another. In addition, for the magnetoresistive random access memories (MRAM) [3], unlike for current forms of nonvolatile memories, switching rates and rewriteability properties surpassing those of conventional RAMs are needed. This can be achieved only by first understanding and then controlling the magnetization dynamics of very confined magnetic elements.

The magnetization dynamics at different timescales is governed by different physical dynamic mechanisms. First, on the nanosecond range (0.1 ns to 100 ns) the dipolar interactions, external fields and spin-lattice interactions are the major driving forces. The magnetization reversal occurs through a process called precessional motion, which is the

primary source of magnetization rotation that is gradually opposed by dampening [4, 5]. This regime is described theoretically by the phenomenological magnetization's equation of motion Landau-Lifshitz-Gilbert (LLG) and is able to describe the precessional reversal mechanism [6]. For shorter time scales of the order of picoseconds (1-100 ps), the electron excitations can not be ignored and electron-phonon, phonon-phonon, and spin-lattice interactions start to be important. In this case the LLG formalism gradually becomes invalid as quantum effects starts to appear. Here, a new mechanism of magnetization reversal is possible, induced by an angular momentum transfer from a magnetically polarized electron current [7-10]. Finally, for very short time scales (1 fs-1 ps), electron–electron and spin-orbit interactions dominate. Magnetic structures can be excited by optical probes that are shorter than fundamental timescales such as spin-lattice relation times and precession times. This regime has became accessible only recently when novel pulsed magneto-optical pump-probe experiments were developed, being capable of studying the spin dynamics at femtosecond resolution [11, 12].

This work focuses on investigating some properties of magnetization dynamics in various magnetic thin film structures in the first regime among those mentioned above, with original contributions on the study of one of the MRAM's essential component, the synthetic antiferromagnet (SAF) structures. In spite of continuous efforts on studying SAF magnetization dynamics, there are several experimental physics issues which remain poorly explored including the critical curve determination. Specifically, in this dissertation the study of magnetization switching will be performed through magnetic susceptibility experiments based on the formalism of the critical curve. The critical curve is a very important concept

for both, theoretical and experimental study of switching mechanism in magnetic system and device applications, as MRAM.

The critical curve was first discussed by Slonczewski [13] and then developed further by André Thiaville [14]. However, the term of "critical curve" basically comes from the Stoner-Wohfarth model, which was early introduced by Stoner and Wohfarth to describe the simplest case of the uniaxial, single domain particles [15]. Based on the remarkable properties of the critical curve, the hysteresis and the corresponding transverse susceptibility curves can be constructed, providing a lot of useful information about magnetic materials. It is clear, therefore, that the critical curve is the key to the understanding of the static behavior of magnetic materials.

There are several techniques that have been developed to measure the critical curve. In this work the quasi-static case will be considered where a new method for measuring the static critical curve using the reversible susceptibility measurements is proposed. This method will be theoretically presented and experimentally validated in the case of several magnetic nanostructures: both uncoupled and coupled.

The main goal is to develop a method capable of completely describing the magnetization switching through the critical curve for any nanostructured magnetic system, including the case of single layer or multilayer coupled thin films. The experimental difficulties related to the complexity of the critical curve for coupled magnetic layers systems, like SAF, are discussed. Our results and analysis suggest a new experimental procedure capable of characterizing this important MRAM component and will provide a precise description of its operation.

To be more specific, an outline of the format of the dissertation follows:

Chapter 1, *Magnetic Free Energy. Stoner Wohlfarth Model,* gives an overview of the background information required for a full understanding of the remainder of the dissertation. These theoretical sections includes the overview of the magnetic anisotropies, free energy of magnetic systems, as well as the overview of Stoner-Wohlfarth model.

Chapter 2, *Susceptibility of a Magnetic Nanostructure,* begins with a brief description of the magnetic susceptibility measurement method and a literature review of its development. Then the Aharoni Model is presented in detail and we end with the theoretical derivation of the critical curve derived from susceptibility measurements for two-dimensional (2D) magnetic systems.

Chapter 3, *Tunnel Diode Oscillator Method for Susceptibility Experiments,* presents the most important experimental techniques used for susceptibility measurements from literature and we introduce the Tunnel Diode Oscillator (TDO) method. Afterwards, we continue with a review of the main contribution in developing the TDO technique. A detailed presentation of the original TDO-based experimental setup designed and used in our laboratory shows the originality of the improvements we brought to this technique.

Chapter 4, *Experimental determination of Critical Curve for Uncoupled Magnetic Nanostructures,* discusses the TDO experiments performed in our lab on several magnetic nanostructures. Among the most significant samples we chose to present the CrO_2 single layer – half-metallic thin film samples, FeCo/IrMn multilayers - having exchange bias anisotropy and Co/SiO_2 multilayers – series of three samples that shows an interesting evolution in the critical curve aspect ratio. All these experiments provide a good illustration of the capability of the TDO-based susceptibility measurement method.

Chapter 5, *Experimental Recording of the Critical Curve for Coupled Thin Films,* discusses our original contribution to the study of coupled thin films, in particular the synthetic antiferromagnet (SAF) structures, is described in detail. The chapter starts out with a introduction of SAF concepts and application (the most important being MRAM). Afterwards we present the TDO experiments performed on SAF in our laboratory with their theoretical foundation, a new experimental procedure, original results and technical difficulties.

Chapter 6, *Conclusions,* presents the conclusions of all the work done for this dissertation, and discusses the potential extensions of this work in future.

Each of the five chapters ends with a *summary* that briefly presents the essential information such way that one can faster focus its attention on a specific section.

The *Appendices* section covers several essential aspects that were not included in the body of the dissertation in order to provide a smooth transition between different sections of this work. The first appendix presents the derivation of the parametric equations that describes the critical curve and the second appendix shows details of the transverse susceptibility expression in Aharoni's model. The third appendix provides a comprehensive description of the technological application of SAF. In the fourth appendix we review the theoretical work previously published about the magnetization switching and critical curve for magnetically coupled thin films and SAF.

The dissertation ends with a *list of author's publications* and a short *Vita*.

Chapter 1

Magnetic Free Energy. Stoner Wohlfarth Model

The following section is intended to facilitate the understanding of the concept of the energy of magnetic systems. To achieve static equilibrium, a system will go through a process of minimizing its total free energy.

The magnetic energy concept is employed together with the Stoner-Wohlfarth model (SW) [15]. By finding the total energy minima, it is possible to predict the magnetization switching behavior of the particle under the influence of an applied field. This concept can also explain the existence of domain structure in ferromagnetic materials through the minimization of the total free energy.

The apprehension of the energy terms and their role in the magnetic behavior of the system depends on understanding of how energy terms play a role in contribution of the total free energy of the system. In the following, we present the most important energy terms.

1.1. Magnetic anisotropy energy

Magnetic anisotropy [16] is the way in which the magnetic properties of a material are dependent on the direction in which they are measured. In practical terms we find that many materials are easier to magnetize in one direction than they are in another. The directions of easy magnetization are referred to as easy axes and those that are more difficult to magnetize, hard axes.

Because the applied field must do the work against the anisotropy force to turn the

magnetization vector $\mathbf{M}$ away from the easy direction, there must be energy stored in the crystal if the $\mathbf{M}$ is not along the easy direction.

1.1.1. Magnetocrystalline anisotropy

Crystal anisotropy is the only type of anisotropy that is intrinsic to the material, all the others types are extrinsic. The disposition of the magnetic moments in a magnetic crystal reflects the symmetry of the lattice. A coupling of the electron orbital to the lattice causes the anisotropy, and in the easy direction of magnetization this coupling is such that these orbitals are in the lowest energy state. Therefore the interactions of the magnetic moments between themselves or with the lattice are affected by the crystal symmetry and will generate anisotropic energy contributions, collectively termed the magnetocrystalline anisotropy [17].

There are directions in the space lattice which are easier to magnetize than other directions; these directions are called easy directions or easy axes. For the simple case of the uniaxial magnetic anisotropy, and considering that the uniaxial anisotropy axis, or easy axis, is parallel to one of the axis of the crystal, the anisotropy energy is invariant with respect to rotations around the anisotropy axis, and depends only on the relative orientation of magnetization vector $\mathbf{M}$ with respect to that axis. As $\mathbf{M}$ rotates away from that axis, the anisotropy energy initially increases with θ, the angle between the axis and the magnetization vector, then reaches a maximum value at $\theta = 90^0$, and decreases to its original value at $\theta = 180^0$. Therefore, the minimum of anisotropy energy occurs when the magnetization points in either the + or – direction along that axis. The expression of this energy density is:

$$F_K = K_0 + K_1 \sin^2\theta + K_2 \sin^4\theta + \ldots \qquad (1.1)$$

The coefficients K_n $(n = 0,\ 1,\ 2....)$ are the anisotropy constants, having the dimension of energy per unit volume. The higher-order terms above K_2 are negligible being in general very small. The K_0 term is a constant; therefore, it also can be disregarded. For small deviations of the magnetization vector from the equilibrium position, the anisotropy energy density can be approximated, to second order in θ, as:

$$F_K \cong K_1\theta^2 \cong 2K_1 - 2K_1\cos\theta = 2K_1 - \mathbf{M}\cdot\mathbf{H}_K \qquad (1.2)$$

where: $H_K = \dfrac{2K_1}{M_s}$, with M_s being the magnitude of the magnetization vector $\mathbf{M}$; H_K is the anisotropy field, offering a measure of the strength of the anisotropy effect and of the torque necessary to take the magnetization away from the easy axis;

In a crystalline magnetic material the magnetic properties will vary depending on the crystallographic direction in which the magnetic dipoles are aligned.

For cubic crystals, the anisotropy energy density can be expressed in terms of the direction cosines $(\alpha_1,\ \alpha_2,\ \alpha_3)$ of the magnetization vector with respect to the 3 cube edges:

$$F_K = K_1(\alpha_1^2\alpha_2^2 + \alpha_2^2\alpha_3^2 + \alpha_3^2\alpha_1^2) + K_2\alpha_1^2\alpha_2^2\alpha_3^2 \qquad (1.3)$$

Another example is the hexagonal crystal structure of Co that can be magnetized easily in the [0001] direction (along the c-axis), but has hard directions of magnetization in the <1010> type directions, which lie in the basal plane (90° from the easy direction), as represented in Fig. 1.1.

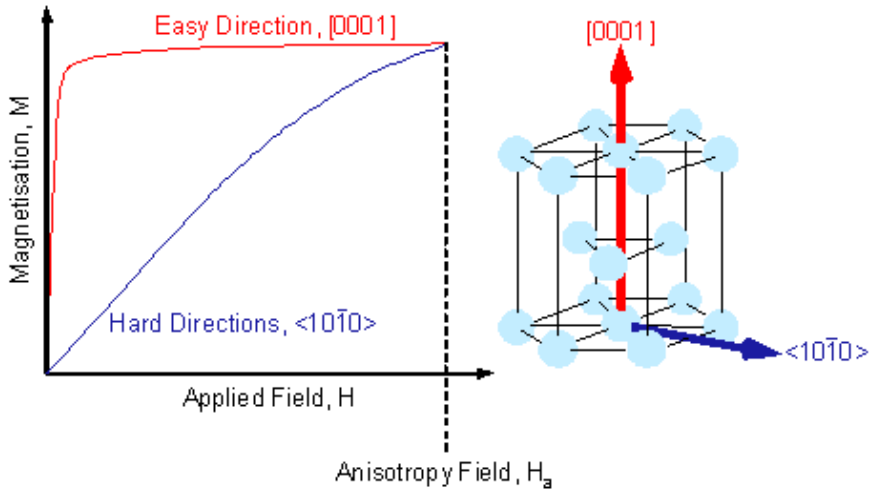

Figure 1.1. The magnetocrystalline anisotropy of cobalt

1.1.2. Shape Anisotropy

The magnetostatic energy is creating the shape anisotropy. The behavior of magnetization for a magnetic specimen depends on its susceptibility and also on its geometry.

When a specimen of finite size is magnetized by an external magnetic field, at its ends will appear so-called free poles. The free poles will produce a magnetic field oriented opposite to the magnetization of the specimen [17]. The only bodies which can be uniformly magnetized, when they are placed in a uniform field, are the ellipsoidal bodies. From an experimental point of view, the prolate spheroids are a good approximation to cylinders, oblate spheroids to disks, and oblate ellipsoids to films.

The demagnetizing field is given by

$$\mathbf{H}_d = -\vec{N} \cdot \mathbf{M}\,, \qquad (1.4)$$

where N is the demagnetizing factor, dependent only on the shape of the specimen.

For a single domain particle, the magnetostatic energy is related to the magnetization components and it can be only expressed exactly if the particle has an ellipsoidal shape. If we take the principal axes *a*, *b*, and *c* of the ellipsoid as xyz axes, the magnetostatic energy density takes the form:

$$F_D = \frac{1}{2}(N_a M_x^2 + N_b M_y^2 + N_c M_z^2) \tag{1.5}$$

where: N_a, N_b and N_c are the demagnetizing factors corresponding to the three principal axes, and satisfying the equation $N_a + N_b + N_c = 4\pi$ (cgs).

The longer the principal axis, the lower is the corresponding demagnetizing factor and the lower is the energy when $\mathbf{M}$ points along that direction.

1.1.3. Stress anisotropy and magnetostriction

If a mechanical stress is applied to a magnetic specimen, its shape and volume change and will induce a change in the magnetic properties along the stress directions. The reverse phenomenon is called magnetostriction. The magnetostriction is the phenomenon in which the shape and volume of a magnetic specimen change during the process of magnetization.

The reason for this behavior is that the crystal lattice inside each magnetic domain is spontaneously deformed in the direction of domain magnetization and its strain axis rotates with the rotation of the domain magnetization, thus resulting in a deformation of the specimen as a whole [17]. The magnetoelastic energy density for the stress anisotropy and for its reverse, the magnetostriction, is given by:

$$F_\sigma = \frac{3}{2}\lambda_s \sigma \sin^2 \theta_s \tag{1.6}$$

where: θ_s is the angle between the magnetization and the stress direction, λ_s is the magnetostriction constant, and σ is the uniaxial stress applied along a certain direction.

1.2. Zeeman energy

The interaction between the magnetization and the external applied field is called the Zeeman energy. The energy density in this case is given by

$$F_H = -\mathbf{M} \cdot \mathbf{H} \tag{1.7}$$

1.3. Exchange energy

The exchange interaction was first introduced by Heisenberg in 1928 to interpret the origin of the enormously large molecular fields acting in ferromagnetic materials[17]. This interaction is of the quantum mechanical nature. It is the result of the fact that the wave function of indistinguishable particles is subject to exchange symmetry, that is, the wave function describing two particles that cannot be distinguished must be either unchanged (symmetric) or inverted in sign (antisymmetric) if the labels of the two particles are changed.

The energy density for exchange interaction is given by:

$$F_E = -2\sum_{ij} J_{ij} \mathbf{S_i} \cdot \mathbf{S_j} \tag{1.8}$$

where: $\mathbf{S_i}$, $\mathbf{S_j}$ are the spin operators of the two electrons. The term J_{ij} is a pure quantum mechanical term and is called the exchange integral. We have $J_{ij} > 0$ for the case when the two spins are parallel to each other (ferromagnetism) and $J_{ij} < 0$ when the two spins are anti-parallel to each other (antiferromagnetism). Although the consequences of the exchange interaction are magnetic in nature, the cause is not; it is due primarily to electric repulsion and the Pauli Exclusion Principle, from quantum mechanics. Indeed, in general, the direct

magnetic interaction between a pair of electrons (due to the electron's magnetic moments) is negligibly small compared to this electric interaction.

From a practical point of view, it is interesting to discuss the exchange anisotropy in the case of thin film structures. The exchange coupling of ferromagnetic and antiferromagnetic films across their common interface causes a shift in the hysteresis loop of the ferromagnet, along the field axis, called exchange bias (see Fig. 1.2). The shift can be useful in controlling the magnetization in nanodevices, such as spin valves which sense changing magnetic fields through the giant magnetoresistance effect [18]. Read heads based on this effect are used in magnetic disk data storage.

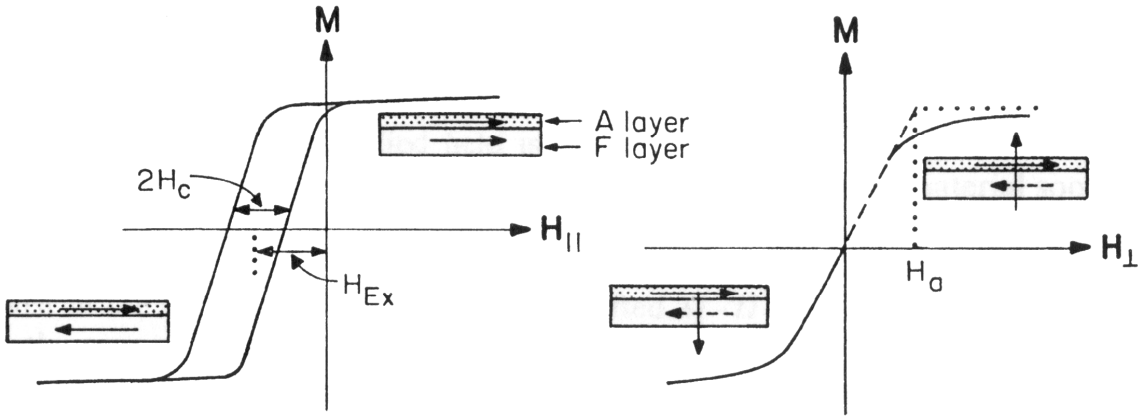

Figure 1.2. The effect of exchange coupling on M vs. H loop for a material with an antiferromagnetic (A) surface layer and a soft ferromagnetic (F) interior [18]

This exchange coupling refers to a preference for specific relative orientations of the moments of two different materials when they are in intimate contact with each other (or less than 60 Å between the layers) [18]. This proximity will allow spin information to be communicated between the materials. One of them is generally ferromagnetic and the other is harder or is antiferromagnetic (see Figure1.3).

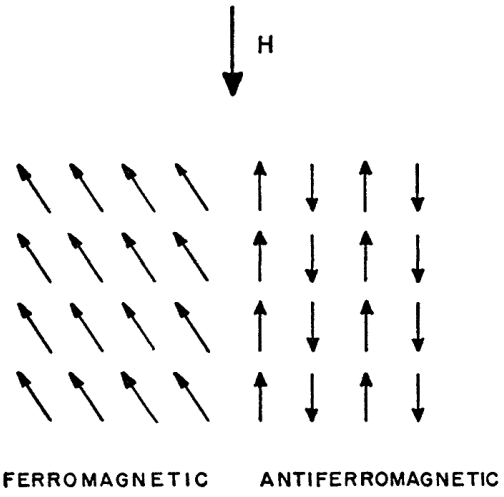

Figure 1.3. Ferromagnet-antiferromagnet interface with a small field applied

In order for the exchange anisotropy to appear during a measurement, the sample temperature should be lower than Néel temperature, T_N, of the antiferromagnetic material. Below this temperature the antiferromagnetic material acts as paramagnetic, and the exchange anisotropy does not appear [19].

When the field is applied in the same direction during cooling, $H_{\|}$, the hysteresis loop is shifted toward the negative field direction by H_{ex}. The coercivity is half the width of M vs. $H_{\|}$ loop at M = 0. No exchange shift in the loop is observed if the external field is applied orthogonal to the direction of the field present during cooling. The hard axis loop serves to define the anisotropy field, H_a, of the system. The coercivity is 0 in $H_{\perp}$ direction [18].

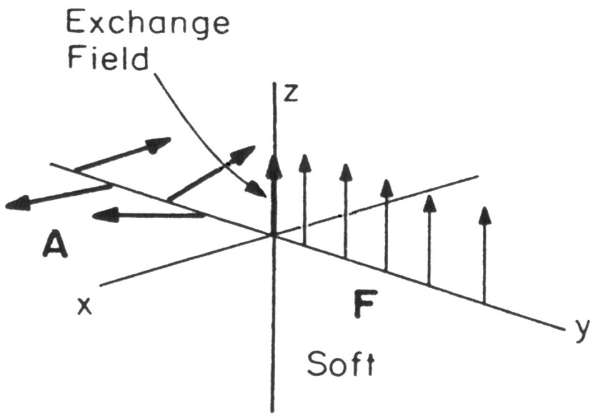

Figure 1.4. Direction of the spins near the interface between *A* and *F* layers after cooling through T_N of *A* material [18]

The exchange coupling across the interface is such that the moments in the antiferromagnetic material, ***A***, is on the axis that is orthogonal to the ferromagnetic material, ***F***, at the time of the cooling through T_N . This is the lower energy configuration because it is easy to align the ***A*** moments in the direction of an orthogonal field, and it is difficult to align in the direction of the field which is parallel to the preferred ***A*** axis. For ***A*** the orthogonal susceptibility is larger than the parallel susceptibility, $\chi_{\perp} > \chi_{\parallel}$. This moment's arrangement generates an exchange field parallel to the direction of the ***F*** moments during field cooling (see Figs. 1.2 and 1.5).

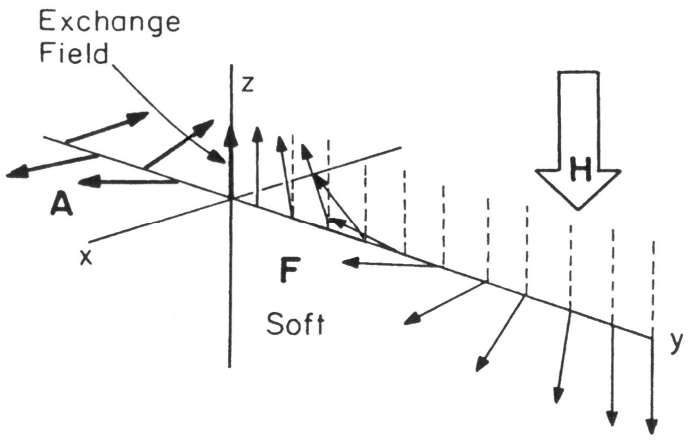

Figure 1.5. Effect on spins in soft material of a applied field opposite to the exchange field [18]

If we apply a weak field to an exchange coupled system, the soft material will tend to follow the field subject to the coupling at the interface. For semi-infinite media on each side of the interface, most of the twist in magnetization field caused by the field would occur in the soft material. This twist occurs over a length comparable to a domain wall thickness. Because the magnetic anisotropy in ***F*** layer is small and the external field exerts no net torque on the ***A*** moments (they sum to zero and are held to a particular crystallographic direction by the strong magnetocrystalline anisotropy) the twist occurs in the soft material layer [18].

Several parameters are important in exchange coupling: the strength of the interface exchange, *J*, the anisotropy-thickness products of the two materials and the magnetization-thickness product of the soft layer (see Fig. 1.6).

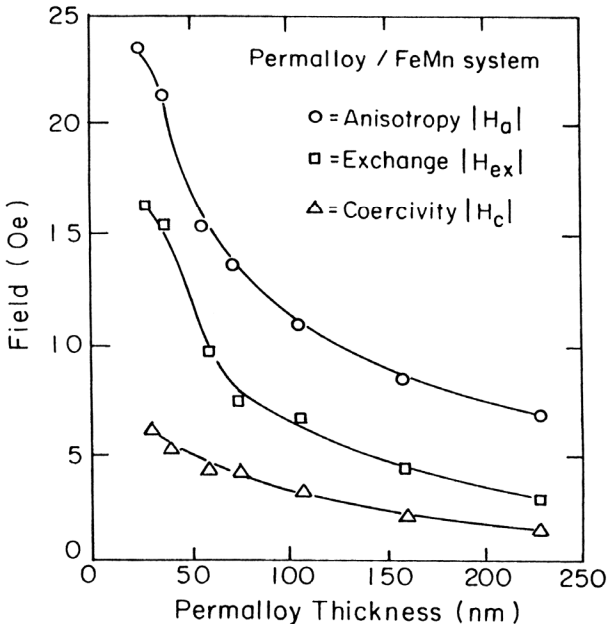

Figure 1.6. Anisotropy, exchange and coercive fields as function of material thickness [20]

1.4. Magnetization through Coherent Rotation. Stoner-Wohlfarth Model

The understanding of energy terms defined previously will offer us a way to study the magnetization process of magnetic systems through various models. A magnetic body consists of many domains and therefore it acts as a multi-domain structure. That means it is divided into uniformly magnetized domains separated by domain walls in order to minimize its total free energy. However, due to the energy cost of domain wall formation, the balance with the magnetostatic energy limits the subdivision in domains to a certain optimum domain sizes. There is a corresponding lower limit in the crystal size, below which a single-domain structure exists [21], since the energy increase due to the formation of domain walls in this case is higher than the energy decrease obtained by dividing the single domain into smaller domains.

The SW model is one of the simplest and successful approaches followed to explain the magnetization behavior of a single domain ferromagnetic particle or nanostructure.

The basic idea of the model is that a single magnetization vector is sufficient to describe the state of the whole system of single domain particles, which results in a coherent rotation. This model can describe well the systems of small magnetic particles when the thermal fluctuations of magnetic particles are neglected. However, when the system of single domain particles have their sizes lower than some critical value, the thermal effect needs to be taken into account since in this case the thermal energy of the system would be comparable to the magnetic anisotropy energy barrier of single domain particles. The anisotropy energy of a uniaxial single domain particle is given by $KV\sin^2\theta$ where K is the anisotropy constant and θ the angle between the magnetization vector and the easy axis. Thus, the energy barrier, separating easy directions is KV, proportional to the volume V. Therefore, by decreasing the particle size the anisotropy energy decreases, and for a domain size lower than a certain value, it may become comparable to, or even lower, than the thermal energy, kT. This implies that, the energy barrier for magnetization reversal may be overcome, and then the magnetic moment of the particle can thermally fluctuate from one easy direction to the other, even in the absence of the applied field, like a single spin in a paramagnetic material.

The magnetic behavior of an assembly of such small particles is called superparamagnetism [21]. In the case of studying of a system of magnetic nanoparticles where the superparamagnetism occurs, the SW model fails to describe such a system.

The thermal fluctuation of the magnetic moments of a single-domain particle and its decay toward thermal equilibrium was then introduced by Néel [22] and further developed by

Brown [23]. For the samples and situations considered in our study the effects of thermal relaxation are negligible and the hypotheses of Stoner-Wohlfarth model are valid.

1.4.1. The Critical Curve

The model proposed by Stoner and Wohlfarth [15] in 1948 attempted to explain the hysteretic behavior of a single domain magnetic particle, by determining its energy as a function of applied field and the angle of the magnetization vector. The model assumes that the magnetic moments within the particle remain parallel to one-another (coherent) during rotation and switching. Hence, the particle will have a constant intensity of magnetization, which changes only in direction. By finding the total energy minima it is possible to predict the magnetization switching behavior of the particle under the influence of an applied field.

This reduces the number of degree of freedom to one. The approach is idealized and should not be expected to always give accurate prediction of the behavior of real systems. This model applies for a monodomain particle in which the exchange interaction will be able to keep the elementary spins parallel with respect to each other so that the whole system can be considered uniform as a big single magnetization vector (see Fig. 1.7). One additional notable exception of SW model is that the temperature of the system is not taken into account or can be considered to be equal to zero.

This is reasonable to assume when the sizes of all ferromagnetic particles are still large enough so that the thermal energy is negligibly small, compared to the anisotropy energy. In this case the magnetic relaxation (superparamagnetism) phenomena can be disregarded. Also, the SW model does not take into account the interaction between particles.

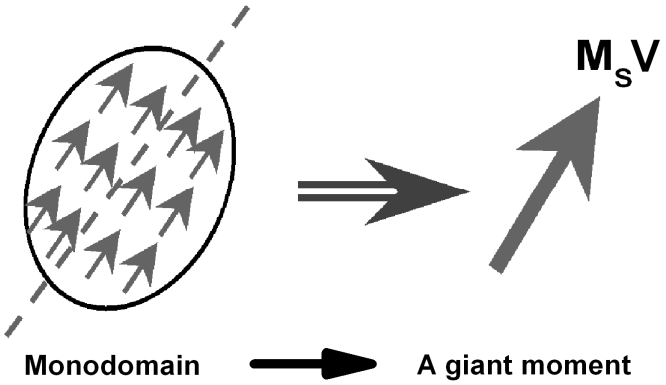

Figure 1.7. An assembly of small magnetic particles considered as a big magnetic particle having a big single moment

In what follows we will describe the free energy of a SW particle. The free energy of the uniaxial particle per unit volume is composed of two terms, the magnetocrystalline anisotropy energy and the energy of interaction with the external field, described as

$$F(\theta,\mathbf{H}) = K_1 \sin^2\theta - M_s H \cos(\theta - \theta_K) \tag{1.9}$$

where: K_1 is the first anisotropy constant, $\mathbf{H}$ the external field, θ and θ_K the angles made by normalized vectors $\mathbf{m} = \dfrac{\mathbf{M}}{M_S}$ and $\mathbf{h} = \dfrac{\mathbf{H}}{H_K}$ with the easy axis direction (see Fig. 1.8).

We write Eq. 1.9 in dimensionless form, by introducing the dimensionless quantity

$$g = \frac{F}{2K_1} \tag{1.10}$$

With this, Eq. 1.9 becomes:

$$g(\theta,\mathbf{h}) = \frac{1}{2}\sin^2\theta - h\cos(\theta - \theta_K) \tag{1.11}$$

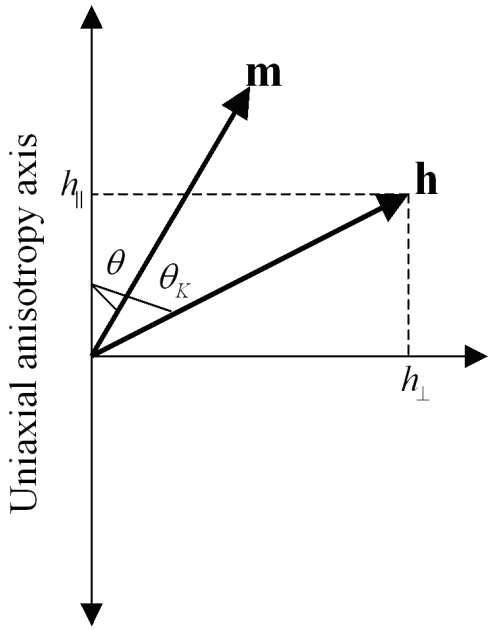

Figure 1.8. Orientation of uniaxial anisotropy axis, magnetization unit vector, **m** , and external field, **h** .

By using the field components perpendicular and parallel to the easy axis ($h_{\perp} = h\sin\theta_K$; $h_{\|} = h\cos\theta_K$), we obtain:

$$g(\theta, \mathbf{h}) = \frac{1}{2}\sin^2\theta - h_{\perp}\sin\theta - h_{\|}\cos\theta \qquad (1.12)$$

Next, we show how to test the change of the free energy function when we move in the plane determined by $h_{\perp}$ and $h_{\|}$. By taking the first and second derivative of the energy function (1.12) and by imposing the condition $\frac{\partial g}{\partial \theta} = 0$; $\frac{\partial^2 g}{\partial \theta^2} = 0$ we obtain the equations that describe the energy in this plane:

$$h_{\|} = -\cos^3\theta \quad \text{and} \qquad (1.13)$$

$$h_{\perp} = \sin^3\theta\,. \qquad (1.14)$$

The detailed derivation of these last two equations is presented in Appendix A.1.

Eq. (1.13) and (1.14) are the parametric equations that describe the critical curve - the astroid - when θ varies in the interval $(0,\ 2\pi)$, as shown in Fig. 1.9.

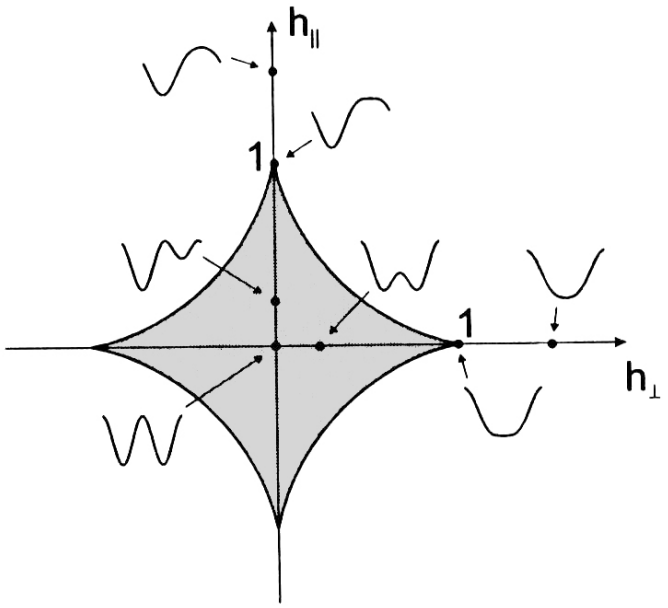

Figure 1.9. Plane of coordinates $h_{\|}$ and $h_{\perp}$. The astroid curve is defined by Eq. 1.13 and 1.14. Simplified illustrations of the dependence of the system energy g from (1.12) on θ at different points in $h_{\|}$ and $h_{\perp}$ space

The curve generated by (1.13 and 1.14) when θ varies in the interval $(0,\ 2\pi)$ as shown in Fig. 1.9 is the critical curve or astroid curve [24] in its simplest representation. The energy profiles can be obtained from (1.12) as a function of θ at different values of the applied field corresponding to the points inside and outside astroid.

The orientations of **m** for a given field **h** can be determined by drawing the tangents to the astroid, passing through the point **h** of the plane $h_{\perp}$ and $h_{\|}$. (see Fig. 1.10). Each tangent may identify either a stable or an unstable state. The stable orientation provides an energy minimum, and it can be selected using the two conditions:

$$\frac{\partial g}{\partial \theta} = 0; \quad \text{and} \quad \frac{\partial^2 g}{\partial \theta^2} > 0 \tag{1.15}$$

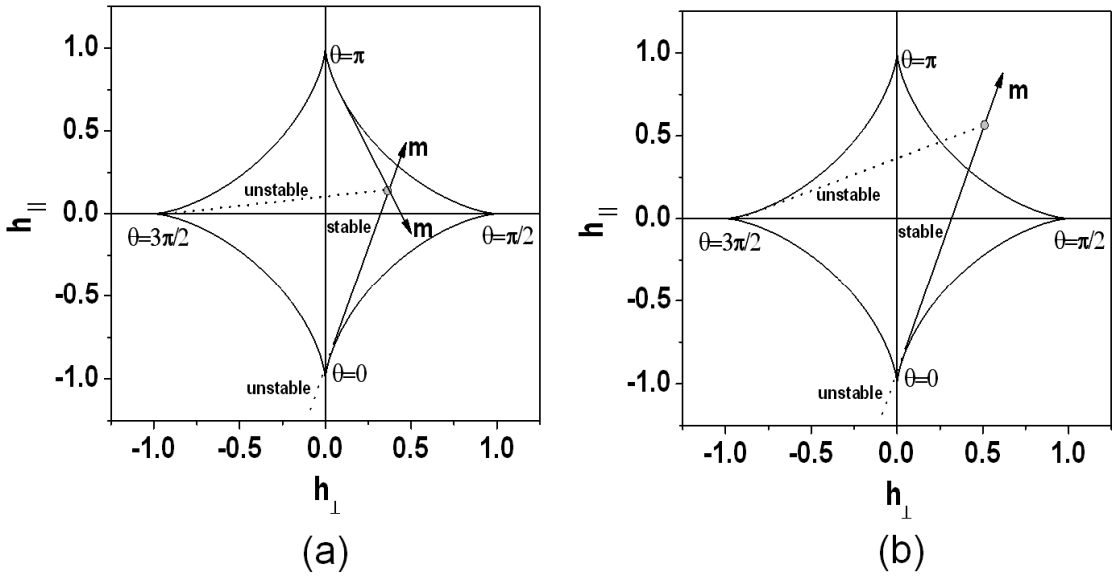

Figure 1.10. Graphical construction defining the possible **m** orientations for a given applied field: (a) Inside the astroid. (b) Outside the astroid. The straight half-lines marked as "stable" ("unstable") are sets of local energy minima (maxima) characterized by the same **m** orientation. θ values are showing how the angle parameter of (1.13 and 1.14) varies along the astroid [24].

There is only one stable solution when the point is located outside the astroid, whereas there are two stable tangents that can be drawn when the point is inside the astroid.

As seen in Fig. 1.11, the stable states corresponding to a given field can be easily determined according to the method [13] explained next. We start by drawing a tangent from the field point $\left(h_x, h_y\right)$ to the critical curve such that the tangent is pointing toward the field point. The orientation of the tangent will be a stable state for the given field if and only if the angle θ, as measured from the $+h_x$, axis, falls within the range labeled on the corresponding part of the critical curve.

Based on this rule, it is found that for field values within the critical curve, one of two possible stable states can occur, depending on the history of magnetization (the tangent's starting point).

Outside the critical curve, only one stable state is possible. When the critical curve is crossed during field change, switching (or discontinuous change in magnetization orientation) may or may not occur (again depending on the tangent's starting point).

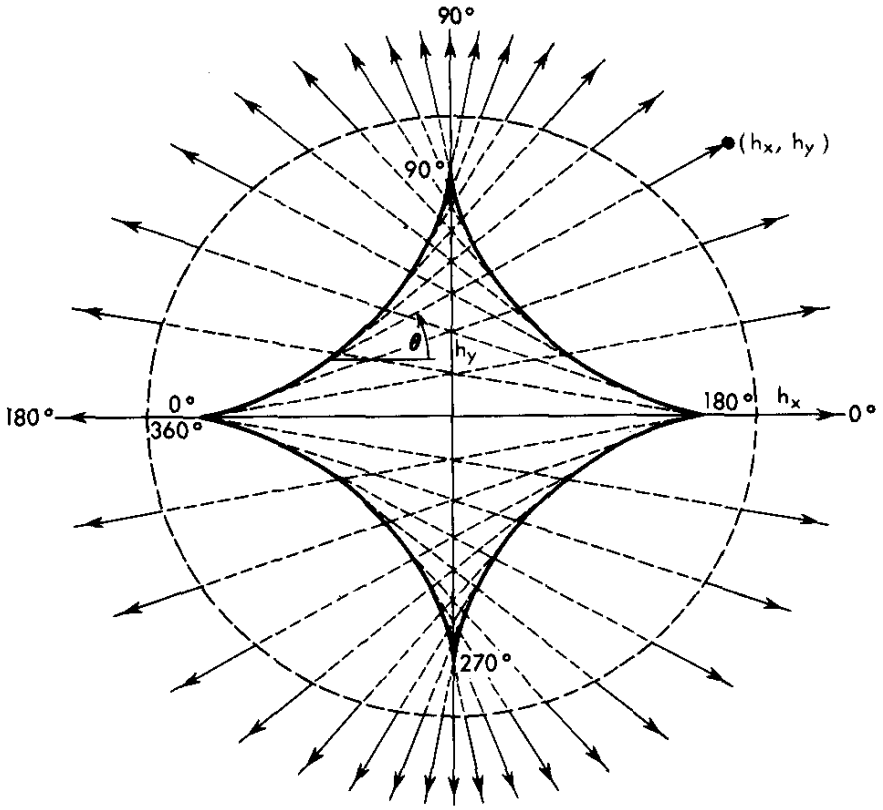

Figure 1.11. Critical Curve and stable-state lines for a uniaxial film [25]. In this case the angle θ is between 0° and 90° and the intersect with the critical curve (in the 2nd quadrant) is also between 0° and 90°.

1.4.2. Hysteresis

The typical properties of the astroid curve are the basis for the analysis of the phenomena that takes place when the field is slowly varied over time. The magnetization

process under alternating field, where **h** oscillates between opposite values along a fixed direction, is shown in Fig. 1.12. The field vector orientation moves back and forth in the plane along a fixed straight line. The **m** orientation at each point is obtained by the tangent construction discussed in the preceding subsection.

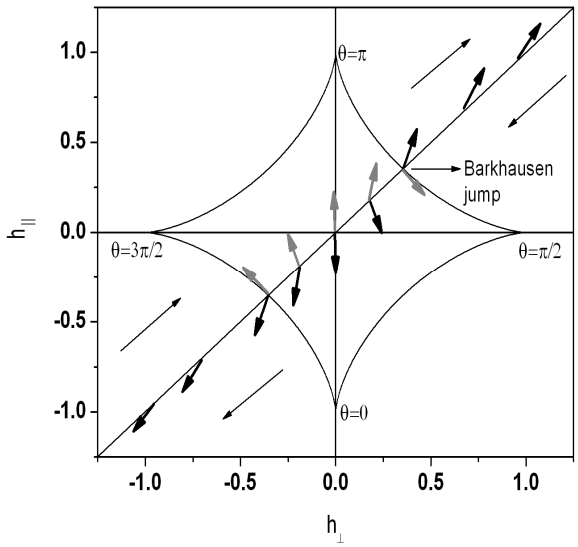

Figure 1.12. Magnetization process under alternating field. Black arrows represent the **m** orientation in the state occupied by the system, gray arrows in the other state available to the system [24].

Inside the astroid, two orientations are possible, and the only one actually realized depends on the past history (hysteresis). If the field oscillation were all contained inside the astroid, the magnetization would reversibly oscillate around the orientation initially occupied. If the field can cross over the astroid boundary, a magnetization reversal (Barkhausen jump) takes place [24], and a hysteresis loop can be recorded (see Fig. 1.13).

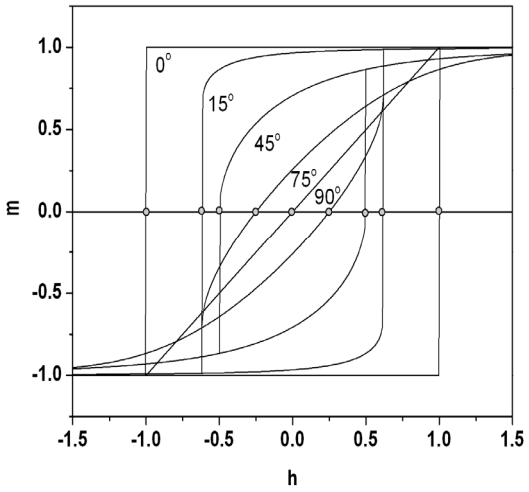

Figure 1.13. Hysteresis loops for different values of θ_K [24]

1.5. Summary

In this chapter we discussed the different energy terms contribution in magnetic systems and how they influence the magnetization switching. In particular, for a magnetic system with uniaxial anisotropy, we determined the magnetization curves using the Stoner-Wohlfarth model.

The problem of magnetization switching can be addressed in general, if one knows the free energy F of the magnetic system. The free energy landscape for every magnetic system at a given value of applied magnetic field presents a series of relative minima and maxima separated by energy barriers. At equilibrium the magnetic system will be found in one of its stable state corresponding to one of the free energy minima. As the field is changing, the configuration of maxima and minima will be altered and the stable states of magnetization will shift, and if precessional effects are neglected, the system will remain in its state of free energy minimum. However, for a critical field value the energy barrier adjacent to the system's energetic minimum will disappear and the stable state will switch to

a neighboring minimum. The critical curve is in essence the locus of these critical field values. In the case of a single magnetic film, a sufficient condition for a critical state is to have $\frac{dF}{d\theta}=0$, $\frac{d^2F}{d\theta^2}=0$, and $\frac{d^3F}{d\theta^3}\neq 0$ simultaneously, where the angle θ describes the magnetization's orientation. For a Stoner-Wohlfarth system (uniaxial anisotropy) the critical curve is an astroid, as it was shown in this chapter.

As the critical curve is the locus of points for which the magnetization reversal occurs [14], any experimental method able to probe the discontinuous and irreversible changes in magnetization orientation can be employed to determine this polar map of the switching fields.

Several methods were developed to determine the critical curve for 2D magnetic systems through magneto-resistance [26], [27], [28], micro-superconducting quantum interference device technique [29], [30] and, lately, through reversible susceptibility experiments [31], [32]. As it will be shown later, the reversible susceptibility method can be applied to magnetic systems with any type of anisotropy. This is the method we used in our study and it will be discussed in the next chapter.

Chapter 2

Susceptibility of a Magnetic Nanostructure

Magnetic susceptibility measurements reveal important information about the switching fields and anisotropies of magnetic materials. We begin our study by exploring the susceptibility of a Stoner-Wohlfarth (SW) particle due to the relative simplicity of the theoretical model used. We will proceed in the next chapters with the susceptibility studies for more complicated systems.

The magnetic susceptibility is a quantity which describes the capability of a magnetic material to magnetize in response to a magnetic field. The magnetic susceptibility χ is defined by the ratio between the induced magnetization of a magnetic sample and the inducing magnetic field; therefore, it describes the material's response to an applied magnetic field.

Taking into account that both magnetization and magnetic field are vectors, the magnetic susceptibility of a ferromagnetic substance is not a scalar.

This response is dependent upon the state of sample and may occur in directions other than that of the applied field. To accommodate this, a general definition using a second rank tensor derived from derivatives of components of magnetization M with respect to components of applied field H, called the differential susceptibility, describes ferromagnetic materials, where i and j refer to the directions (e.g., x, y and z in Cartesian coordinates) of the magnetization and applied field, respectively. The differential susceptibility is written as:

$$\chi_{ij} = \frac{\partial M_i}{\partial H_j} \tag{2.1}$$

The susceptibility tensor describes the response of the magnetization in the i^{th} direction from an incremental change in the j^{th} direction of the applied field. Generally the susceptibility tensor should have 9 components, but, in fact, a maximum of 3 can be independent, because, by appropriate choice of the orientation of the body-fixed coordinate system, the susceptibility tensor can be reduced to its diagonal form. The general tensor behavior of the susceptibility is, in fact, related to the anisotropy of magnetic properties. The diagonalization of the susceptibility tensor takes place when the privileged directions of magnetization become parallel with coordinate system's axis.

If the change of the applied field provides only reversible change of magnetization (i.e., processes that involves no loss of energy) we have a reversible susceptibility.

If the $0z$ axis is in the direction of the biasing field then the diagonal elements of the tensor are the parallel susceptibility χ_{zz}, measured in the field direction, and the two transverse susceptibilities χ_{xx} and χ_{yy}, measured perpendicular to the field direction.

These susceptibilities will be considered in the case of a Stoner-Wohlfarth [15] particle, outlining briefly the derivation of Aharoni [33] as presented in section 2.3.

2.1. Magnetic Susceptibility Method

The transverse susceptibility of a material is a measure of the magnetic susceptibility (ease of magnetization) of the material in a direction transverse to an applied bias field, H_{dc}.

In order to measure the susceptibility of the sample, a small ac probe field, H_{ac}, is applied in the direction in which the susceptibility is to be measured and a coil winding

around the sample is used to measure the magnetic flux change in this direction, which is proportional to the change in magnetization of the sample. The *ac* probe field is very small so that we may assume that the measured change in magnetization in phase with the probe field is due to reversible oscillation of the particle moments and not switching behavior.

If we assume that the magnetic material is composed of small single-domain particles, we will use the Stoner-Wohlfarth [15] model to show how the transverse susceptibility changes as a function of the applied bias field.

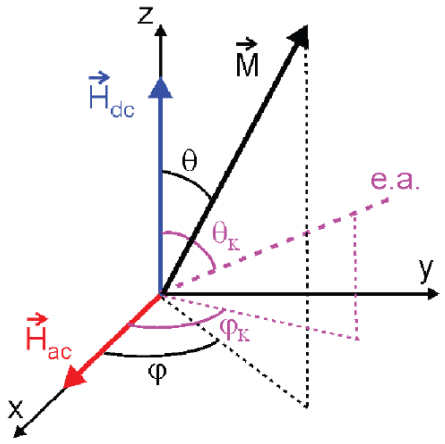

Figure 2.1. Schematic representation of the transverse susceptibility experiment for a uniaxial single domain ferromagnetic particle; the angles notation complies with the original model proposed by Aharoni [33]

Further on let's see how the free energy landscape, as described in subchapter 1.4.1 - Eq. 1.11, is determining the magnetization switching. Let's consider now different directions for the applied bias field, $h = \frac{H}{H_k}$, with respect to the SW particle's easy axis, given by the angle θ_K :

a) θ_K = 180°

For a particle where θ_K = 180° (i.e. the applied field is antiparallel to the easy axis) the energy as a function of angle formed by magnetization with the easy axis, $(\theta_K - \theta)$, is shown in Fig. 2.2.

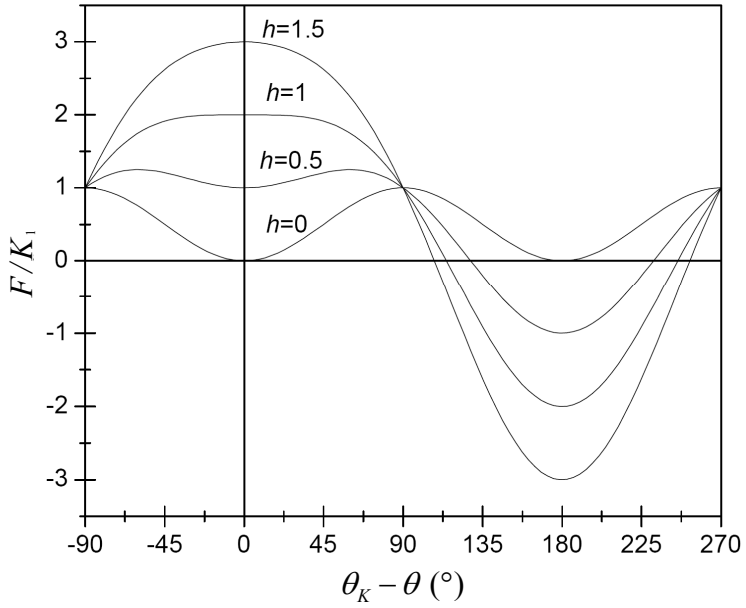

Figure 2.2. Energy as a function of h and $(\theta_K - \theta)$ for a SW particle at θ_K=180°

With zero applied field (h=0) the energy function has two minima, at $\theta_K - \theta = 0^\circ$ and $\theta_K - \theta = 180^\circ$. As we increase the field, the depth of the energy well at $\theta_K - \theta = 0^\circ$ decreases. We can see that the stable equilibrium at $\theta_K - \theta = 0^\circ$, transforms into an unstable equilibrium at a field value of h = 1. Above this field, a moment with an angle $\theta_K - \theta = 0^\circ$ would switch to the $\theta_K - \theta = 180^\circ$ position. The value of h at which this occurs is known as the switching field, h_c. For Fig. 2.2, where $\theta_K = 180^\circ$, we can see that $h_c = H_k$.

b) $\theta_K = 90°$

If we consider a particle where a field is applied perpendicular to the easy axis direction, (i.e. $\theta_K = 90°$) the energy function is as shown in Fig. 2.3. We can see that as the field is increased the angular position of the minima changes, causing the magnetization vector to rotate. Neither one of the minima disappears at higher fields; instead they merge to form a single minimum at $\theta_K - \theta = 90^\circ$ when $h = 1$.

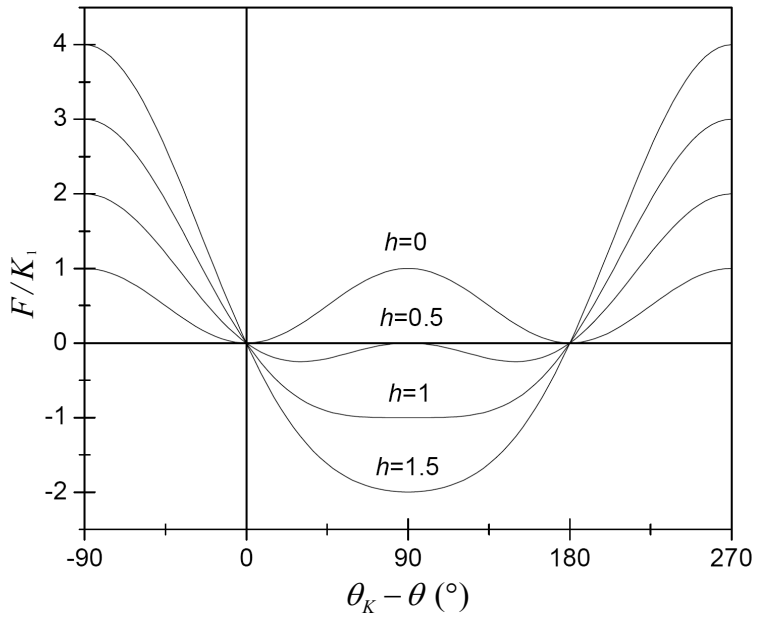

Figure 2.3. Energy as a function of h and $(\theta_K - \theta)$ for a SW particle at $\theta_K = 90°$

The effect of this is that the magnetization will rotate continuously from the easy axis to the hard axis direction without any switching behavior. The particle moment will be aligned with the applied field (hard axis direction) at an applied field $h \geq 1, (H \geq H_k)$.

c) $90° < \theta_K < 270°$

For a particle where a field is applied at an angle greater than 90° from the easy axis direction a combination of rotation and switching governs the magnetization of the particle

(with θ_K = 180° as a special case where the reversible rotation component is zero). Figure 2.4 shows the energy function for a particle where θ_K = 135°. In this case we can see that the angular position of the minimum at $\theta_K - \theta = 0^\circ$ starts to change as the field is applied, causing the magnetization vector to rotate.

At a field value between $h = 0.4$ and $h = 0.6$ (actually at $h = 0.5$ for this particular angle) the minimum changes to a point of inflection and at this point the magnetization will switch to the remaining minimum. Subsequent increases in the field continue to rotate the magnetization vector towards the field direction but saturation in the direction of the field ($\theta = 0^\circ$) will only be achieved when $h = \infty$. In this case the switching occurs at a field where $h < 1$, and nothing significant happens at the field value $h = 1$.

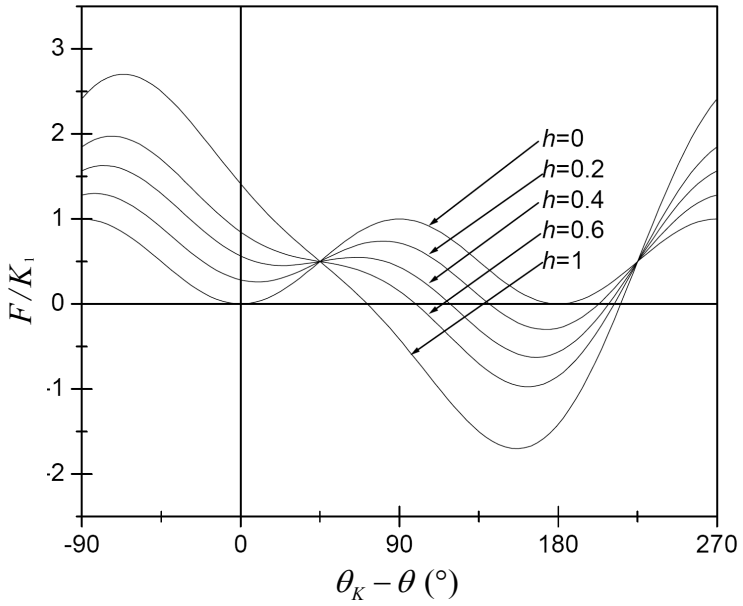

Figure 2.4. Energy as a function of h and $(\theta_K - \theta)$ for a SW particle at θ_K =135°

d) General case

For the special case where $\theta_K = 180°$ there is no change in the magnetization vector as a result of increasing field until the field reaches $h = 1$, when the particle switches and the magnetization is subsequently saturated in the field direction.

Also, for the special case where $\theta_K = 90°$ the magnetization rotates continuously with increasing field until the field reaches $h = 1$, at which point the magnetization vector is aligned with the applied field and the magnetization is saturated in the field direction. For all other cases the magnetization rotates towards the applied field direction tending to saturate in the field direction as the field approaches infinity. When the magnetic moment orientation angle at $h = 0$ is greater than 90° from the direction of the applied field, $(\theta > 90^\circ)$, a switching event will also occur at some point during the rotation.

In order to determine at what angle, $(\theta_K - \theta)_c$, and at what field, h_c, a switching event will occur we consider the conditions for switching. In order for a moment to switch, the energy minimum in which the moment rests must become a flat point-of-inflection. Hence

$$\frac{dF}{d(\theta_K - \theta)} = 0 \text{ and } \frac{d^2F}{d(\theta_K - \theta)^2} = 0 \tag{2.2}$$

For the ease of notation, we will use $(\theta_K - \theta) = \beta$

Hence $$\frac{dF}{d\beta} = 0 \text{ and } \frac{d^2F}{d\beta^2} = 0 \tag{2.3}$$

The solution of Eqs. 1.9 and 1.11 (rewritten using $(\theta_K - \theta) = \beta$) are:

$$F(\beta, \mathbf{H}) = K_1 \sin^2 \beta - M_s H \cos(\beta - \theta_K) \tag{2.4}$$

$$g(\beta, \mathbf{h}) = \frac{1}{2}\sin^2 \beta - h\cos(\beta - \theta_K) \tag{2.5}$$

where $g = \dfrac{F}{2K_1}$

for these conditions - (2.4) and (2.5) – transforms in the following two equations [16],

$$\tan^3 \beta_c = -\tan \theta_K \tag{2.6}$$

$$h_c^2 = 1 - \frac{3}{4}\sin^2 2\beta_c \tag{2.7}$$

From these equations it is possible to determine the switching angle as a function of the applied field angle, and the switching field as a function of the switching angle.

The last equation is an interesting result as it shows that the maximum switching field is equal to H_K, and occurs only where the switching angle β_c, is 0° or 90°, with respect to the easy axis direction. The switching field, h_c, as a function of the switching angle, β_c, is shown in Fig. 2.5.

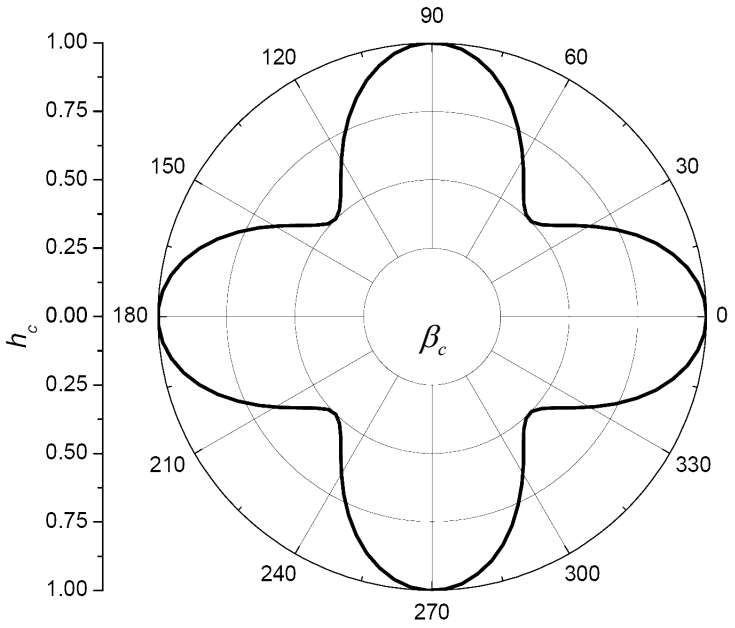

Figure 2.5. Switching field, h_c, as a function of switching angle, $(\theta_K - \theta)_c = \beta_c$

The Stoner-Wohlfarth model is the foundation in the theoretical modeling of systems of magnetic particles. The behavior of a Stoner-Wohlfarth particle can be completely described by defining the two parameters, M_s and H_k.

Figures 2.2, 2.3 and 2.4 are showing the energy of a particle as a function of magnetic moment angle, β, and reduced field, h, for different angles, θ_K, of the applied field. The application of a *ac* field causes a small oscillation of β within the local energy minimum. Considering the width of the energy minima we can see that for θ_K=180°, just before switching, the energy minimum becomes a point of inflection the base of which becomes flat. Also, in the case where θ_K=90° and $h=1$ (see Fig. 2.3) the two minima merge to form a single wide, flat-based minimum. In both of these cases the flat segments on the energy curve means that there is no restoring force acting on the moment such that the transverse susceptibility becomes infinite at these points. Aharoni [33] used the Stoner-Wohlfarth model to predict the transverse susceptibility for a SW particle, as it will be presented in next section.

The physical origin of the infinite susceptibility features can be explained by reference to the changing shape of the energy minima in which the particle moment sits. The features related to the anisotropy field are associated with those particles with easy axes aligned with the *ac* field direction. Referring to Fig. 2.3, this corresponds to particles with angle θ_K = 90°. The energy as a function of reduced field, h, and moment angle, β, is shown in Fig. 2.6 and we can see that as h increases from zero, the energy minima rotate towards one another.

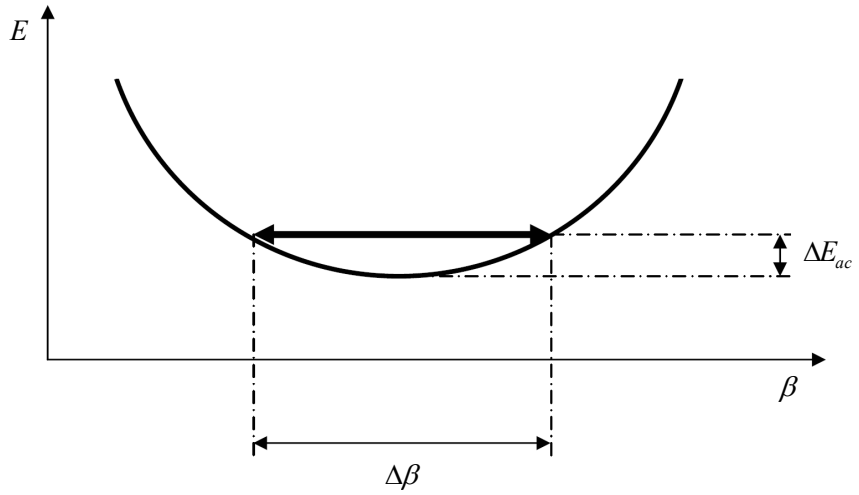

Figure 2.6. Representation of the energy minimum showing relationship between shape of curve, *ac* field energy, ΔE_{ac}, and oscillation angle, $\Delta\beta$

Figure 2.6 shows the relationship between the shape of the minimum, the *ac* field energy, ΔE_{ac}, and the moment oscillation angle, $\Delta\beta$. As the *ac* field is constant, changes in the susceptibility signal (which is a function of $\Delta\beta$) are solely due to changes in the shape of the minimum. For those particles with easy axes aligned with the *ac* field, as H_{dc} approaches H_K ($h \simeq 1$) the two narrow minima begin to merge until the point where $H_{dc} = H_K$, when they form one minimum with a very wide flat base (see Fig. 2.3). At this point $\Delta\beta$, and the susceptibility signal, become very large.

Subsequent increases in H_{dc}, to values greater than H_K, cause the single minimum to narrow reducing $\Delta\beta$. So, for $H_{dc} = H_K$ the minimum is the broadest, and any arbitrary *ac* field, however small, will cause an oscillation of the magnetic moment, and consequently the theory of Aharoni predicts a singular point of the TS at $H_{dc} = H_K$.

Therefore, the susceptibility signal goes through a sharp maximum when $H_{dc} = H_K$.

Particles with easy axes orientation not perpendicular to H_{dc} will not show this single, wide minimum. Instead, one of the minima progressively deepens, while, at same time, the other becomes shallower until the shallow minimum disappears (see Fig. 2.4). As no wide minimum occurs at $H_{dc} = H_K$ there is no feature in the susceptibility signal associated with the anisotropy field of these particles, instead as H_{dc} approaches H_c, the shallow minima becomes wider and flatter until at $H_{dc} = H_c$ it becomes a flat point of inflection (an unstable equilibrium) and hence $\Delta\beta$ again becomes very large. As H_{dc} increases further the equilibrium position disappears and the moment switches irreversibly into the single narrow minimum causing $\Delta\beta$ to become small again.

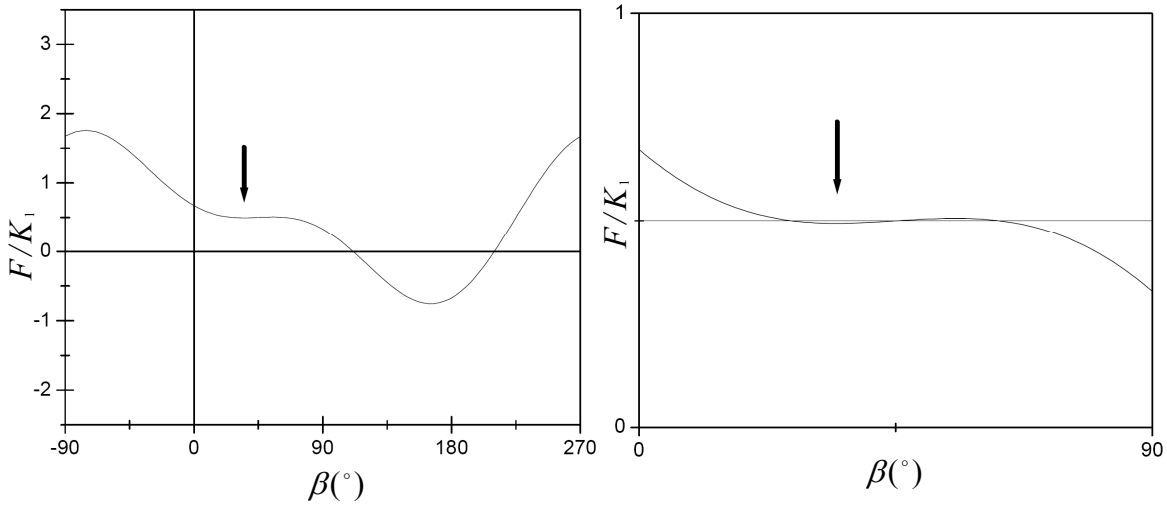

Figure 2.7. Energy F/K_1 as a function of β at $H_{dc} = 0.95H_c$; arrow indicates broad minimum (*left*), expanded view of broad minimum (*right*)

Figure 2.7 shows the energy as a function of moment angle for a particle where $H_{dc} = 0.95H_c$ (θ_K = 135° in this example). A broad minimum exists at an angle just below the switching angle (45° for θ_K = 135°) and can be seen in more detail in the expanded view of Fig. 2.7 (right).

2.2. Timeline for Magnetic Susceptibility Studies

The transverse susceptibility, TS, was first discussed by Gans [34] in 1909. The transverse susceptibility is defined as the initial susceptibility of a material measured in a transverse direction to an applied bias field and its usual notation is χ_t.

A theoretical expression for the reversible transverse susceptibility (RTS), was derived by Aharoni et al in 1957 [33] which suggested that the χ_t for a Stoner-Wohlfarth system with a random distribution of easy-axis directions would show three cusps, at the coercive field, $-\mathrm{Hc}$ (assuming that the bias field is swept from positive to negative values), and at the anisotropy fields, $\pm\mathrm{Hk}$.

In 1987 Pareti and Turilli [35] demonstrated that the Aharoni model was only applicable to particulate media where the particle size was below the required volume for multiple domain formation.

In 1993 Hoare et al [36] published experimental and theoretical studies of the effect of texture and anisotropy field distributions on the transverse susceptibility of particulate media. These showed that the shape of the χ_t plot was highly dependent on the texture of the media and that a highly aligned system enhanced the anisotropy peaks. The addition of an orientation texture distribution and particle's H_K distribution to the Aharoni model gave broadened peaks rather than cusps and that the H_K peaks were enhanced in a material with a preferred orientation direction aligned with the *ac* field. These findings were consistent with the results of experimental measurements.

In 1995 Yang [37] published extensions to transverse susceptibility theory showing the effects of thermal switching and interactions (using a mean field approach). These studies

indicated that the anisotropy information in the χ_t was not affected by thermal switching, whilst the coercivity information was reduced. They also found that the anisotropy peak shifted to lower field values and eventually merged with the coercivity peak as the interactions in the system were increased.

In 1995 Zimmermann [38] published his progress in investigating the influence of remanent magnetization on the low-field χ_t which showed deviations from the Stoner-Wohlfarth model due to inhomogeneous magnetization states and particle-particle interactions.

The experimental work published in 1999 by Spinu et al [39] describes the design and use of a high-frequency tunnel diode oscillator based susceptometer capable of measuring the χ_t for nanoscale particle systems as a function of temperature. This experiment shows the loss of anisotropy information as the particles became super-paramagnetic.

Numerous contemporary research efforts are dedicated to the development of characterization methods that can easily probe various properties of nanostructured materials. The transverse susceptibility method was used for many years as a versatile technique to measure anisotropy in particulate media. The method consists in the simultaneous application of two fields: one *dc* and one *ac*, the direction of these fields being perpendicular.

During the TS experiment it is measured the magnetic moment component parallel to the *ac* field direction. What it is know from the original model given by Aharoni, it is that the TS signal has sharp peaks located at the *dc* field values equal to anisotropy field of the material.

2.3. Aharoni Model

Very often the magnetic nanostructured systems have a uniaxial anisotropy that can be determined by the crystalline anisotropy, shape anisotropy, stress anisotropy or a combination of all of the above. Aharoni in 1957 [33] gave a complete theoretical description of the reversible susceptibility tensor for a uniaxial anisotropy system. The field dependence of the transverse susceptibility predicted by Aharoni's model with characteristics peaks located at the anisotropy field and switching field values allowed TS to become an important tool to characterize the magnetic anisotropy and magnetization switching in magnetic materials. Below is given a short presentation of Aharoni's model.

Let us consider the geometry from Fig. 2.1 with a *dc* field H_{dc} acting along the $0z$ axis of a rectangular coordinates system and the *ac* field, $H_{ac} = H_{ac,0}\sin\omega t$, acting along the $0x$ axis. Let us consider a particle whose magnetization M reverses by coherent rotation. Let's assume that $|M| = M_s$, where M_s is the saturation magnetization. The particle has the uniaxial anisotropy constant $K > 0$, with the easy axis defined by the spherical polar angles θ_K and φ_K. Similarly, M has coordinates θ and φ. For low values of the frequency of the *ac* field it may be assumed that the processes leading to a certain value of M have characteristic relaxation times much shorter than the time scale over which M varies significantly and the system approaches equilibrium, that is, the magnetization M lies in a minimum of the free energy at any moment. With these the transverse susceptibility can be written as:

$$\frac{\chi_t}{\chi_0} = \frac{3}{2}\lim_{h_{ac}\to 0}\frac{d(\sin\theta\cos\varphi)}{dh_{ac}} = \frac{3}{2}\left(\cos\theta^0\cos\varphi^0\lim_{h_{ac}\to 0}\frac{d\theta}{dh_{ac}} - \sin\theta^0\sin\varphi^0\lim_{h_{ac}\to 0}\frac{d\varphi}{dh_{ac}}\right) \qquad (2.8)$$

where $\chi_t \equiv \chi_{xx}$, $\chi_0 = \mu_0 \frac{M_S^2}{3K}$ is the initial transverse susceptibility for a randomly oriented system, $h_{ac} = \frac{H_{ac}}{H_K}$, $H_K = \frac{2K}{\mu_0 M_s}$ is the particle's anisotropy field, θ^0 and φ^0 are the magnetization's coordinates corresponding to the free energy minimum in the absence of the *ac* field.

The free energy density is:

$$F = K\left[-2h_{dc}\cos\theta - 2h_{ac}\sin\theta\cos\varphi + 1 - \left(\sin\theta\sin\theta_K\cos(\varphi-\varphi_K) + \cos\theta\cos\theta_K\right)^2\right] \quad (2.9)$$

where $h_{dc} = \frac{H_{dc}}{H_K}$. In order for magnetization of the particle to be in an extreme of the free energy, there are 2 necessary conditions that need to be satisfied:

$$\begin{cases} \frac{\partial F}{\partial \theta} = 0, \\ \frac{\partial F}{\partial \varphi} = 0. \end{cases} \quad (2.10)$$

Using the derivation presented in A.2. one can obtain the transverse susceptibility from Eq. 2.8 as

$$\frac{\chi_t}{\chi_0} = \frac{3}{2}\left(\cos^2\varphi_K \frac{\cos^2\theta_i^0}{\cos 2(\theta_i^0 \mp \theta_K) + h_{dc}\cos\theta_i^0} + \sin^2\varphi_K \frac{\sin(\theta_K \mp \theta_i^0)}{h_{dc}\sin\theta_K}\right) \quad (2.11)$$

The expression (2.11) is the transverse susceptibility given by the Aharoni's model.

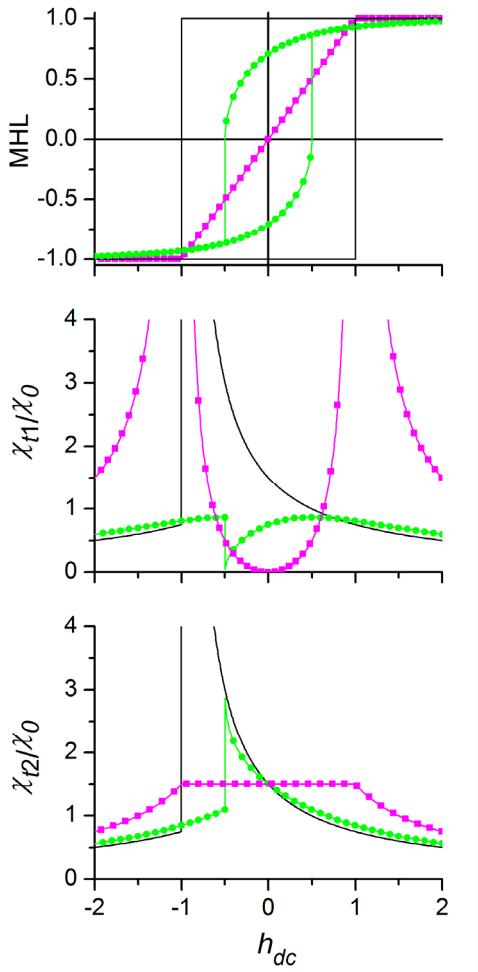

Figure 2.8. Field sweep for a single domain particle [40].

In figure 2.8 are presented the major hysteresis loop (MHL), $\chi_{t1} \equiv \chi_{xx}$ and $\chi_{t2} \equiv \chi_{yy}$ for a single domain particle with uniaxial anisotropy, as the *dc* field is swept from positive saturation to negative saturation, for $\theta_K = 0^\circ$ (black line), $\theta_K = 45^\circ$ (green circles), and $\theta_K = 90^\circ$ (magenta rectangles). The major hysteresis loop for a single domain particle given by the Stoner-Wohlfarth model shows a discontinuity in the magnetization at a certain field, called critical field.

At the same value for the *dc* field there is a discontinuity in the TS; just before the discontinuity of the magnetization the TS becomes very large, because the curvature of the

total energy becomes smaller, vanishing at the jump. After the discontinuity, the TS for $-h_{dc}$ is equal to that for h_{dc}. In addition, it should be noted that $\chi_{t2} \equiv \chi_{yy}$ is always finite. Besides these points the TS also has high values in the vicinity of $h_{dc} = 1, \theta_K = 90^\circ, \varphi_K = 0^\circ$, which is not accompanied by a discontinuity in the magnetization. This behavior is caused by the special symmetry of this case, the first non-vanishing energy's derivative is forth order. Therefore, the minimum is very broad and any arbitrary, very small *ac* field will cause an oscillation of the magnetic moment.

The Eq. 2.11 represents the response from a single particle. For a system of particles with a texture function $f(\theta_K, \varphi_K)$ the response may be obtained by integrating Eq. 2.11 over θ_K and φ_K. For a system with the easy axes randomly distributed in the 3D space the TS has three discontinuous points, namely $h_{dc} = \pm 1$, called anisotropy peaks, and $h_{dc} = -0.5$, called coercivity switching peak. The left-hand derivative at $+1$ and the right-hand derivative at -0.5 are infinite.

The peaks at $h_{dc} = \pm 1$ are always present, and they reflect the behavior of the particles having the easy axes oriented perpendicular to the *dc* field. Therefore, the detection of the anisotropy peaks offers a versatile and simple method for direct evaluation of the anisotropy field and easy axes texture. In addition, one observes that the magnetization switching is more visible in TS curves than in the hysteresis loops and TS can be used to track down the critical switching fields for different orientations of the applied field. In the next section it will be shown how this characteristic of the transverse and longitudinal components of the reversible susceptibility tensor can be used to measure the critical curve of nanostructured magnetic systems.

2.4 Critical Curve derived from Susceptibility Measurements

In the case of two-dimensional (2D) devices used in magnetic data storage, the magnetization dynamics is determined by the 2D magnetization switching properties since the magnetic field is also applied in two dimensions in the plane of the device. Therefore, it is important to study the response of such magnetic systems to fields applied along different directions with respect to easy and hard axes.

The study of 2D magnetic switching enables us to determine the critical curve, which constitutes the fingerprint of the switching behavior and provides information about micromagnetic and structural properties of magnetic systems. The magnetic critical curve for a single-domain particle with uniaxial magnetic anisotropy as it results from the Stoner–Wohlfarth model [15] is an astroid, which is a geometrical construction known in mathematics as a four-cusped hypocycloid [41].

The critical curve shape depends on the magnetic system anisotropy, and for some symmetries the critical curve can be a closed hypocycloid. For example, in the case of combinations of cubic and uniaxial anisotropies, the critical curve is a hypocycloid with three cusps (deltoid) [42] or an eight-cusped hypocycloid, as in the case for a biaxial magnetic system [14].

Several methods were developed to determine the critical curve for 2D magnetic systems through magneto-resistance [26], [27], [28], micro-superconducting quantum interference device technique [29], [30] and, lately, through reversible susceptibility experiments [31], [32]. As we will show in this chapter the reversible susceptibility method is very general and it can be applied to magnetic systems with any type of anisotropy.

As the critical curve is the locus of points for which the magnetization reversal occurs [14], any experimental method able to probe the discontinuous and irreversible changes in magnetization orientation can be employed to determine this polar map of the switching fields. One of the most sensitive methods for switching field measurements is the transverse susceptibility (TS). TS is usually employed as a technique for determining the anisotropy in magnetic particulate media due to the fact that it offers a simple method of direct evaluation of the anisotropy field H_K, independent of the size and orientation distributions of particles in the system.

Uniaxial systems with random orientation in magnetic easy axes show sharp peaks located at H_K, and switching fields H_S [33], [35]. Recent experimental developments of TS have afforded higher sensitivity to this method, enabling the study of systems with low concentration of magnetic moments, such as magnetic nanoparticles [43] and thin films [44]. In addition, recent theoretical advancements of the original model of TS due to Aharoni [33] allowed the possibility of describing the TS for systems with types of anisotropy other than those initially considered [45], [46].

Recently it was shown [47], using the Landau-Lifshitz-Gilbert (LLG) magnetization equation of motion, that the traditional TS experiment is in fact the zero-frequency limit of the ferromagnetic resonance (FMR), and allows one to find the TS for virtually any magnetic system if an expression for the magnetic free energy density F is known. The susceptibility expression that was derived is identical with the one found through Aharoni's model, for a uniaxial system.

As mentioned before, for TS experiments, two magnetic fields are required: a *dc* field, H_{dc}, and small perturbing *ac* field, h_{ac}, oriented at a right angle to the *dc* field. The

quantity which is measured is the magnetization variation along the *ac* field direction, transverse to H_{dc}. If the *dc* field is assumed to be applied along the *z* axis and the *ac* field along *x* axis of a Cartesian reference system, the susceptibility measured along the *x* axis is in fact the TS.

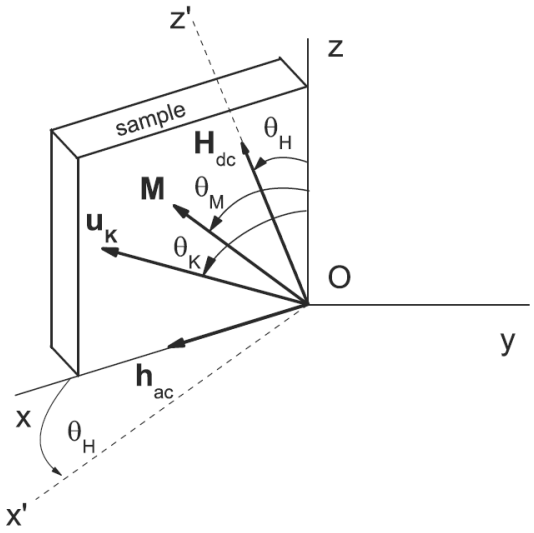

Figure 2.9. Schematic of the coordinate system for thin-film samples.

For the limiting case in which the frequency of the *ac* field is very small, that is, the process for which equilibrium prevails throughout very small variations [47], the reversible TS is given by:

$$\chi_{xx} = \frac{M^2}{F_{\theta\theta}F_{\varphi\varphi} - F_{\theta\varphi}^2}\left[\sin^2\theta_M \sin^2\varphi_M F_{\theta\theta} + \frac{\sin 2\theta_M \sin 2\varphi_M}{2} F_{\theta\varphi} + \cos^2\theta_M \cos^2\varphi_M F_{\varphi\varphi}\right] \qquad (2.12)$$

where θ_M and φ_M are the equilibrium polar and azimuthal angles of magnetization vector M, respectively, and $F_{\theta\theta}$, $F_{\theta\varphi}$ and $F_{\varphi\varphi}$ are second derivatives of the free energy density at the equilibrium position (θ_M, φ_M) where F has a minimum.

As shown by Eq. (2.12), the TS can be used for probing the switching field because the denominator of χ_{xx}, $D(\theta_M,\varphi_M)=F_{\theta\theta}F_{\varphi\varphi}-F_{\theta\varphi}^2$, is the curvature (discriminant) of the free energy surface $F(\theta,\varphi)$, at the equilibrium (where *F* is minimum) position (θ_M,φ_M). For the two-variable function, $F(\theta,\varphi)$, the points for which $D(\theta_M,\varphi_M)=0$ are the critical points that make the transition from one minimum toward the other, and are, in fact, the switching points.

Therefore, the switching points of a system described by the free energy $F(\theta,\varphi)$ satisfy the equation $D(\theta_M,\varphi_M)=0$ and can be found from singular points of susceptibility $\chi_{xx}\propto\frac{1}{D(\theta_M,\varphi_M)}$. This condition is generally valid for any magnetic system, being independent of the free energy expression.

For thin-film samples, in principle, by performing TS experiments with the *dc* field applied at different orientations in the sample's plane, it is possible to plot the angular variation of the switching fields, from which the critical curves can be determined. As a reminder it is worth mentioning that TS geometry conditions requires only *ac* field and *dc* field to be perpendicular and does not require a specific orientation for the easy axis besides the fact that *ac* field, *dc* field and easy axis should be all in the same plane.

Although we will comeback with a detailed explanation of the experimental technique in chapter 3, it is worth mentioning that there are two approaches on how to change the sample orientation with respect to the *dc* field.

In the classical approach, is required to physically rotate the sample with respect to the assembly of perpendicular fields: *ac* field and *dc* field. The sample is located inside a

sensing coil with a small diameter; therefore the sample's rotation with precision is very difficult.

A new approach [32] is to rotate the *dc* field H_{dc} in the plane of the sample, while keeping the sample fixed inside the sensing coil (and therefore fixed in the lab reference system xOz). It is shown [31] that, in this case, the susceptibility χ_{xx} no longer represents the TS, but a combination of both transverse and longitudinal susceptibilities that still preserve the same singularities characterizing the switching fields.

Let us briefly explain the previous affirmation. In the arrangement given by Fig. 2.9, the free energy density is given by the equation:

$$F = -K_1 \left(\hat{\mathrm{u}}_K \cdot \mathrm{M}\right)^2 - \mathrm{M} \cdot \mathrm{H}_{dc} \tag{2.13}$$

where $\hat{\mathrm{u}}_K$ is the unit vector corresponding to the direction of the uniaxial anisotropy axis of anisotropy constant K_1. Following a similar proof like in Aharoni's paper [33], from Eq. (2.11) can be determined the susceptibility signal measured along the Ox direction:

$$\chi_{xx}\left(\theta_H\right) = \frac{3}{2}\chi_0 \frac{\cos^2\theta_M}{\cos 2(\theta_M - \theta_K) + h\cos(\theta_M - \theta_H)} \tag{2.14}$$

where $\chi_0 = \dfrac{M^2}{3K_1}$.

It was proven [31] that because the denominator of $\chi_{xx}\left(\theta_H\right)$ is the same as the one of $\chi_{xx} = \chi_t$ from Eq. (2.11), the signal detected along the Ox axis, even out of TS geometry $\left(\theta_H \neq 0\right)$, has the same singularities as in the case of a regular TS geometry, but for different orientations of the easy axis with respect to the applied *dc* field direction. In other words, as the field is ramped from positive saturation to negative saturation the detected signal will

present a singularity at the field value, called the switching field, $h_S = \frac{H_S}{H_K}$, for which $F = 0$, i.e., the curvature of free energy vanishes $\frac{d^2F}{d\theta_M{}^2} = 0$. When the magnetic field is ramped from positive saturation to negative saturation for each field value the magnetization vector reaches an equilibrium position when $\frac{dF}{d\theta_M} = 0$. Further, for a specific field value h_S the second derivative also vanishes, $\frac{d^2F}{d\theta_M{}^2} = 0$. The locus of solutions of the two equations system $\begin{cases} \frac{dF}{d\theta_M} = 0 \\ \frac{d^2F}{d\theta_M{}^2} = 0 \end{cases}$ represents the critical curve, which in the simple case of a magnetic system with only uniaxial anisotropy is an astroid.

In the Figure 2.10 it is shown how the critical curve for a uniaxial system is determined using the singularities in the susceptibility signal (right) measured along Ox axis while the *dc* field H_{dc} is applied along different directions, θ_H, in the sample's plane. The detected signal for each field orientation (left) shows a sharp peak located at the field values associated with the singularity in the detected signal.

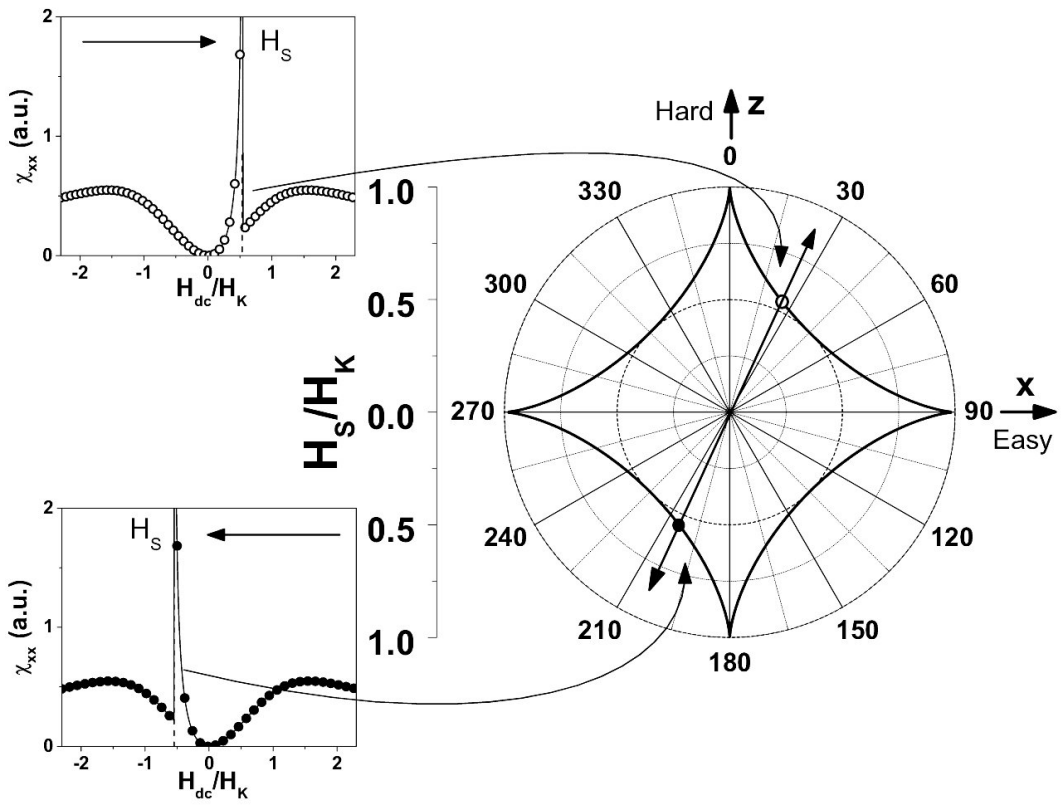

Figure 2.10. *Left:* Susceptibility signal χ_{xx} detected along the Ox axis, for increasing (top) and decreasing (bottom) field sweeping for $\theta_H = 25^\circ$ and $\theta_K = 90^\circ$. *Right:* Theoretical critical curve (astroid) determined from susceptibility measurements for a uniaxial anisotropy system [32]

The critical curve is obtained plotting the switching field values $H_S(\theta_H)$ in polar coordinates. The critical curve could be obtained using only one *dc* field sweeping direction (either increasing or decreasing) while θ_H varies between 0° and 360°. However, by using the values of H_S determined from both susceptibility curves corresponding to increasing and decreasing fields, it is possible to reduce the angular domain for θ_H to (0°, 180°). Thus, the right half of the critical curve will be obtained from the increasing *dc* field curves while the left half from the decreasing *dc* field curves.

In the chapter 5 it will be presented, in a similar fashion, the determination of the critical curve for coupled magnetic systems.

2.5. Summary

Magnetic susceptibility χ measurements reveal important information about the switching fields and anisotropies of magnetic materials. The magnetic susceptibility is a quantity which describes the capability of a magnetic material to magnetize in response to a magnetic field. We explore the susceptibility of a Stoner-Wohlfarth particle outlining briefly the derivation of Aharoni that gave a complete theoretical description of the reversible susceptibility tensor for a uniaxial anisotropy system.

The physical origin of the infinite susceptibility features can be explained by reference to the changing shape of the free energy minima in which the particle moment sits. Critical curve constitutes the fingerprint of the switching behavior and provides information about micromagnetic and structural properties of magnetic systems. We show how it can be derived from susceptibility measurements.

As the critical curve is the locus of points for which the magnetization reversal occurs, any experimental method able to probe the discontinuous and irreversible changes in magnetization orientation can be employed to determine this polar map of the switching fields.

One of the most sensitive methods for switching field measurements is the transverse susceptibility (TS).

$$\chi_{xx} = \frac{M^2}{F_{\theta\theta}F_{\varphi\varphi} - F_{\theta\varphi}^2}\left[\sin^2\theta_M \sin^2\varphi_M F_{\theta\theta} + \frac{\sin 2\theta_M \sin 2\varphi_M}{2} F_{\theta\varphi} + \cos^2\theta_M \cos^2\varphi_M F_{\varphi\varphi}\right]$$

TS can be used for probing the switching field because the denominator of χ_{xx}, $D(\theta_M, \varphi_M) = F_{\theta\theta}F_{\varphi\varphi} - F_{\theta\varphi}^2$, is the curvature (discriminant) of the free energy surface $F(\theta, \varphi)$. Therefore, the switching points of a system described by the free energy $F(\theta, \varphi)$ satisfy the equation $D(\theta_M, \varphi_M) = 0$ and can be found from singular points of susceptibility $\chi_{xx} \propto \frac{1}{D(\theta_M, \varphi_M)}$. This condition is generally valid for any magnetic system, being independent of the free energy expression.

The locus of solutions of the two equations system $\begin{cases} \frac{dF}{d\theta_M} = 0 \\ \frac{d^2F}{d\theta_M{}^2} = 0 \end{cases}$ represents the critical curve, which in the simple case of a magnetic system with only uniaxial anisotropy is an astroid. The critical curve is obtained by plotting on a polar map the position of the susceptibility peaks (singularities).

Chapter 3

Tunnel Diode Oscillator Method for Susceptibility Experiments

We will shortly review first the key notions regarding the magnetic susceptibility presented in the second chapter and we will present the generalities regarding magnetization dynamics and susceptibility measurements, in order to make the transition smother toward this experimental section that deals mostly with the Tunnel Diode Oscillator (TDO) method use by us to measure the magnetic susceptibility.

3.1. Methods for susceptibility measurements

Magnetization dynamics may be probed by either time-domain or frequency-domain measurements. Each approach has its merits. The first one provides a direct insight into time sequential steps in the magnetization process, while, on time other hand, frequency-domain measurements relate more directly to the energetics of magnetization dynamics and are accompanied by immediate insight into time energy-level structure, especially in the case of resonant phenomena.

The general principle underlying all frequency-domain magnetic measurements at frequencies between 100 kHz and 10GHz consists of applying an *rf* magnetic field, then measuring the magnetic response of the system being studied in terms of the real and imaginary parts of its magnetic susceptibility from which magnetization dynamics may be modeled.

The magnetization dynamics divides loosely into resonant and non-resonant phenomena. Resonant magnetic phenomena involve transitions between quantum states which may be those of an isolated atom or may even be the consequence of collective effects. They generally demand tight selection rules which impose constraints on the way the magnetic fields should be applied.

Non-resonant magnetic phenomena generally have different behavior. Many arise as a relaxation processes consequent upon a diagonal perturbation which commutes the energies of two magnetic states, for example, by Zeeman interaction with an oscillating applied magnetic field. If the timescale of the applied field is comparable with the longitudinal relaxation time, the populations' level will adjust to the energy modulation. Energy dissipation results with consequent variation in the imaginary part of susceptibility, χ'', for the magnetic system. Similar considerations apply to the motion of domain walls between two magnetization states which are alternately stabilized and destabilized by commuting the applied field. The characteristic relaxation time involved in this case is related to the velocity of the domain wall motion.

The common feature of all the frequency-domain magnetic investigations is that, irrespective of whether the phenomena under study are resonant or non-resonant, the parameter being measured is the magnetic susceptibility. This has two components χ' and χ'' which are, respectively, its real and imaginary parts.

A variation with frequency in one component also leads inevitably to variation in the other. In resonant phenomena where the variations are localized in frequency space, their amplitudes can be very pronounced. The form of χ'' is symmetric about the center frequency, whereas that of χ' is anti-symmetric.

Understanding the magnetization dynamics behind the susceptibility variation requires measurement of χ' and χ'' as a function of amplitude, frequency, temperature, nanostructure dimensions, etc. with high precision and reliability.

To obtain maximum sensitivity in such measurements, it is usual to employ some form of electrically or even mechanically resonant structure to generate the magnetic field which interrogates the sample; the electrical resonance has the dual merits of maximizing the applied radio-frequency magnetic flux and employing the quality factor of the resonant circuit to enhance the detected signal.

A variety of such resonators are currently used for measurements. They include series and parallel inductance/capacitance resonant circuits for use from 100 kHz to 3 GHz, cavities for frequencies from 300 MHz to 10 GHz, microwave stripline designs for use from 500 MHz to 10 GHz and above, and microwave acoustic resonators for frequencies from 300 MHz to 10 GHz.

As discussed, variations of χ' and χ'' with frequency, magnetic field, etc. are closely correlated. This implies that if a resonant circuit or cavity is being employed to measure variations in χ'' the associated variations in χ' will cause the electrical resonance to detune with, consequently producing false signals. This is a known problem with electron spin resonance cavities especially when highly magnetic materials are being examined which have sharp variations in susceptibility; a variety of tracking/feedback techniques are used to overcome this, by themselves introducing unwelcome complexity to the dynamic response of the instrumentation.

This experimental difficulty is an overriding argument for the use of self-oscillating detectors which use the resonant structure itself to determine the oscillation frequency at

which the experiment is conducted, like the TDO used in our lab. Usually a low-frequency parallel resonant tank circuit is the electrically resonant element. This principle has universal application across the entire frequency range of 100 kHz - 10 GHz. If correctly designed, such spectrometers constitute nice, compact, predictable, well-behaved, high signal to noise ratio (SNR) instrumentation which may additionally be adapted to cryogenic operation without the usual problems of phase lags and thermal conduction generally associated with cryogenic coaxial cables and waveguides. Moreover, self-oscillating spectrometers provides great economy of operation because two parameters are simultaneously extractable: the operating frequency and the magnetic losses and these translate directly into the desired information about changes in χ' and χ'' in the sample.

Magnetic measurements frequently need to be performed at low temperatures, and this requires physical separation between the ambient temperature electronics and the sample/resonator assembly. Such a separation is satisfactory, provided that the length of the connecting lead between the two is less than $\lambda/10$. For greater separations, the associated phase shift militates against the performance of the oscillator. The most ingenious cryostat design provides a sample-to-ambient distance of 30 cm minimum for liquid helium operation, and the $\lambda/10$ criterion translates this into an upper frequency limit of about 100 MHz.

Above this limiting frequency, the solution is to integrate the electronics and sample into a single cryogenic package, and several new constraints now appear. Evidently, components that can function at 4 K are now required, and this excludes such items as bipolar transistors, silicon JFETs, tantalum and electrolytic capacitors, and carbon resistors.

Different resonator schematics are appropriate for the different frequency regimes and also for different sample types. At low frequencies, resonant circuits comprising discrete inductance and capacitance are practical and desirable. At higher frequencies, generally above a few hundred MHz, cavity or stripline are recommended.

Special considerations apply to thin film samples and hence also to nanostructured thin films. It is possible, at the cost of SNR, to examine thin film samples in resonators made for bulk samples, but it is evidently desirable to attempt to tailor the resonator structure to give the best performance with thin magnetic films. For oscillators that use as measuring element a coil, the problem arises from the fact that the coil inner volume is much larger than the magnetic sample volume.

This translates into a low filling factor (ration between the two volumes) and decreases the sensitivity of the method. The usual solution is to replace only the inductor with a lithography-manufactured coil directly on the sample, or to manufacture a flat-spiral coil and place the sample in its immediate vicinity [48]. Another approach is the one we chose for our susceptibility measurements which is using a flatten-circular coil that will be presented in detail in the third part of this chapter.

The most obvious resonator design to choose for thin films, if one has access to a deposition system, is that of a stripline in which the sample is placed between the live strip and the ground plane. Layers of insulator above and below the sample prevent it from shorting the stripline. Evidently, this approach requires fabrication of a dedicated stripline in the same process as makes the sample itself, but the extra effort and complexity is repaid by much improved SNR. However, there are inherent problems which revolve around the manner in which the stripline is electrically characterized. The method of analyzing a

composite stripline/sample is to measure its scattering parameters using a network analyzer and back-calculate to extract changes in χ' and χ''.

In electromagnetism, the magnetic susceptibility, referred shortly in this dissertation as susceptibility, is the degree of magnetization of a material in response to an applied magnetic field.

The magnetic susceptibility, represented by the symbol χ, is defined by the relationship

$$\mathrm{M} = \chi \mathrm{H} \ (SI) \tag{3.1}$$

with M being the magnetization of the material and H is the magnetic field strength.

The magnetic induction B is related to H by the relationship:

$$\mathrm{B} = \mu_0(\mathrm{H} + \mathrm{M}) = \mu_0(1+\chi)\mathrm{H} = \mu_0\mu_r\mathrm{H} = \mu\mathrm{H} \ (SI) \tag{3.2}$$

where μ_0 is the free space magnetic permeability (a constant), $\mu_r = 1 + \chi \ (SI)$ is the relative permeability of the material and $\mu = \mu_0(1+\chi) = \mu_0\mu_r \ (SI)$ is the magnetic permeability.

Therefore, we can see that $\chi \propto \mu$ i.e. the susceptibility is direct proportional with the permeability of the material. We will make use of this proportionality in the next steps in order to explain how we detect the susceptibility variations.

The dimensionless SI value of volume susceptibility is multiplied by 4π to give the dimensionless cgs volume susceptibility value, $\chi^{SI} = 4\pi\chi^{cgs}$.

The magnetic susceptibility can be measured, almost directly, by the force change felt upon the application of a magnetic field gradient or by inductive methods, generically known as time or frequency-domain measurements.

Early measurements were made using the Gouy balance where a sample is hung between the poles of an electromagnet. The change in weight when the electromagnet is

turned on is proportional to the susceptibility. Today, high-end measurement systems use a superconductive magnet. An alternative is to measure the force change on a strong compact magnet upon insertion of the sample. This system, widely used today, is called the Evan's balance.

As a frequency-domain method, the most used one is the ferromagnetic resonance (FMR) spectroscopy and its derivates [49]. In particular, when an *ac*-field is applied perpendicular to the detection direction (called the "transverse susceptibility" regardless of the frequency), the effect has a peak at the ferromagnetic resonance frequency of the material with a given static applied field. One of the particular case of the FMR is the TDO based experiment [47].

3.2. Timeline of experimental methods based on TDO

A tunnel diode or Esaki diode is a type of semiconductor diode which is capable of very fast operation, well into the microwave frequency region, by using quantum mechanical effects. It was invented in 1958 by Reiona Esaki, from Sony, who in 1973 received the Nobel Prize in Physics for discovering the electron tunneling effect used in these diodes.

The tunnel diodes have a heavily doped p-n junction only about 10 nm wide. The heavy doping results in a broken bandgap, where conduction band electron states on the n-side are more or less aligned with valence band hole states on the p-side.

Tunnel diodes were manufactured by General Electric and other companies from 1960, and are still made in low volume today. Tunnel diodes are usually made from germanium, but can also be made in gallium arsenide and silicon materials. They can be used as oscillators, amplifiers, frequency converters and detectors.

Under normal forward bias operation, as voltage begins to increase, electrons at first tunnel through the very narrow p-n junction barrier because filled electron states in the conduction band on the n-side become aligned with empty valence band hole states on the p-side of the p-n junction. As voltage increases further these states become more misaligned and the current drops - this is called negative resistance, because current decreases with increasing voltage. As voltage increases yet further, the diode begins to operate as a normal diode, where electrons travel by conduction across the pn junction, and no longer by tunneling through the pn junction barrier. Thus, the most important operating region for a tunnel diode is the negative resistance region. The typical forward bias value necessary to bring the tunnel diode at the middle of the negative resistance region is between 50 to 100 mV.

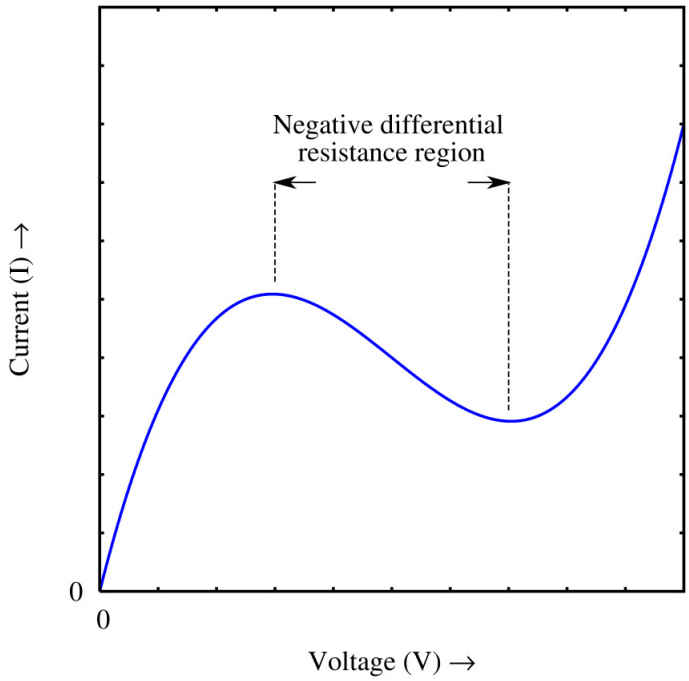

Figure 3.1. Theoretical IV curve for a tunnel diode, showing the negative differential resistance region

In a conventional semiconductor diode, conduction takes place while the p-n junction is forward biased and blocks current flow when the junction is reverse biased. This occurs up to a point known as the 'reverse breakdown voltage' when conduction begins (often accompanied by destruction of the device). In the tunnel diode, the dopant concentration in the P and N layers are increased to the point where the reverse breakdown voltage becomes zero and the diode conducts in the reverse direction. However, when forward-biased, an odd effect occurs called 'quantum mechanical tunneling' which gives rise to a region where an increase in forward voltage is accompanied by a decrease in forward current. This negative resistance region can be exploited in a very fast oscillator, like the one we use throughout our experiments, called TDO – tunnel diode oscillator.

The tunnel diode showed great promise as an oscillator and high-frequency threshold (trigger) device since it would operate at frequencies far greater than the early transistors would, well into the microwave bands. Applications for tunnel diodes included local oscillators for UHF television tuners, trigger circuits in oscilloscopes, high speed counter circuits, and very fast rise time pulse generator circuits. The tunnel diode can also be used as low-noise microwave amplifier. Practical tunnel diodes operate at a few mA and a few tenths of a volt, making them low-power devices. However, since its discovery, more conventional semiconductor devices have surpassed some of its qualities, but nevertheless it is still used for research equipment and as frequency calibration standards.

First paper presenting the measurement of kinetic inductance of superconducting structures was published in 1969 by Meservey [50]. It describes the construction and use of a TDO operating at 15 MHz. The coil in the LC tank in this oscillator contains the sample under investigation. This technique allows measurement of the carrier concentration or

penetration depth in films and wires of superconducting materials. The measured frequency changes are proportional to $z = \left[\lambda(t)/\lambda(0)\right]_{BCS}$ for wires and thick films. The setup is made of 2 parts; the amplifier, counter and power supply at room temperature and the TDO with the LC tank at liquid He temperature.

A second publication by Clover [51] published in 1970 uses a similar circuit like Meservey for paramagnetic susceptibility measurements at frequencies from 3 to 55MHz and at temperatures from 1.2K to 77K and in magnetic fields of up to 18kG. It also presents a semi-empirical mathematic formula describing the frequency of operation for the TDO.

Another paper by Kingma [52] in 1971 propose the use of the negative resistance oscillator for application like proximity detection. It uses a similar circuit like the previous authors but it has two critically coupled LC tanks.

In a paper by Aslam [53] in 1973 in presented a tunnel diode NMR spectrometer for studies of ferromagnetic material at VHF an UHF. The important improvement over the previous designs is that the used TDO is tunable and can operate in a relatively broad frequency range.

Van Degrift [54] in 1975 published the results of a systematic study of the design considerations of a low-temperature tunnel diode oscillator. The circuit is similar to the one presented in the previous papers. The main contribution of this paper is the calculations describing the measured frequency noise and dependence on bias voltage, magnetic field, and temperature of the TDO. This circuit's performance is claimed to allow measurement of changes in the resonant frequency of an LC circuit with a precision of 0.001 ppm. One can thereby detect extremely small changes in a number of material properties such as thermal expansion, surface impedance, and electric and magnetic permeability.

In 1986 Brisson [55] combines the ease of construction of a discrete element TDO with the quick response times and immunity to stray reactance of the reentrant cavity TDO into a transmission-line tunnel diode oscillator.

Revisiting one of his earlier papers, Meservey [56] publish in 1986 his work on developing a low temperature magnetic susceptometer for thin films based on a TDO. The inductance is in this case a superconducting meander line. The device is capable to detect a change in susceptibility equal to that of a change in Fe thin film thickness of 0.03 atomic layers.

In 1999 a paper by Srikanth [57] describes the use of a TDO for precise measurements of relative impedance changes in materials. The impedance changes are determined directly from the measured shift in TDO resonance frequency.

Coffey [58] in 2000 is presenting details of an apparatus that extend the tunnel diode techniques to measure the properties of materials in pulsed magnetic fields. The sample is placed in the inductor of a small *rf* tank circuit powered by a tunnel diode and the conductivity, magnetization, or penetration depth is measured. It is explained in this article how the sample and configuration of the radio frequency fields determine which property is measured. The major innovation is the stabilization the tunnel diode oscillator during a magnet pulse by using compensated coils in the tank circuit.

In a series of papers spanning from 1998 to 2004, Gevorgyan [48, 59-66], is improving the TDO technique and achieves high resolution measurement of magnetic field penetration depth of radio frequency fields into thin films or plate like superconductors being able to characterize superconductive transitions in various materials. The main novelty and improvement of the TDO technique is the replacement of the solenoid testing coil by a open

flat, spiral, coil. The advantage of the flat coil geometry is the high filling factor that makes the sensitivity increase significantly.

In 2001 Spinu [67] published a paper where, using the sensitive resonant method based on a TDO, has, for the first time, mapped the complete variation of $\chi(T)$ in the H-T plane in several nanoparticle systems covering the superparamagnetic and blocked regimes. The variation is well described using theoretical models that take into account the thermal relaxation and anisotropy field distribution.

In 2002 Agosta [68] presents measurements of resistivity and penetration depth in *dc*- and pulsed-magnetic fields of the organic superconductors α-$(ET)_2NH_4Hg(SCN)_4$, and κ-$(ET)_2Cu(NCS)_2$ using a resonant rf circuit powered by a tunnel diode oscillator.

Ohmichi [69] has published in 2004 experiments regarding a noncontact technique of resistivity measurement in pulsed high magnetic fields of up to 40 T with use of a tunnel diode oscillator. An LC tank circuit powered by a tunnel diode oscillates at frequency of $f \sim 1/\sqrt{LC}$, which is typically in a megahertz range. A sample is placed in the LC tank coil, and a small change in the resonant frequency f of the circuit is measured. For metals, the frequency change is related to the change in skin depth, which is converted to resistivity via $\delta = \sqrt{\rho/\pi\mu f}$.

In 2005 Woods [70] published a paper presenting temperature and field-dependent reversible transverse susceptibility (TS) measurements on a $La_{0.85}Sr_{0.15}MnO_3$ (LSMO) single crystal at radio frequency (10 MHz) using a resonant tunnel-diode oscillator technique. These dynamic experiments probe the coupled electronic, magnetic and structural transition in LSMO giving rise to the ferromagnetic transition and the charge-ordered phase.

As we notice from this review of the main contributions to the deployment of the TDO related experiments as a one of the important techniques in materials study, these technique can be applied in various fields: for London penetration depth, for magnetic and meta-magnetic transitions, superconductor's characterization, and the one of interest for us, the magnetization switching characterized via susceptibility studies.

3.3. TDO – based experiment designed and used in our laboratory

The sensitivity of techniques for measuring the dynamic susceptibility varies significantly with frequency and with the way the signal is obtained. Amplitude-domain measurements with lock-in amplifiers operate at relatively low frequencies and are prone to waveform distortions and phase drift. Frequency-domain measurements are much more sensitive, but require high-Q circuits and frequency scanning to find the resonance frequency. The most sensitive probes utilize microwave cavity perturbation at typical frequencies of 1 to 100 GHz. However, at these frequencies, nonlinear magnetic effects as well as the anomalous skin effect may be of importance and interpretation of the results becomes difficult.

Tunnel diode oscillators (TDO) are well suited to fill the spectral gap between these two extremes since TDO can be tuned to operate in the radio-frequency range, as was suggested by Clover [51]. A TDO is essentially a self-resonating LC tank circuit driven by a tunnel diode. A properly constructed circuit allows one to measure changes in the magnetic moment on the order of a pico-emu. In addition, the excitation field is very small, of the order of tenths of mOe, which is very useful in cases of highly nonlinear and/or hysteretic samples.

The main component of a TDO is a tunnel diode. As mentioned before, the device exhibits a bias region with negative differential resistance. When biased to this voltage

region, the diode can be used to drive the tank circuit resulting in a self-resonating LC oscillator.

The frequency is always at the resonance, which is the main advantage of this device. Careful design and good thermal stability resulted in a circuit that resonates in the rf range with a stability of 4 ppm over days. The sample under study is placed in a coil which acts as the inductor in the LC tank circuit. In the Figure 3.2 is shown the electrical diagram of the TDO circuit used for our experiments (top) and the magnified image of the PCB (bottom).

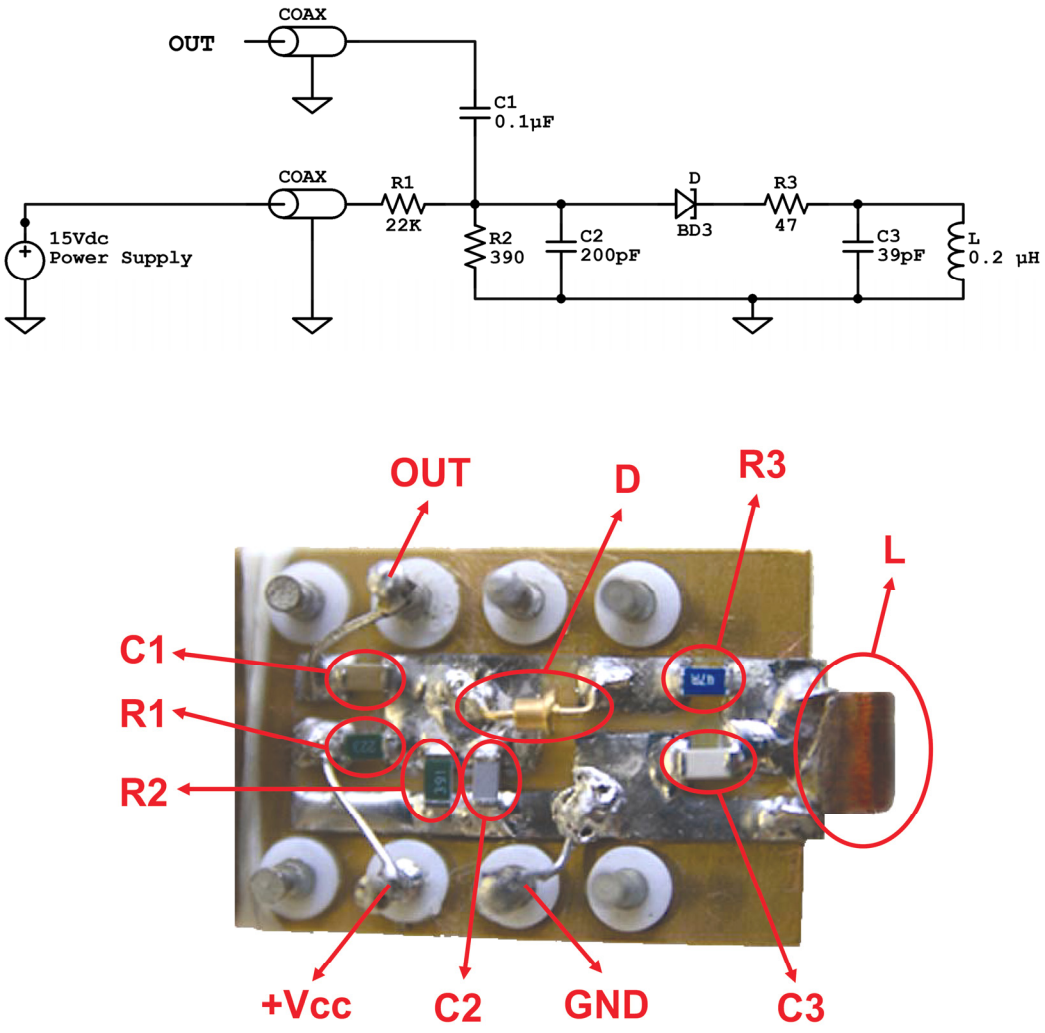

Figure 3.2. Electrical diagram of the TDO circuit used for our experiments (top) and the electronic components on the PCB (bottom).

Although our design of the TDO oscillator derives from two main sources, the published work by VanDegrift [54] and Srikanth [57], its configuration and characteristics are mostly original.

In Fig. 3.2, top, the circuit elements on the left of the coaxial cables are the ones that constitute the actual TDO and, during experiments, are placed in a continuous flow liquid He cryostat with a temperature range of 4.2 to 300 K. The TDO's PCB is placed at the end of the cryostat insert, with the coil extending 1 mm further down from the PCB (to the right in Fig. 3.2, bottom). The TDO auxiliary elements are a power supply, a signal conditioning block and a frequency counter.

The core of the circuit is the tunnel diode D, whose current-voltage characteristic has a negative slope region where the diode acts as a negative *ac* resistance that cancels the losses of the LC tank circuit. The diode we use is MBD3057-E28X manufactured by Aeroflex / Metelics [71]. In contrast to other semiconductor devices, the tunnel diode is very heavily doped so that at low temperatures it becomes increasingly temperature independent. Moreover, its characteristics are not magnetic field dependent so that it can be used over a very wide temperature and field ranges.

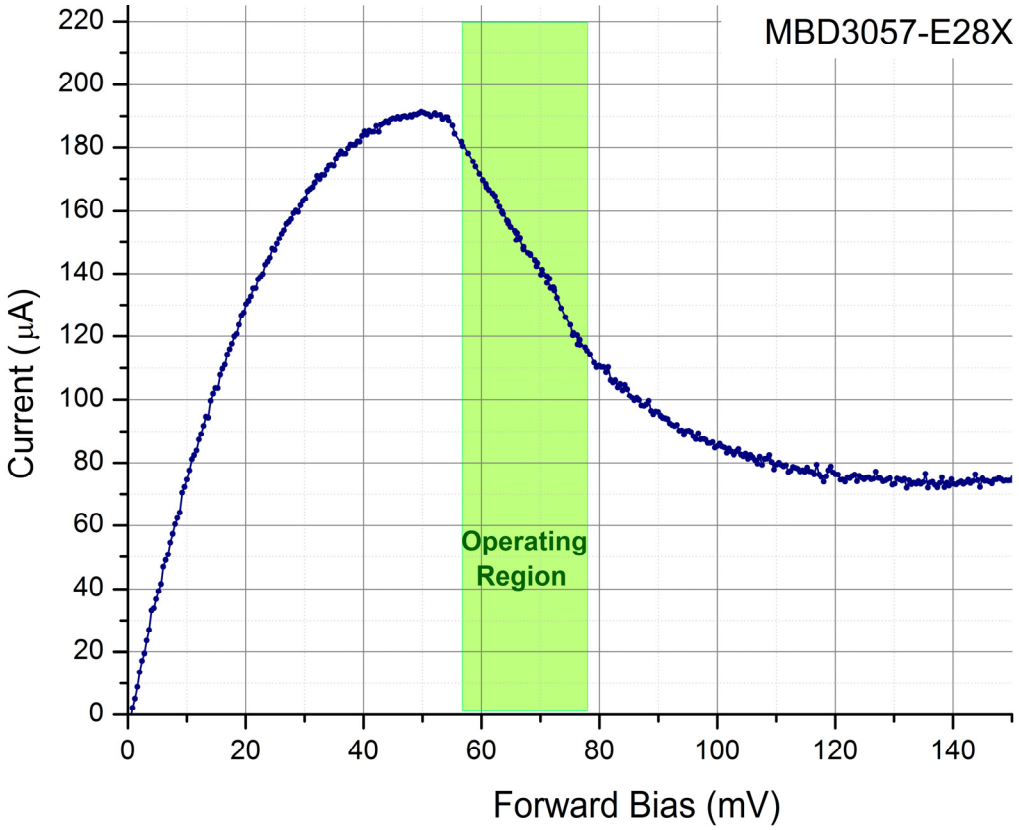

Figure 3.3. Experimental IV curve for the MBD3057-E28X tunnel diode used in our TDO. The green shaded area denotes the negative resistance optimal operating region

In the Figure 3.3 is shown the experimental IV curve, obtained in our lab, for the MBD3057-E28X (shortly BD3) tunnel diode used in our TDO. The green shaded area denotes the negative resistance optimal operating region. In order for the oscillator to function in a stable regime, the diode's bias is chosen to be in the middle of the linear negative *ac* resistance region, in our case about 70 mV.

The resistors R1 (22KΩ) and R2 (390Ω) form a *dc* voltage divider chosen to provide the proper *dc* bias for the diode.

The output coupling capacitor, C1 (0.1μF), will let pass only the *rf* signal up the coaxial cable, toward the amplifiers and frequency counter, while eliminating the *dc* component.

The bypass capacitor C2 (200pF) is chosen high enough to appear as a short circuit at the operating frequency and serves to several purposes; its value is a compromise between signal amplitude and noise; C2 closes the *rf* circuit for the oscillator, suppress the *rf* noise coming on the power cables and stops the signal from propagating up, toward the *dc* power supply.

The parasitic suppression resistor, R3 (47Ω), is needed to prevent oscillation of the tuned circuit unintentionally formed by the stray capacitance of the diode and any inductance from the circuit board. Although such high frequency parasitic oscillations can seriously degrade all aspects of the oscillator performance, our experience shows that R3 can oftentimes be discarded.

The LC tank is formed by the capacitor C3 (39pF) and the measuring coil, L (0.2μH). The L and C3 values will set the operating frequency:

$$f = \frac{1}{2\pi\sqrt{LC_3}} \approx 70MHz \tag{3.3}$$

The typically peak current in the LC tank, when driven by the diode is $\approx 10\mu A$ [54].

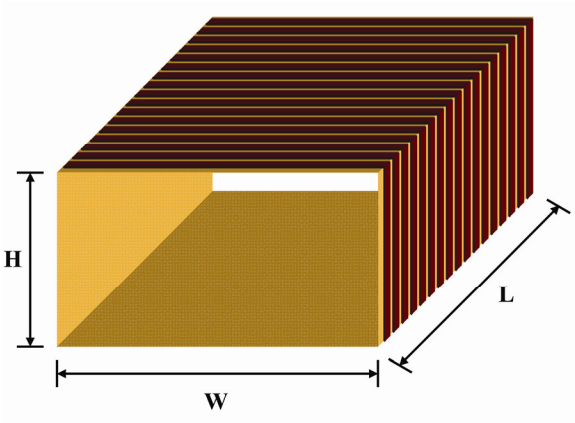

Figure 3.4. Measuring coil L design and dimension: length 7 mm, width 8 mm, height 2 mm. 10 turns, CuEm AWG24

Figure 3.4. shows the flat-cylindrical (almost a rectangular prism) coil design. The coil has a length of 7 mm, width of 8 mm and height of 2 mm. The winding is done "on air" and is potted in dielectric epoxy for mechanical stability. The coil has 10 turns of CuEm AWG24 wire that gives an inductance of about 0.2 μH.

Since most of the samples under study in our case are a piece of thin film, the flat-cylinder shape provides an increase in the filling factor over a regular cylindrical coil. Moreover, the lack of coil support case increase the filling factor and also eliminates the background signal we have got from the case material.

Over the past years we made progress in decreasing the size of the circuit board while optimizing its design. This offers the advantage of reducing considerably the capacitance and inductance added by the board. There is another, more important advantage of having a smaller board. The space on the low temperature cryostat insert is limited so that, in the previous design [57], entire TDO circuit, except the coil, was placed outside the cryostat. The coil was connected through a semi-rigid coax cable to the TDO circuit board. In many cases, the inductance of this cable is higher than the one of the coil, so that it gives the major contribution to the resonant frequency. This arrangement of the TDO components drastically reduces the sensitivity of the TDO and also the resonant frequency.

Using smaller, surface mount (SMD) electronic components available today, we were able to design boards with the dimension of several mm. Moreover, we were able to fit the measuring coil on the same PCB and completely eliminate the coaxial cable, so that the resonant frequency is much higher, of about 70MHz. By doing this, the change in frequency is due to the coil inductance alone.

We found that, differently from any design published or used so far in the previous TDO related experiments, the TDO works the best when the power supply coaxial cable and the output signal coaxial cable are separated, and only the TDO itself is placed inside cryostat. Since our cryostat was factory equipped with two coaxial connectors would also be inefficient to use only one cable. This way, the signal quality is dramatically improved over the previous design style [54].

The measured physical property in the case of the TDO experiment is the change in the resonance frequency of the oscillator, due to the change in the sample's properties.

We will briefly explain now how we get the information regarding susceptibility from the change in frequency. The resonant frequency of oscillation for an inductor-capacitor circuit with inductance L and capacitance C is given by:

$$f_0 = \frac{1}{2\pi\sqrt{LC}} \tag{3.4}$$

If the inductance changes by a small amount to $L + \Delta L$ the new frequency is written:

$$f_0 + \Delta f = \frac{1}{2\pi\sqrt{(L + \Delta L)C}} \tag{3.5}$$

Expanding this expression for small values of ΔL gives, to first order,

$$\Delta f \approx \frac{1}{2}\frac{\Delta L}{L} f_0 \tag{3.6}$$

If a magnetic sample is acting as the core of the solenoid, we have, in a first approximation, the magnetic flux density given by:

$$B = \frac{\mu_0 \mu_r N i}{l} \text{ (SI)} \tag{3.7}$$

where μ_0 is the permeability of free space, μ_r is the relative permeability of the material

within the solenoid, N the number of turns, i the current and l the length of the coil.

Ignoring end effects the total magnetic flux through the coil is obtained by multiplying the flux density B by the cross-section area A and the number of turns N :

$$\Phi = \frac{\mu_0 \mu_r N^2 i A}{l} \quad \text{(SI)} \tag{3.8}$$

from which it follows that the inductance of a solenoid with magnetic core is given by:

$$L = \frac{\mu_0 \mu_r N^2 A}{l} \quad \text{(SI)} \tag{3.9}$$

Expressed in terms of magnetic susceptibility, the inductance becomes:

$$L = \frac{\mu_0 (\chi + 1) N^2 A}{l} \quad \text{(SI)} \tag{3.10}$$

and (3.6) can be written as:

$$\frac{\Delta f}{f_0} \approx \frac{1}{2} \frac{\Delta \left[\frac{\mu_0 N^2 A}{l} (\chi + 1) \right]}{\frac{\mu_0 N^2 A}{l} (\chi + 1)} \quad \text{(SI)} \tag{3.11}$$

Therefore the change in TDO's frequency of resonance is proportional with the change in the susceptibility of the material placed inside the measuring coil:

$$\frac{\Delta f}{f_0} \propto \frac{\Delta \chi}{\chi} \tag{3.12}$$

We mainly use the TDO-based experiments to explore the magnetic susceptibility for various thin film samples. To record the critical curve one has to identify first the susceptibility peaks appearing when a *dc* field is swept from negative to positive saturation in the space where the measuring coil (containing the sample) is placed, for different orientation of the *dc* field with respect to the sample's anisotropy axis.

It is obviously easier to rotate with high accuracy the magnetic field direction with respect to the sample and measuring coil than would be to precisely rotate the sample inside the tiny measuring coil while keeping the magnetic field direction fixed. It was very ingeniously proven [31] that, even though the experiment geometry is different comparing to the generally known TS experiment, the singularities detected this way preserves the switching information of the original TS experiments.

Therefore, we are always using the following geometry in our experiments: the sample is placed inside the measuring coil with its anisotropy axis parallel with the coil axis (*rf* field direction). We need to remind that the direction of the magnetic moment of the sample for our samples geometries is in the thin film plane, therefore the *dc* field, *rf (ac)* field and the anisotropy axis needs to be always in same plane. During experiments, the *dc* field is applied at different orientation with respect to the anisotropy axis, and for each direction its amplitude swept between negative and positive saturation of the sample's magnetization.

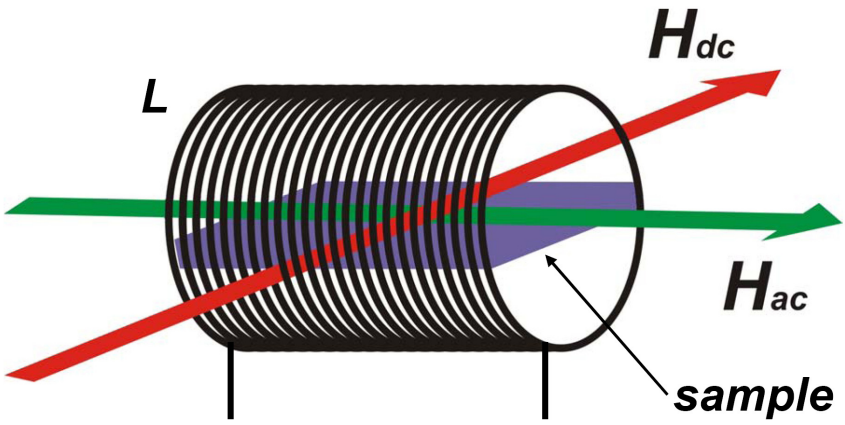

Figure 3.5. Sample placed inside the measuring coil L with the *ac* and *dc* fields in plane

The other important components of the TDO setup are, as presented in Fig. 3.6, the tunnel diode's bias power supply, the signal conditioning block, the frequency counter, the *dc*

magnetic field controller, the electromagnet, the temperature controller, the cryostat and the computer that controls all the experimental parameters and records the data.

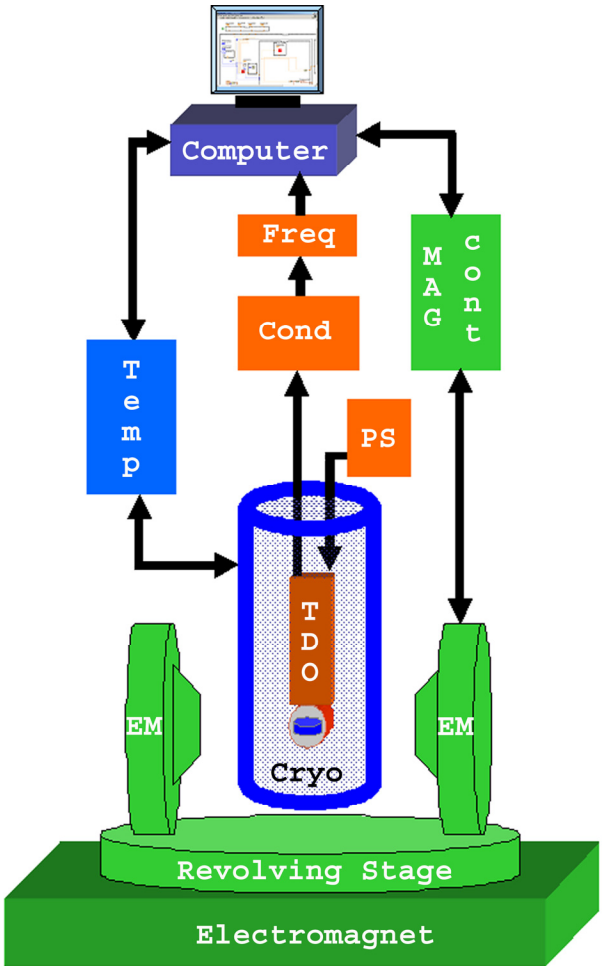

Figure 3.6. TDO-based experimental setup used for susceptibility measurements.

The diode's bias power supply (*PS*) used in our experiment is a programmable power supply (Agilent Model E3643A) but, generally, any power supply with low voltage drift can be used to power the TDO; we experimented with a battery and the results are good as well. We have chosen the value of 15V for the power supply's output because we can use the same voltage for the signal conditioning amplifiers.

The signal conditioning block (*Cond*) is optional and contains a series of amplifiers (Mini-Circuits Model ZFL-1000LN), a signal splitter (Mini-Circuits Model ZFSC-2-4-S) for visualization on the oscilloscope (Tektronics Model TDS 5104), a frequency mixer (Mini-Circuits Model ZFM-2) and a reference signal generator (Agilent Model 33250A) for the situation when a shift in signal frequency is desired, a band pass filter (Mini-Circuits Model SBP 21.4) is added after the mixer to select only the useful frequency. The signal coming from TDO needs to be further amplified sometimes if its amplitude is too small for the frequency counter.

The route of the signal coming from the TDO is as follows: the signal is amplified in a selectable one or two stage broadband monolithic amplifiers, afterwards goes via a passive splitter toward the oscilloscope for visualization and also to the frequency mixer where it will mixed with a stable reference sinusoidal signal of about 50MHz. At the exit from splitter we place a narrow band-pass filter with the center frequency of about 20MHz, this way selecting only the low frequency resulted from mixing and eliminating the higher frequency. Further, the signal is amplified again by a broad band amplifier and is sent toward the frequency counter. The greatest advantage of intercalating a signal conditioning block is the fact that we provide a strong, less noisy signal to the frequency counter.

The frequency counter (*Freq*) used by us (HP Model 53181A) provides 0.1 Hz resolution when measuring up to 200MHz signals. The frequency counter will read the frequency and transmit the data via a GPIB interface to the computer that controls the experiment.

The *dc* magnetic field controller (*MAG cont*) is composed of two parts: the electromagnet's bipolar power supply (Kepco Model BOP 20-10M) and a 3-axes Gaussmeter

(LakeShore Model 460). The computer, via GPIB interface, will send a voltage control command to the power supply and the Gaussmeter will report back to the computer what is the field value that was achieved for the specific voltage setting sent to the power supply. Although the power supply is used as a voltage power supply in order to obtain the maximum field resolution, and the field value is dependent on the electromagnet winding resistance (temperature), it does not affect our experiment since we always record the current magnetic field value, not only the voltage at the power supply output.

The electromagnet has an adjustable gap and is placed on a 360° revolving stage. It can be rotated with 1° precision. The maximum *dc* field created is about 3000G, suitable for all our susceptibility experiments. As we will explain in chapter 5, the original electromagnet was fitted with another smaller electromagnet, placed also in the horizontal plane but at 90° with respect to the original electromagnet magnet axis. Both electromagnets are mounted on the same revolving stage. For the small electromagnet another similar power supply was added, and another Gaussmeter channel is used to measure the magnetic field on the 90° direction.

Having a 2D electromagnet assembly provides the advantage of being able to apply an additional *dc* field during experiments or to rotate the resulting vector field in the horizontal plane. However, this improvement comes with a sacrifice in field uniformity due to field lines closing between the two electromagnets poles and great caution needs to be paid in order to compensate for this. There are two main corrections made in the recorded magnetic field values and power supplies output setting. We need to multiply the field value acquired near the pole with a correction factor in order to obtain the field value at the sample's position. The actual voltage sent to the one or the other electromagnet (*X* or *Y* field

direction) needs to be corrected accordingly to the influence exercised upon that magnet by the other one (*X* influences *Y*, therefore the *Y* needs to be modified and vice versa). These inconvenient correction procedures will be eliminated if the pair of electromagnets is replaced by a pair of superconducting coils. In the current configuration, with the two electromagnets operating, and with the necessary four poles separation, it is possible to obtain 800G in one direction and 300G in the perpendicular direction, in the sample immediate vicinity.

Another important asset our experimental setup is the continuous flow liquid He cryostat (Janis Model STVP-300) controlled by an auto tuning temperature controller (LakeShore Model 330). The duo of continuous flow cryostat and temperature controller is very economical to use having a very low liquid He consumption (less than 5 liters per day) and also provides great long term temperature stability (less than 0.1 K per day variation). The TDO circuit, including the measuring coil, is mounted on a removable insert that is placed inside this cryostat. As shown in Fig. 3.6, the cryostat is placed between the electromagnet poles. During the low temperature experiments the cryostat is permanently connected to a liquid He Dewar and to a diaphragm vacuum pump that provides a low but continuous flow of He through the cryostat. Additionally, since the cryostat is made from stainless steel, it provides a very good shielding for the TDO.

The command center of this setup is the computer that reads and controls all the experimental parameters and records the raw data. The computer communicates with all the instruments via a GPIB (IEEE 488) interface. In order to automate the experiment, extensive LabView programming was done and several other experimental setups used by our group are now controlled by programs inspired by the software that controls the TDO.

The LabView program will generate a step by step sweep of the *dc* field wile measuring the real magnetic field in the samples space and the resonant frequency of the oscillator. A typical field sweep data is shown in Fig. 3.7.

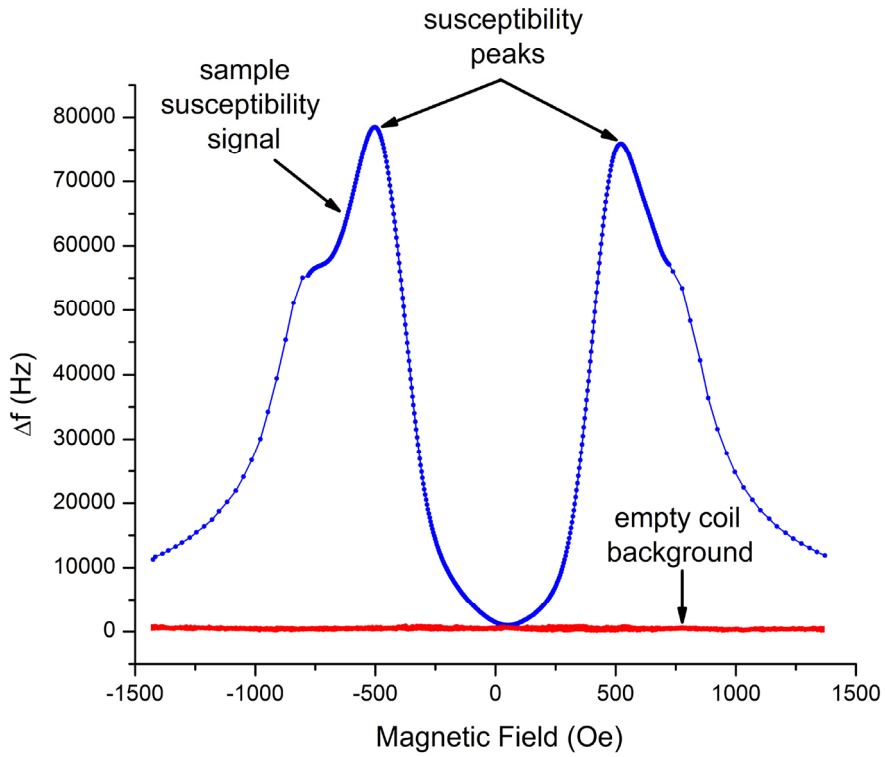

Figure 3.7. Susceptibility signal given by a CrO_2 sample (blue) and the background signal recorded with the empty measurement coil (red). The susceptibility signal has, in this case, very pronounced peaks

Similar TDO-based experiments have been conducted in our lab using the Physical Property Measurements System (PPMS) as a platform for magnetic field and temperature. From our experience it seems more appropriate to use the TDO-electromagnet setup for field scans and the TDO-PPMS combination for temperature scans. When using the TDO with the PPMS we can place the circuit on a horizontal rotator, in order to measure the susceptibility in different directions. A different, complete, LabView application allows us to control at the same time the PPMS's field and temperature and read the TDO frequency's response.

In Fig. 3.8 it is shown the cryostat mounted on the electromagnet support and connected to the vacuum pump and liquid He Dewar.

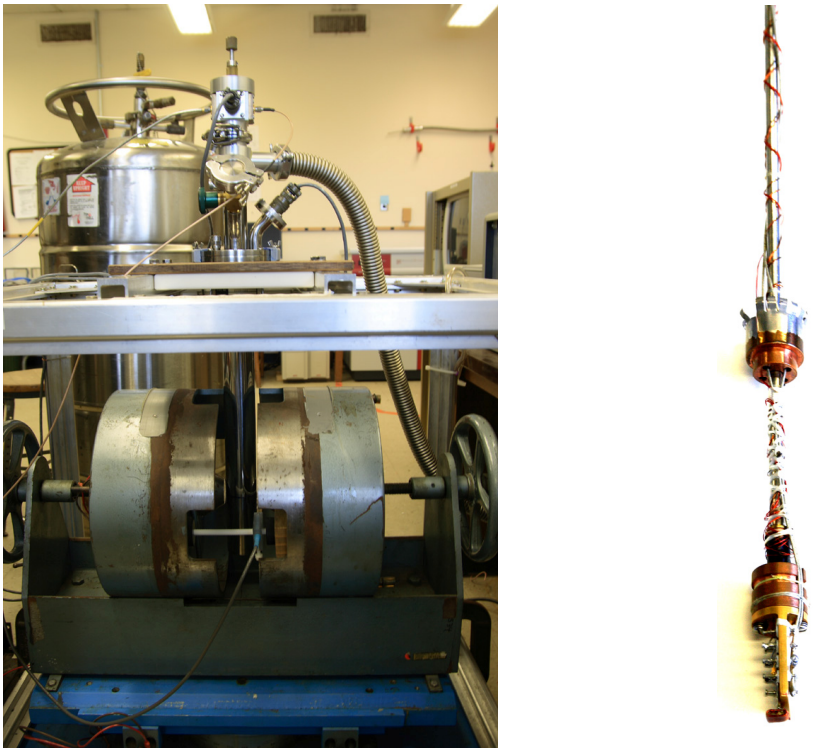

Figure 3.8. Cryostat placed between the electromagnet poles (left). Detail showing the TDO placed on the cryostat insert (right)

From the description of the technological issues involved with the TDO based experiments we can conclude that this experimental method, once mastered, can offer a very sensitive and versatile way of measuring the susceptibility. The challenging part of these experiments is to increase the sensitivity, i.e. change in frequency, without increasing the noise over imposed on the signal, so the peaks positions are clearly discernable.

3.4. Summary

We present the Tunnel Diode Oscillator (TDO) experimental method and our original contributions for the measuring of the magnetic susceptibility.

The main component of a TDO is a tunnel diode. When polarized in the negative resistance region, the tunnel diode is used to drive the tank circuit resulting in a self-resonating LC oscillator. The sample under study is placed in a LC tank's coil. The susceptibility is direct proportional with the permeability of the material ($\chi \propto \mu$). The measured physical property in the case of the TDO experiment is the change in the resonance frequency of the oscillator, that is proportional with the change in the susceptibility of the material placed inside the measuring coil, $\Delta f / f_0 \propto \Delta\chi / \chi$.

This technique can be applied in various fields: for London penetration depth, for magnetic and meta-magnetic transitions, superconductors, and in our case, the magnetization switching. We perform measurements in a temperature range of 4.2 to 300 K. Since most of the samples under study in our case are a piece of thin film, the coil was given a flat-cylinder shape providing an increase in the filling factor over a regular cylindrical coil. As a novelty, the power supply coaxial cable and the output signal coaxial cable are separated and only the TDO itself is placed inside the cryostat. We also built a 2D electromagnet assembly that provides the advantage of being able to apply an additional *dc* field during experiments or to rotate the resulting vector field in the horizontal plane.

Even though the experiment geometry is different comparing to the generally known TS experiment, the singularities detected by rotating the magnetic field direction with respect to the sample and measuring coil instead of the sample inside the tiny measuring coil preserves the switching information of the original TS experiments and it is more practical.

During experiments, the *dc* field is applied at different orientation with respect to the anisotropy axis, and for each direction its amplitude swept between negative and positive saturation of the sample's magnetization.

Chapter 4

Experimental Determination of Critical Curve for Uncoupled Magnetic Nanostructures

In this chapter we present the experimental results we obtained in our lab for measuring the critical curve of various uncoupled nanostructured magnetic systems. These structures are significant magnetic materials with wide area of technological applications. The success in these explorations will enable us to further expand the use and understanding of our research method.

4.1. Strain influence on the magnetic properties of epitaxial Chromium Dioxide thin film

Magnetic materials exhibiting a high degree of spin polarization are being actively investigated for their use in tunnel junctions and other magneto-electronic devices. Of particular interest are systems with complete spin polarization, termed as half metallic [72], that are metallic for one spin direction while at the same time semiconducting for the other spin direction.

Chromium dioxide (CrO_2) is a ferromagnetic oxide that has been widely used as a particulate magnetic recording medium. Theoretical and experimental [72] studies have confirmed that CrO_2 is a half-metallic solid with a nearly 100% spin polarization in the conduction band. This half-metallic behavior makes CrO_2 a good material candidate for

magnetic tunnel junctions and other magneto-electronic devices that require a large spin polarization.

4.1.1. Sample description

Fabrication and characterization of epitaxial CrO_2 films are essential for fundamental studies and potential applications. It remains a challenging task to synthesize CrO_2 films, as this particular phase is a metastable oxide. High-quality single-crystal CrO_2 films have been prepared using the technique of chemical vapor deposition (CVD) on the single crystal (100) substrate of TiO_2. The samples were provided by Prof. Arunava Gupta from MINT Center, University of Alabama at Tuscaloosa.

Bulk CrO_2 has a rutile structure with a tetragonal unit cell (a=b=4.421Å and c=2.916Å) consisting of two formula units. The chromium ions are in the Cr^{+4} state with a magnetic moment of $2\mu_B$ per ion. Bulk TiO_2 has a rutile structure with a tetragonal unit cell (a=b=4.593Å and c=2.958Å).

The close lattice matching between CrO_2 and the substrate is necessary to stabilize the growth of the CrO_2 phase. The lattice constant difference between CrO_2 and TiO_2 is -3.79% along $\langle 100 \rangle$ and $\langle 010 \rangle$ crystalline axes, and -1.48% along the $\langle 001 \rangle$ axis. Therefore the induced strain ε in the CrO_2 film is expected to be anisotropic for films with in-plane *b* and *c* axis. Earlier, it has been shown [73] that the strain in CrO_2 films affects the magnetic anisotropy significantly in the thickness range of 800 Å - 1200Å. An anisotropic in-plane tensile strain is imposed on the film, with a consequent shrinkage of the *a*-axis lattice parameter perpendicular to the substrate [73].

The studied CrO_2 thin film in our case was a square sample of 5 by 5 mm and 2000 Å thick, grown by CVD at atmospheric pressure. The structural and magnetic properties of this

film has been extensively characterized [74]. An important property of the epitaxial grown CrO_2 (100) thin film is the very large in-plane uniaxial anisotropy, with well-defined magnetic easy axis (*c*-axis) along the [001] axis and hard axis (*b*-axis) along the [010], that is reflected in the magnetic measurements [44].

In Fig. 4.1 it is represented a schematic of the CrO_2 sample with the magnetic easy axis and the average tensile strain in the plane of the sample. The actual easy axis of the sample will be proven to be a resultant of the two anisotropy forces acting on the sample, similar to the case of the two vector's resultant, in mechanics.

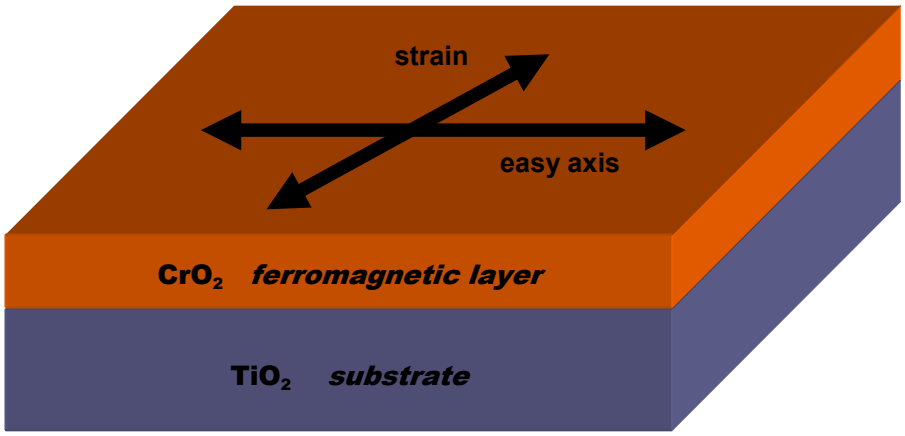

Figure 4.1. CrO_2 thin film sample geometry

4.1.2. Magnetic properties characterization of the Chromium Dioxide (CrO_2)

Next we will demonstrate how the anisotropy of this sample can be probed sensitively and explored in great detail using transverse susceptibility experiments.

The susceptibility χ_T is measured by applying the method presented in chapter 2 using our experimental setup described in chapter 3. The thin films are placed inside the coil that is a part of the TDO.

The change in resonance frequency is measured as the static field is ramped from negative to positive saturation, and vice versa. This quantity is proportional to the change in inductance that in turn is governed by the transverse susceptibility χ_T of the films. It should be noted that the rf field amplitude is very small, of about 20 mOe, and, at the most can be considered only a perturbation that does not affect the magnetization in the film.

In a previous paper [44], the magnetic properties of CrO_2 was investigated by conventional magnetometry techniques but we will demonstrate that using our TDO-based susceptibility experiment the experimental critical curve can be accurately determined. Fig. 4.2 shows the hysteresis curves recorded at room temperature (300K) and at low temperature (10K), for two different angular orientation of the easy axis with respect to the applied *dc* field direction $(\psi = 0^\circ \text{ and } 90^\circ)$.

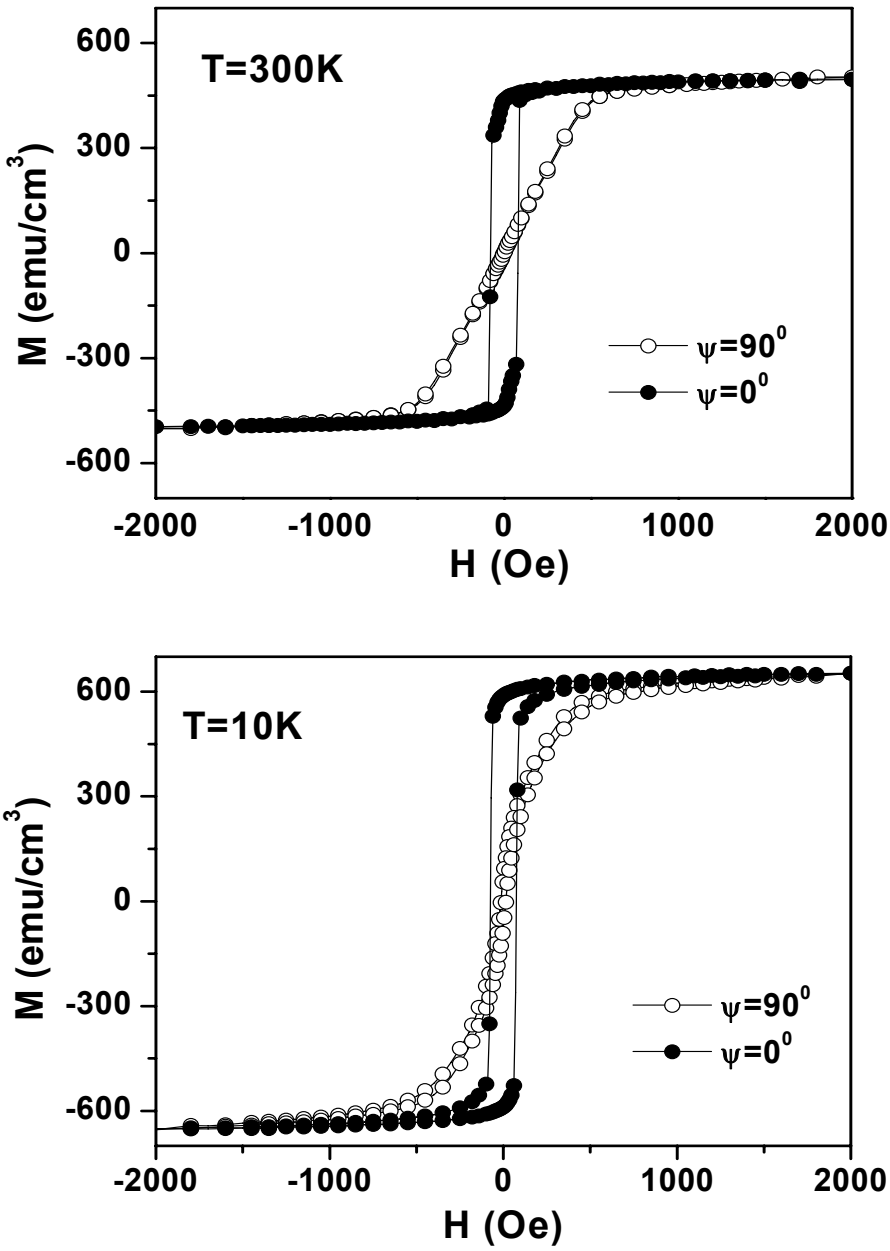

Figure 4.2. Hysteresis loops for CrO_2 thin film sample [44]

The results of the susceptibility experiments done using the TDO-based setup are initially a set of susceptibility curves, like the one presented in Fig. 4.3. Although we recorded all the susceptibility signals for all the orientations between 0° and 180° with a step of 5°, we will show only the 0° and 90° orientations. By collecting all these curves and

identifying the peaks in the signal we will be able to plot the critical curve. In the Figure 4.3 are shown the switching peaks (at the field H_S) as well as the anisotropy peaks (at the fields $\mp H_K$). For this CrO_2 thin film sample the H_K is about 700 Oe and H_S is about 40 Oe.

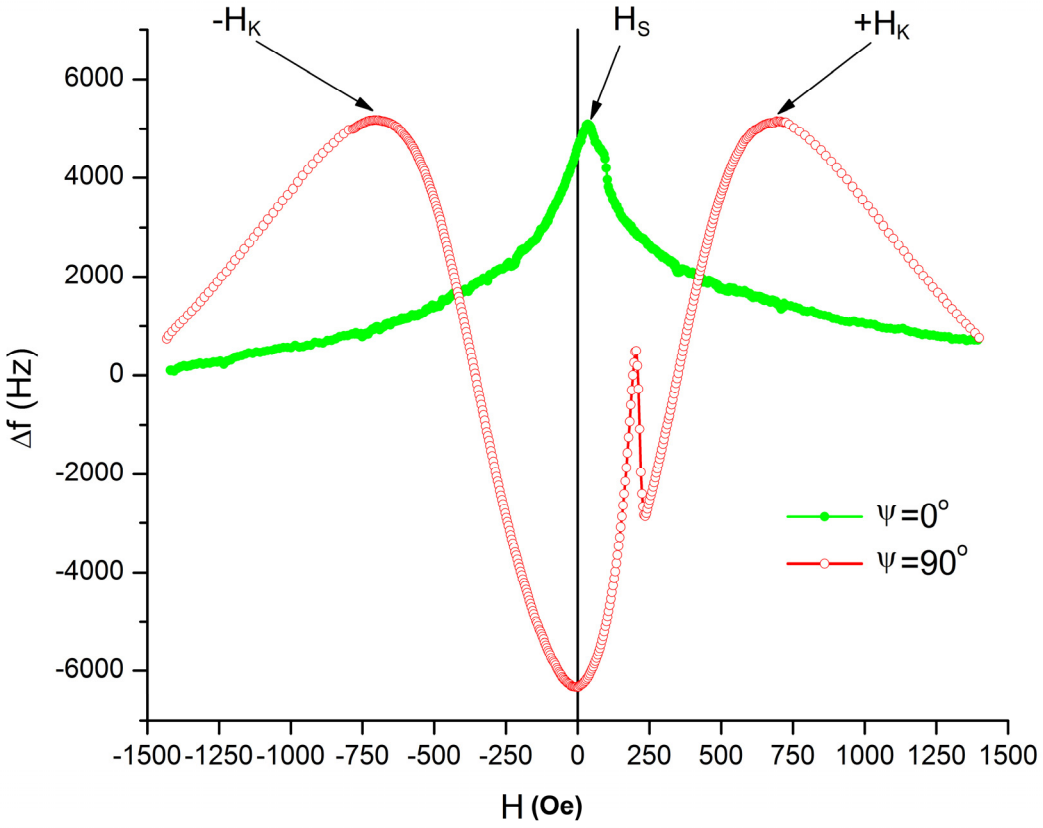

Figure 4.3. Susceptibility curves for parallel (green) and perpendicular (red) orientation for CrO_2 thin film sample.

For clarity in Fig. 4.3 it is shown only the ascending part of the susceptibility signal. Usually we sweep the *dc* field up and down between the negative and the positive saturation, in order to obtain both points on the two sides of the critical curve from a single experiment, for one specific orientation of the *dc* field with respect to the easy axis.

We will focus our attention now on the extra peak observed in the susceptibility signal for the 90° orientation. This extra peak is located on the left of the $+H_K$ anisotropy

peak. In a paper published earlier in our group [44], it was shown how the transverse susceptibility (TS) signal features evolves when the experiment is performed at different temperatures (from 300K down to100K), fact shown in Fig. 4.4.

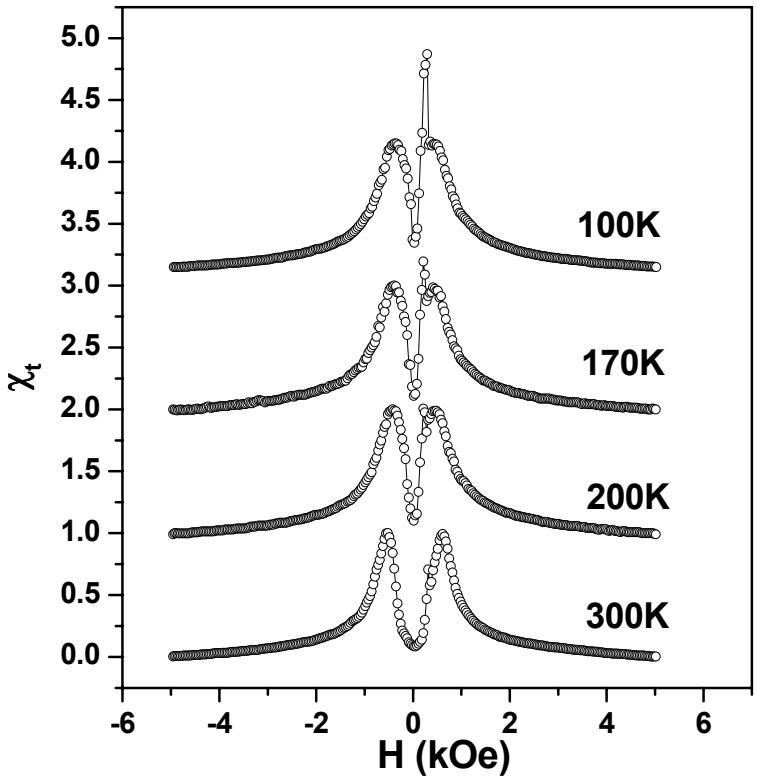

Figure 4.4. Transverse Susceptibility curves recorded at different temperatures for CrO_2 thin film sample [44].

We notice that the peak that was barely visible at 300K increases dramatically in amplitude and around 100K it is almost completely masking the anisotropy peak $+H_K$.

Since the experimental configuration remains the same at lower temperatures as it is at 300 K, the origin of this peak must lie in the magnetic response intrinsic to the thin-film samples. The evolution of the peak structure was reproduced [44] using the coherent rotation model by introducing a misalignment in angle between H and the easy axis in the perpendicular geometry (TS). This trend is clearly illustrated in Fig. 4.5, which shows a

series of calculated transverse susceptibility curves for several angles deviating from the 90° case considered earlier.

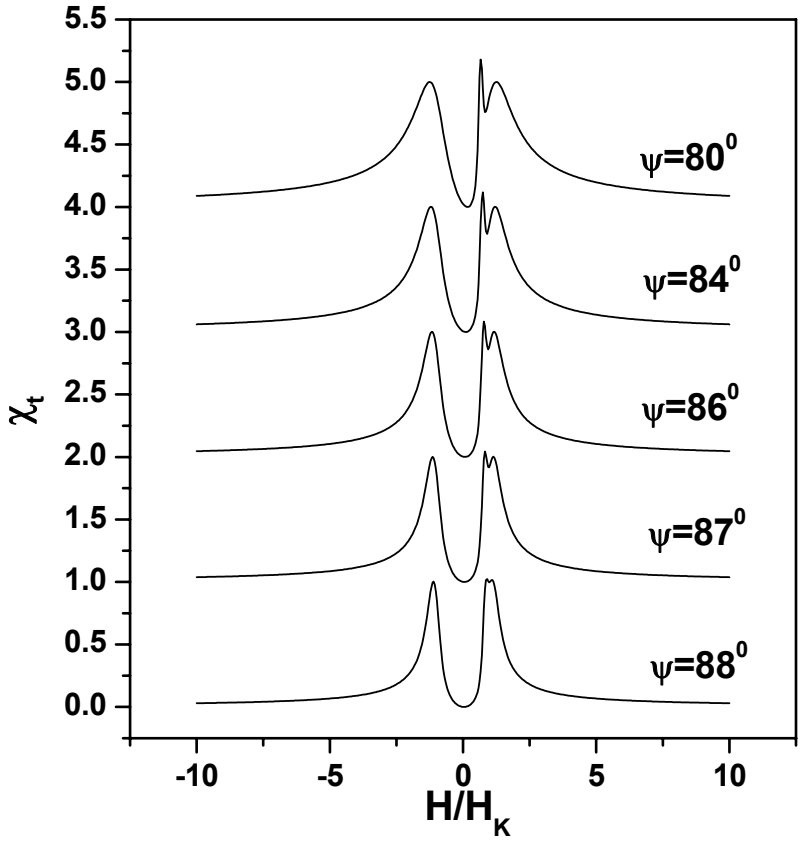

Figure 4.5. Transverse Susceptibility curves calculated for small angular deviation between H and the easy axis [44].

The qualitative similarity between the measured and calculated TS is evident, and suggests that as the temperature is lowered, a gradual angular misalignment develops between the applied static field and the magnetic easy axis in the sample. This effect can be accounted for by considering the influence of strain on the thin films [44]. As noted earlier, the lattice mismatch between the CrO_2 films and TiO_2 substrates introduces an in-plane tensile strain. The angular misalignment as the sample temperature is lowered could be associated with changing strain.

Let's explore now the quantitative dimensions of this predicted effect: As CrO_2 is a ferromagnetic material with uniaxial anisotropy, the total-energy density can be expressed as:

$$F_K(\theta) = K_1 \sin^2\theta - MH\cos(\psi - \theta) \tag{4.1}$$

where K_1 is the anisotropy constant, θ is the angle between the magnetization vector and the easy axis, and ψ is the angle between H and the easy axis. In this expression, the magnetoelastic contribution is neglected, and only the first-order approximation to the magnetocrystalline energy is considered, as is done with standard uniaxial anisotropy.

Considering the saturation magnetization $M_S = 650\, emu/cm^3$ for the CrO_2 thin film, and taking the measured H_K value of 700 Oe from Fig. 4.3 and using the standard relation $H_K = \frac{2K_1}{M_S}$, we estimate the anisotropy constant K_1 to be $2.2\times10^5\, erg/cm^3$.

Introducing the angular deviation between H and the easy axis is equivalent to including a net magnetoelastic energy term in the total anisotropy energy:

$$F_A(\theta) = K_1 \sin^2\theta + K_{\sigma c}\sin^2\theta + K_{\sigma b}\cos^2\theta \tag{4.2}$$

where $K_{\sigma c} = \frac{3}{2\lambda\sigma_c}$ and $K_{\sigma b} = \frac{3}{2\lambda\sigma_b}$ are the stress anisotropy constants in the *c* and respective *b* directions.

The total anisotropy energy including the magnetoelastic term is:

$$F_A(\theta) = \frac{M_S}{2}\left[H_K \sin^2\theta + H_\sigma \sin^2(\theta - \delta)\right] \tag{4.3}$$

where H_σ is the stress field given by:

$$H_\sigma = \frac{3\lambda_S\sigma}{M_S} \tag{4.4}$$

where λ_S is the magnetostriction coefficient, and σ is the stress applied at an angle δ with respect to the easy axis.

The stress can be calculated using $\sigma = Y\varepsilon$ where Y is the Young's modulus for TiO_2, $Y = 2.5\times10^{12}\ dyn/cm^2$, and $\varepsilon = 0.0148$ in the *c* axis direction and $\varepsilon = 0.0379$ in the *b* axis direction. Therefore $\sigma = 3.7\times10^{10}$ and $9.5\times10^{10}\ dyn/cm^2$ in the *c* and, respective *b* axis directions.

In order to calculate λ_S we impose the condition for which the anisotropy along *c* and *b* axis (hard and easy axis) to be equal before the easy axis becomes hard axis and vice versa:

$$K_1 + K_{\sigma c} = K_{\sigma b} \tag{4.5}$$

that gives us $\lambda_S = 1.18\times10^{-6}$ and consequently, $H_\sigma = 200\,Oe$

Transforming Eq. 4.3 yields:

$$F_A(\theta) = \frac{M_S}{2}\left[H^* \sin^2(\theta - \theta^*) + H^* \sin^2\theta^* + H_\sigma \sin^2\delta\right] \tag{4.6}$$

where

$$H^* = \sqrt{H_K^2 + H_\sigma^2 + 2H_K H_\sigma \cos 2\delta} \tag{4.7}$$

and

$$\tan 2\theta^* = \frac{H_\sigma \sin 2\delta}{H_K + H_\sigma \cos 2\delta} \tag{4.8}$$

Therefore, the total anisotropy energy is uniaxial with the effective easy axis rotated with an angle θ^* with respect to the magnetocrystalline easy axis. With the values we obtained from measurements and from literature regarding the thin film deposited on the substrate structure and considering $\delta = 45^\circ$ we can predict a rotation of the easy axis with $\theta^* = 8^\circ$.

We went further and we measured the critical curve at 300K and 10K (see Fig. 4.6)

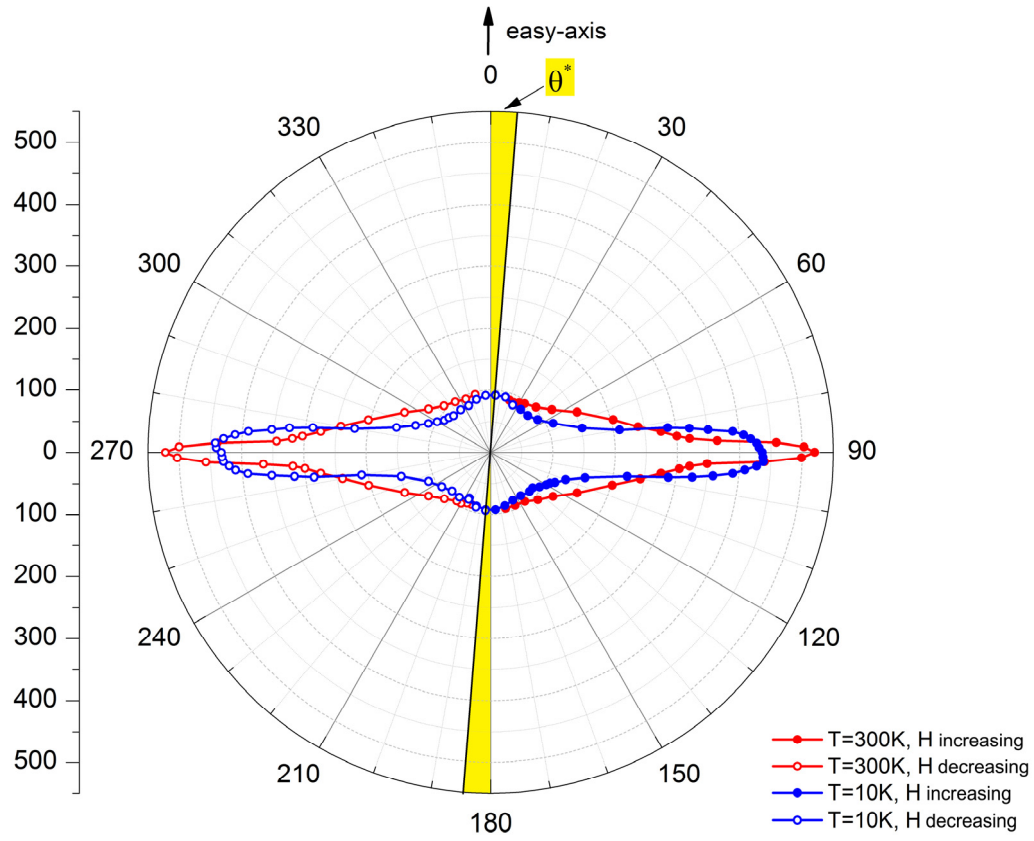

Figure 4.6. Experimental critical curve recorded for CrO_2 thin film sample. The low temperature curve (blue) easy axis is rotated with $\theta^* = 4°$ in comparison to the room temperature curve (red) reference easy axis

With the decrease in the temperature the magnetoelastic effect strengthens, due to the increase in the strain at the interface between CrO_2 and TiO_2 substrate.

The easy axis rotates only half of the theoretical predicted angle. This fact may be due to the error in angle measurements during experiment as well to the approximation made in the theoretical calculation when a simple uniaxial anisotropy was considered.

It has been reported [73] that as the film thickness is reduced to less than 700 Å, the in-plane strain causes switching of the easy axis from the *c* direction to the *b* direction. Our transverse susceptibility results and analyses indicate that this tendency for the easy axis to

gradually deviate by a small angular orientation from the *c* axis towards the *b* axis in plane is evident even for samples with the CrO_2 with a thickness of 2000Å.

Despite the slight mismatch in the rotation angle, this experiment proves the TDO-based susceptibility experiments are a reliable way to identify several important features in the magnetic anisotropy of the epitaxial grown CrO_2 thin films, a technological very important material.

Another aspect of this experiment is the unpredicted rounding of the critical curve around the intersection with the hard axis direction (90°).

One possible explanation for the rounding is the influence of the *ac* field created by the measuring coil. If this field is comparable to the switching fields, then the magnetization can switch at slightly lower *dc* fields, due to the contribution of the *ac* field.

This is a drawback for our method and we need further investigation in order to understand and eliminate it.

4.2. Critical curve at different temperatures for an exchange anisotropy Iron-Cobalt / Iridium-Manganese multilayers structure

Exchange anisotropy (EA) arises from the exchange coupling at the interface between a ferromagnet (FM) and an antiferromagnet (AFM) and it was discovered in 1957 by Meiklejohn and Bean [19]. There is renewed interest in AFM/FM exchange coupling in recent years because of its application to giant magnetoresistive heads for high-density recording systems, Magnetoresistive RAM and sensors. The typical signature of the EA is a displaced hysteresis loop along the field axis with a field value equal to the exchange field, from which the EA can be determined. Different measurement techniques were proposed to assess the EA, such as anisotropic magnetoresistance [75], *ac* susceptibility [76],

ferromagnetic resonance [77], Brillouin light scattering [78], polarized neutron reflectometry [79]. Recently, our group proposed a method to probe the exchange interaction using reversible susceptibility tensor containing transverse and longitudinal susceptibilities [31].

Our method combines the advantages of reversible measurement techniques using a small *ac* field and the simplicity of an irreversible measurement technique, such as the hysteresis loop displacement.

4.2.1. Sample description

The exchange anisotropy sample under investigation is a [FeCo (50 nm) / IrMn (12 nm)] x 4 multilayer with Cu (4 nm) seedlayer deposited on a glass substrate. This was provided by Dr. Ganping Ju from Seagate Technology, Pittsburgh, PA. The sample was fabricated using a HDD disc media sputter deposition system, Unaxis M12. Several detailed methods of fabrication are described in an earlier paper [80]. The sample is cut into 5x5 mm square pieces with one of the edges parallel to the direction of the EA. The multilayer arrangement is shown in Fig. 4.7.

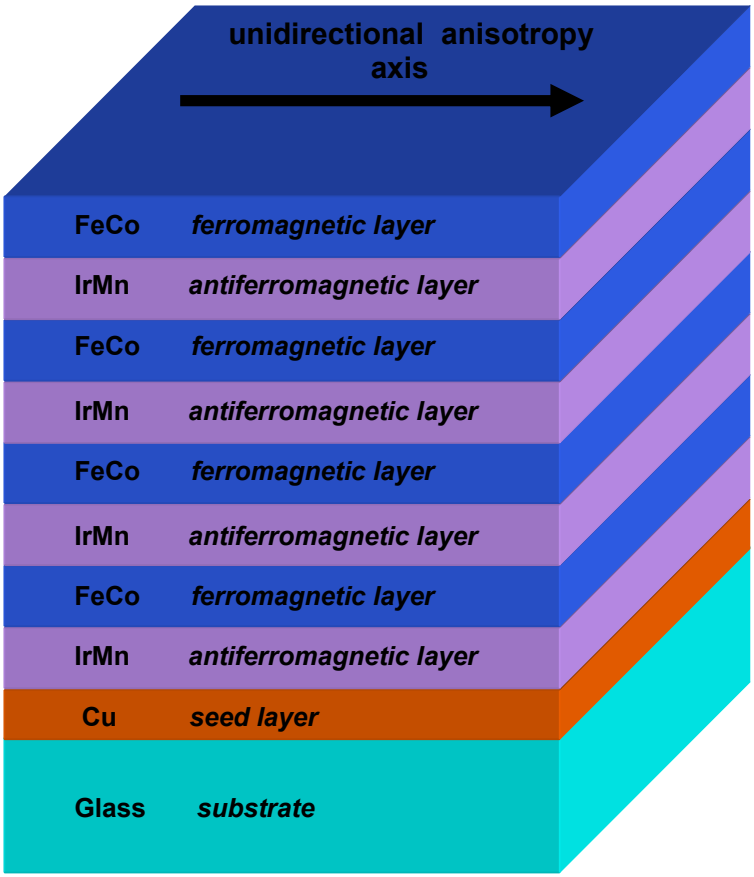

Figure 4.7. FeCo/IrMn thin film sample structure

4.2.2. Exchange anisotropy characterization for the Iron-Cobalt / Iridium-Manganese thin film multilayers sample

For the susceptibility experiment the sample is placed in the sensing coil with both *ac* and *dc* fields lying in the sample plane and the easy axis parallel with the *ac* field, which follows the same procedure like the one described in third chapter. Hysteresis loops at different angles are measured first using a vibrating sample magnetometer.

Figure 4.8 shows the hysteresis loop and the field dependent TS at room temperature, with the static magnetic field H applied parallel to the easy axis of the film.

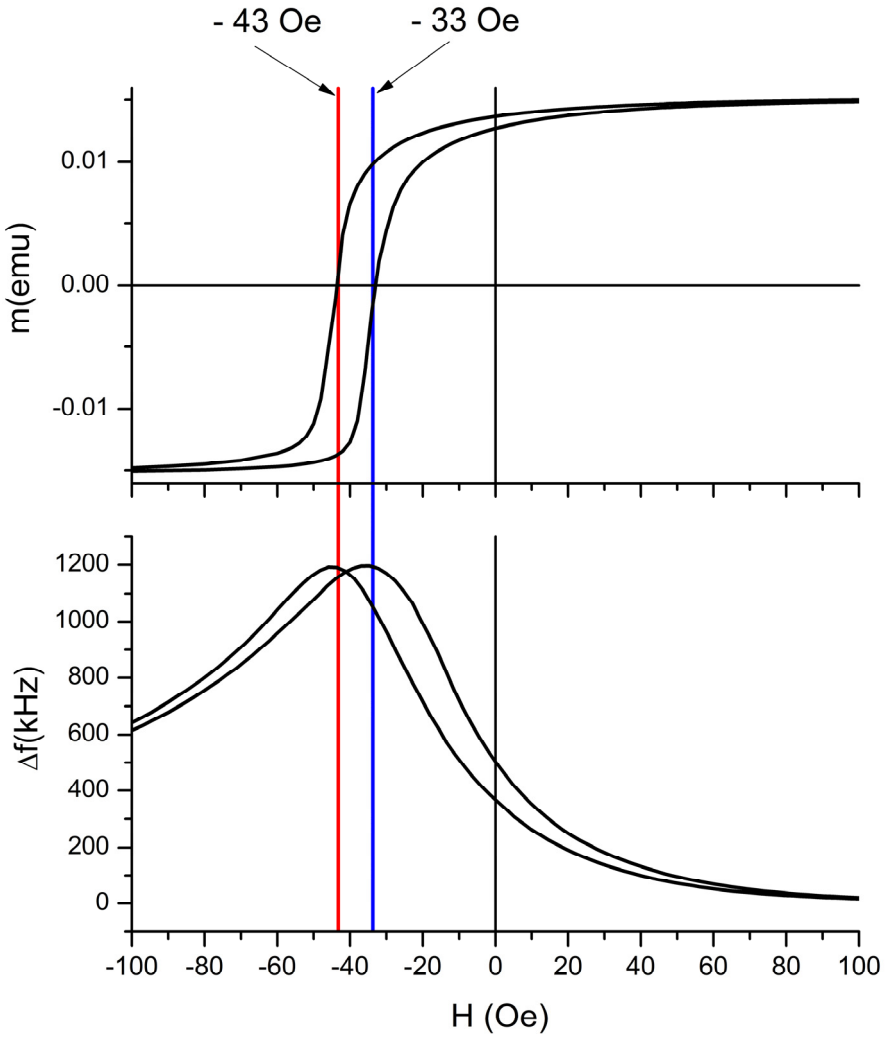

Figure 4.8. Hysteresis loop (top) and susceptibility signal (bottom) for FeCo/IrMn thin film sample measured at room temperature, with *dc* field along easy axis

As is typical for a sample with exchange anisotropy with the *dc* field is along easy axis, the hysteresis loop is displaced, and we show that also the susceptibility signal reflects this characteristic. The asymmetry of magnetization reversal mechanism is evident from TS plot.

In Fig. 4.8, for TS curves we observe a single peak per curve for increasing (red marker) and decreasing (blue marker) field sweeps (i.e., from negative to positive saturation and vice versa). Although we scan in field from – 1500 Oe to +1500 Oe, only the region of

interest from – 100 Oe to +100 Oe, is presented in Fig. 4.8. The observed TS hysteresis has features with symmetry similar to those of the magnetization hysteresis shown in same figure, for the same field orientation. Thus, the shift of the transverse susceptibility hysteresis loop along the field axis clearly indicates the presence of the exchange anisotropy with an exchange field of $H_E = -38\,Oe$ and coercive field in the easy axis direction of $H_C = 5\,Oe$, all these values being confirmed by both hysteresis and susceptibility measurements.

The experimental susceptibility curves when the *dc* field H is applied perpendicular to the easy axis exhibit two peaks per field sweep, symmetrically located around H=0, as expected. For this orientation the effect of the exchange anisotropy is not present, which is similar to the results obtained for uniaxial systems in the same geometry, just like the one presented in the section 4.1.

As it has been shown [81] for the case of an exchange-coupled system, the critical curve is shifted from the origin by a vector given by the exchange anisotropy . By performing experiments at different orientations of the applied field, and tracking the singularities in the detected signal, we obtained the critical curve for the FeCo/IrMn exchange biased system. Both the magnitude and orientation of the exchange field can be determined readily from the critical curve.

The susceptibility signal recorded for different orientations of the applied field with respect to the sensing coil direction and at three different temperatures, 300K, 100K, 50K is used to plot the critical curves, as shown in Fig. 4.9.

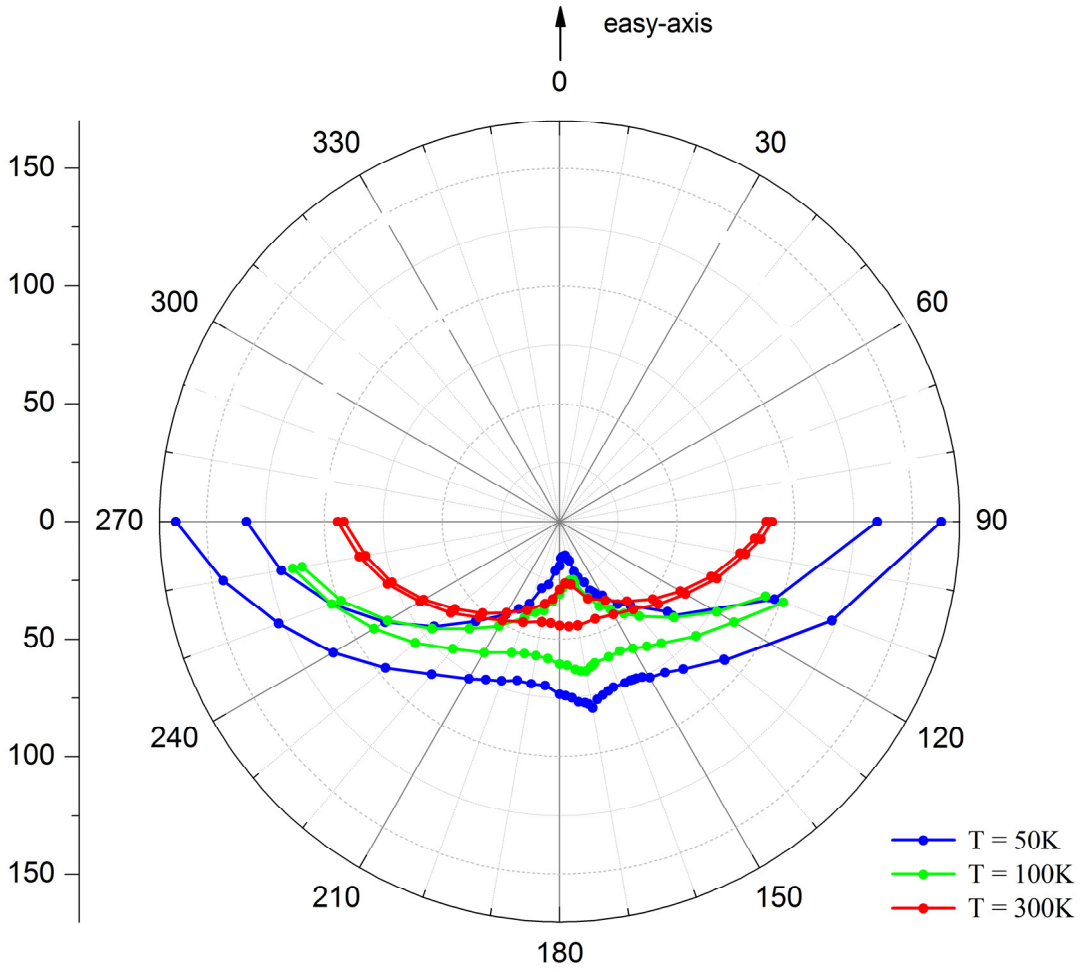

Figure 4.9. Critical curve for FeCo/IrMn thin film sample measured at 300K (red), 100K (green) and 50K (blue)

For all the TDO-based experiments performed in order to obtain the critical curves, we cooled the sample in zero field – typical procedure when the exchange bias is explored.

The experimentally determined critical curves are not symmetric, as the theoretical astroid, but extended along the hard-axis direction and warped towards the ends. Also, we notice the openings along the hard axis, these being associated with the small hysteresis observed even for a field orientation where we would expect a reversible behavior [82]. This

is determined by the existence of a small distribution of the easy axis orientation in our multilayer exchange-coupled sample.

The critical curve representation for the exchange-coupled system has the advantage that it provides comprehensive information about the system from which important features, such as exchange field magnitude and direction or coercivity for any field orientation, can be easily determined.

The offset of the center of the critical curves with respect to the field origin gives exactly the magnitude and direction of the exchange field. As we see from Fig. 4.9 the displacement of the critical curves increases with the decrease in temperature, up to about $H_E = -50\,Oe$, when the temperature reaches 50K. Also, as expected, the coercive field increases with the decrease in temperature, up to about $H_C = 30\,Oe$ at 50K.

The angular exploration of the exchange bias in the studied sample is performed by detecting the susceptibility signal for different orientations of the applied field.

This procedure, that was previously demonstrated theoretically [31] and now experimentally, allows one to obtain the critical curve of the switching fields at different temperatures.

In this way we record the fingerprint of the switching processes from which both magnitude and direction of the directional anisotropy can be determined.

4.3. Critical Curve's shape as a function of Cobalt film thickness in Cobalt / Silicon Dioxide multilayer structure

Granular ferromagnets are immiscible mixtures of two materials, one of which is ferromagnetic in the form of nanoscopic-size polycrystalline grains and the other is

nonmagnetic. The nonmagnetic material can be either metallic (Ag, Au, Cu) or insulating (SiO_2, Al_2O_3) in crystalline or amorphous form.

Magnetic properties of granular ferromagnets are known to depend mainly on the topological structure of the ferromagnetic component [83]. When the size of individual grains is sufficiently large for the existence of ferromagnetism, the isolated nanometer-size ferromagnetic grains are single domains. At low concentration of ferromagnetic material, the individual grains are dispersed in the nonmagnetic matrix. When the space orientation of granular easy magnetic axes is random, the system behaves like a superparamagnet. At high magnetic material volume fraction, the magnetic particles coalesce and form a connected network. In this regime, the magnetic phase percolates throughout the material and the sample appears to be a normal ferromagnet.

The interest in granular ferromagnets was triggered by the discovery of the giant magnetoresistance effect (GMR) in magnetic multilayers and heterogeneous magnetic alloys with ferromagnetic grains embedded in a nonmagnetic matrix.

Discontinuous multilayers, which consist of plane of metallic ferromagnetic particles interspersed within an insulating matrix, are easy to prepare, and they offer several distinct advantages over continuous magnetic layers and especially MTJs. The benefits include less susceptibility to electrical breakdown and greatly reduced likehood of pinhole development across the insulating barrier which often happens to short-circuit the current in a regular MTJ structure.

The systems we are interested to probe with our TDO-based technique are multilayer structures of ferromagnetic Co granular films sandwiched between non-magnetic SiO_2 insulator layers.

4.3.1. Samples description

We investigate several samples of $\left[\mathrm{Co}\left(\mathrm{t_{Co}}\right)/\mathrm{SiO_2}(1\mathrm{nm})\right]\times 10$ multi-layers grown by *dc* (Co) and rf (SiO_2) sputtering on Si substrates held at room temperature. A 10 nm buffer layer of SiO_2 was deposited on the Si substrate before the sequential deposition of Co and SiO_2 layers. Several samples can be obtained by varying the nominal thickness of Co and SiO_2 layers. The samples considered in this work are three metallic samples with Co nominal thickness t_{Co} of 1 nm (sample 90A), 1.5 nm (sample 90B) and 2nm (sample 90C). The samples were cut into 5x5 mm square pieces, with one edge parallel to the easy axis of the ferromagnetic layers. These samples were provided by Dr. Juliano Denardin from Unicamp University, Campinas, Brazil.

The sample structure is shown schematic in Fig. 4.10.

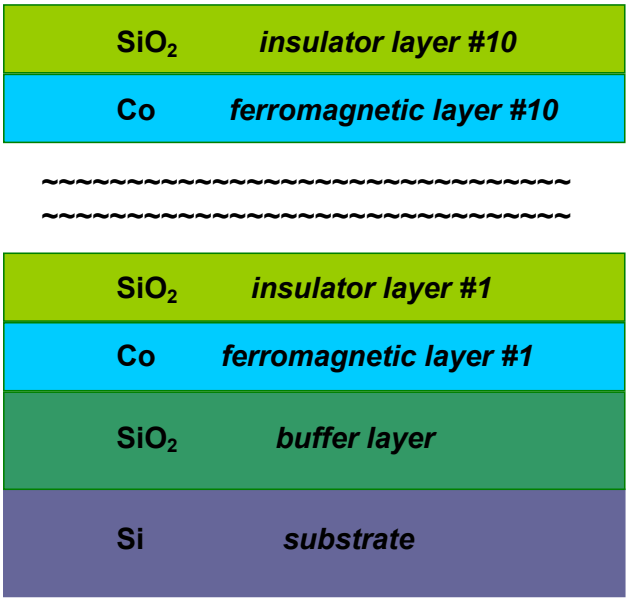

Figure 4.10. Co/SiO_2 sample structure; only the lower and the upper part are shown.

In Fig. 4.11 it is presented a cross-section view of these multilayer structures obtained with the electron microscope.

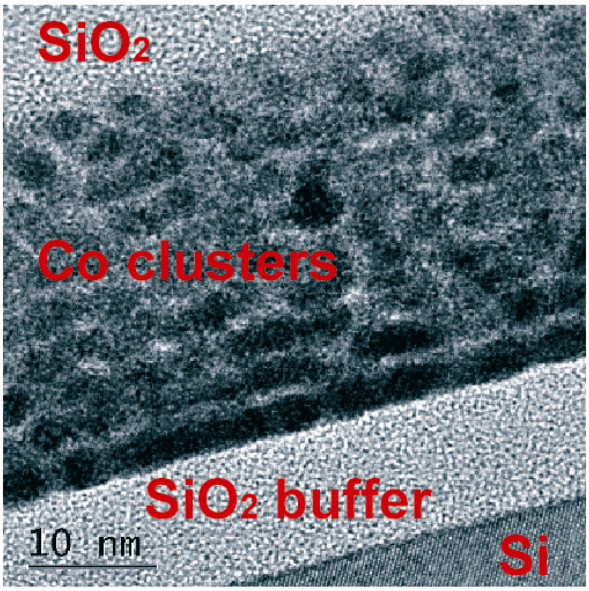

Figure 4.11. Microscope image of the section through the Co/SiO_2 structure.

4.3.2. Critical Curve shape for Co/SiO_2 series of samples

The technique presented in chapter 2 and 3 was employed to determine the critical curves for the Co/SiO_2 samples with different Co layers thickness. The sample was placed in the TDO's measuring coil with both *ac* and *dc* fields lying in the sample plane and the easy axis along the coil axis.

The reversible susceptibility signal was recorded for different orientations of the *dc* field with respect to the sensing coil direction. Starting from $\theta_H = 0^0$ to $\theta_H = 360^0$ with the angle step 5^0, the signals recorded for the sample 90A are presented in Fig. 4.12.

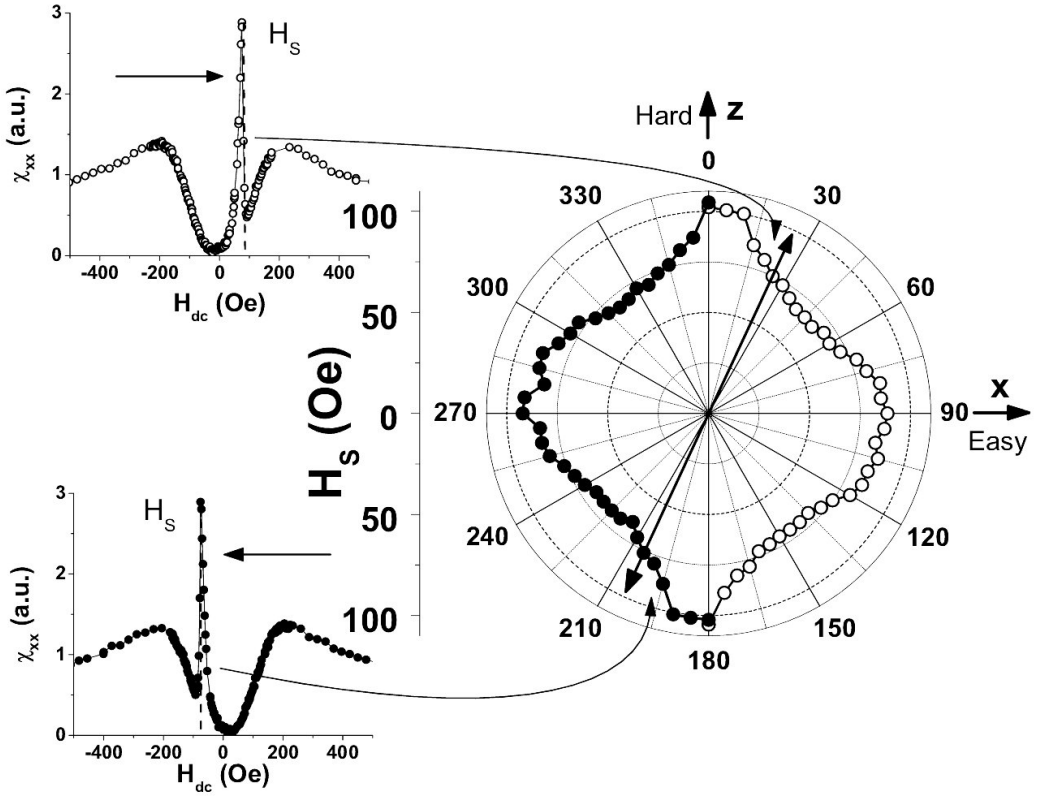

Figure 4.12. Right: Experimental switching critical curve as determined from susceptibility measurements for sample 90A. Left: Experimental susceptibility signal for increasing (top) and decreasing (bottom) field sweeping at $\theta_H = 25^\circ$ [32].

One can observe that the experimental critical curve slightly deviates from the theoretical astroid curve shown in Fig. 2.12. A more dramatic change in the critical curve was observed for sample 90B and 90C, fact shown in Fig. 4.13. They are all smaller compared to the theoretical astroid and rounded along the easy direction.

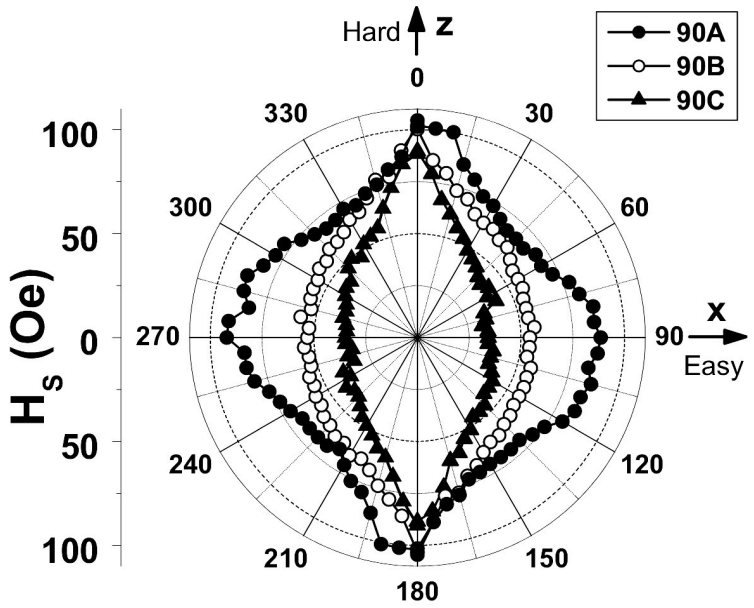

Figure 4.13. Experimental switching critical curves as determined from susceptibility measurements for samples 90A, 90B, and 90C [32].

The dimensions of the critical curve along the hard and easy axes for the sample 90A are 103 and 90 Oe, respectively. One observes that the aspect ratio of the experimental critical curve (defined as the ratio between the maximum length of the critical curve along the easy axis to that along the hard axis) is about 0.87, which is smaller than the unit astroid aspect ratio as predicted by Stoner–Wohlfarth model [15]. The reduced critical curve aspect ratio was already observed for 2D magnetic systems and was connected to the existence of the edge domains or noncoherent rotation switching modes.

A more dramatic change in the critical curve aspect ratio was observed for samples 90B and 90C. Thus, the aspect ratio for sample 90B is 0.55 while for sample 90C it is 0.39, with lengthens of the critical curves along the hard axis of about the same value. The critical curve shape is sensitive to domain formation and switching modes [27]. Hence, incoherent switching modes, as the fanning [84] appearing in the "chain-of-spheres" model [85], are determining a truncated astroid along the easy axis. In our case, the observed shrinkage of the

critical curves along the easy axis as the Co layers thickness increases is consistent with the observation that, for larger thicknesses, the influence of the domain wall motions in the dynamics of magnetization is more important [28].

The TDO-based experimental method has the advantages that it does not require us to put contacts on the sample, as it does in the case of transport measurements.

As seen in this chapter the reversible susceptibility method explored using the TDO experimental technique proves its versatility being able to characterize several types of uncoupled magnetic nanostructures, with crucial application in the modern magnetism studies.

4.4. Summary

We presented some of the experimental results we obtained in our lab when measuring the critical curve of various uncoupled nanostructured magnetic systems.

First we investigate the strain influence on the magnetic properties of epitaxial CrO_2 thin film. This is a system with complete spin polarization, termed as half metallic, that is metallic for one spin direction while at the same time semiconducting for the other spin direction. The samples are high-quality single-crystal CrO_2 films have been prepared using the technique of chemical vapor deposition on the single crystal (100) substrate of TiO_2.

As the temperature is lowered, a gradual angular misalignment develops between the applied static field and the magnetic easy axis in the sample. This effect can be accounted for by considering the influence of strain on the thin films generated by the lattice mismatch between the CrO_2 films and TiO_2 substrates. The total anisotropy energy including the magnetoelastic term is $F_A(\theta) = \frac{M_S}{2}\left[H_K \sin^2\theta + H_\sigma \sin^2(\theta - \delta)\right]$. Therefore, the total

anisotropy energy is uniaxial with the effective easy axis rotated with an angle θ^* with respect to the magnetocrystalline easy axis. We measured the critical curve at 300K and 10K.

Another studied system at different temperatures was an exchange anisotropy FeCo (50 nm) / IrMn (12 nm)] x 4 multilayer structure. Exchange anisotropy arises from the exchange coupling at the interface between a ferromagnet and an antiferromagnet coupling. Their applications are giant magnetoresistive heads for high-density recording systems.

Hysteresis loops at different angles are measured first using a vibrating sample magnetometer. Typical for a sample with exchange anisotropy, when the *dc* field is along easy axis, the hysteresis loop is displaced and we show that also the susceptibility signal reflects this characteristic. The shift of the transverse susceptibility hysteresis loop along the field axis clearly indicates the presence of the exchange anisotropy. The critical curve is shifted from origin by a vector given by the exchange anisotropy. Both the magnitude and orientation of the exchange field can be determined readily from the critical curve at different temperatures, 300K, 100K, 50K . The experimentally determined critical curves are not symmetric, as the theoretical astroid, but extended along the hard-axis direction and warped towards the ends.

We also study a structure of ferromagnetic Co granular films sandwiched between non-magnetic SiO_2 insulator layers $\left[\mathrm{Co}\left(\mathrm{t_{Co}}\right)/\mathrm{SiO_2}(1\mathrm{nm})\right]\times 10$ multilayers. We observe that the experimental critical curve deviates from the theoretical astroid curve. The aspect ratio of the experimental critical curve is smaller than the unit astroid aspect ratio and its evolution as a function of $\mathrm{t_{Co}}$ was connected to the existence of the edge domains or noncoherent rotation switching modes.

Chapter 5

Experimental Recording of Critical Curve for Coupled Thin Films

The technological requirements on magnetic devices are continuously increasing and this fact generates the need for complex structures to be used in modern devices. Following this trend, multi-layer structures are replacing single-layer structures.

This chapter will focus on the study of synthetic antiferromagnet (SAF) - a sandwich of two ferromagnetic thin films antiferromagnetically coupled through a non-magnetic metallic spacer, usually Ru, Os, Re, Cr, Cu, Rh. Due to SAF shape anisotropy, reduced anisotropy field and its capacity for spin transfer [86], SAF has many technological applications as hard layer of exchange coupled composite media [87] , soft under-layer for perpendicular recording [88], pinned and free layers for toggle MRAM cells [89], hard disk reading heads, or magnetic sensors [90].

5.1. Synthetic Antiferromagnet (SAF) concepts

The performance of the devices using SAF structures relies heavily on their switching characteristics, which are governed by the individual reversal of the SAF composing ferromagnetic layers, and the interlayer coupling.

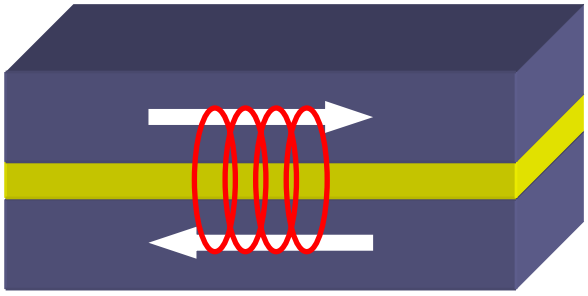

Figure 5.1. Schematic representation of the SAF showing the two ferromagnetic layers antiferromagnetically coupled through an interlayer of non-magnetic material.

The two ferromagnetic layers in a SAF type of structure are coupled together through a Ruderman-Kittel-Kasuya-Yosida (RKKY) type interaction. This type of coupling was first proposed by Ruderman and Kittel and later extended by Kasuya and Yosida to give the theory now generally know as the RKKY interaction. We will briefly explain how this interaction works for SAF: the indirect exchange couples moments over relatively large distances; this is the dominant exchange interaction in metals because there is little or no direct overlap between neighboring magnetic electrons. It therefore acts through an intermediary - which in metals are the conduction electrons (itinerant electrons).

The interaction is characterized by a coupling coefficient, j, given by:

$$j(R_l - R_{l'}) = 9\pi\left(\frac{j^2}{\varepsilon_F}\right)F(2k_F|R_l - R_{l'}|) \tag{5.1}$$

where k_F is the radius of the conduction electron Fermi surface, R_l and $R_{l'}$ are the lattice positions of the point moment, ε_F is the Fermi energy and $F(x) = \frac{x\cos x - \sin x}{x^4}$.

The RKKY exchange coefficient, j, oscillates from positive to negative as the separation lenght changes and has the damped oscillatory nature shown in Fig. 5.2.

Therefore, depending upon the separation between a pair of ions their magnetic coupling can be ferromagnetic or antiferromagnetic. A magnetic ion induces a spin polarization in the conduction electrons in its neighborhood. This spin polarization in the itinerant electrons is felt by the moments of other magnetic ions within range, leading to an indirect coupling.

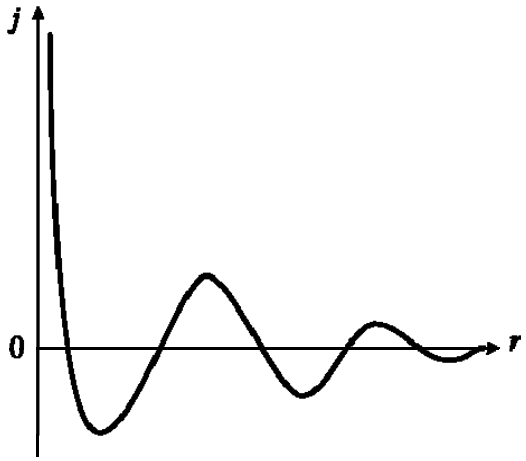

Figure 5.2. Variation of the indirect exchange coupling constant, j , of a free electron gas in the neighborhood of a point magnetic moment at the origin $r = 0$ [91].

In rare-earth metals, whose magnetic electrons in the *4f* shell are shielded by the *5s* and *5p* electrons, direct exchange is rather weak and insignificant and indirect exchange via the conduction electrons gives rise to magnetic order in these materials.

The SAF materials are designed such way that the coupling is antiferromagnetic.

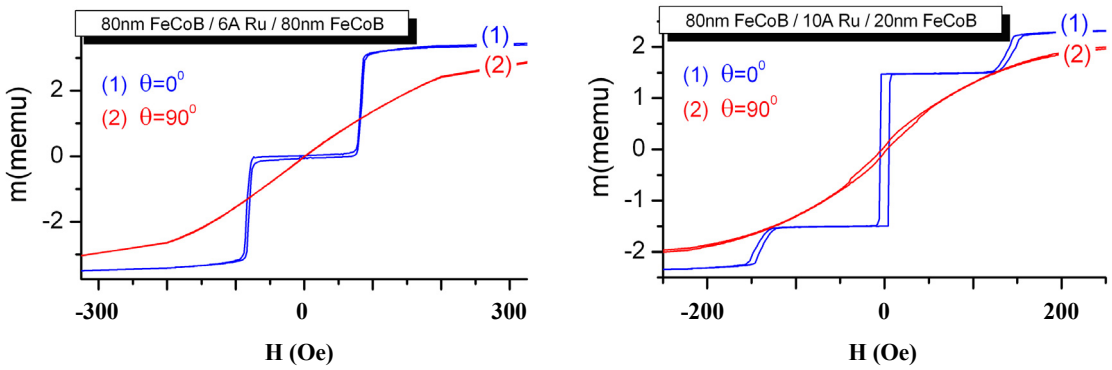

Figure 5.3. Hysteresis loop of the SAF typical samples; on left a structure with symmetric ferromagnetic layer; on right a structure with asymmetric layer thickness [92]

Shown in Fig. 5.3 are two typical examples of the hysteresis loops of SAF samples for two different magnetic field orientations, as presented in a previous paper [92]. On the left we present a hysteresis loop for a symmetric SAF sample with ferromagnetic layers thickness 80 nm separated with a 6 Å Ru interlayer and on the right we present a hysteresis loop of an asymmetric SAF with the ferromagnetic layers thicknesses 80 nm and 20 nm separated with and a 10 Å layer of Ru. Both samples have very well defined anisotropy axes with sharp transitions of magnetization for the field applied along the easy axis ($\theta = 0$). It can be seen the almost perfect compensation of magnetization at zero applied field in the case of symmetric SAF (left) while, as expected, a significant remanent magnetization is observed for the asymmetric SAF structure (right). For the latter sample and in the case of the applied field along the easy axis one observes also a supplementary transition from a $(0,\pi)$ to a $(\pi,0)$ configuration with a direct write field value of about 5 Oe. While clear magnetization transitions are observed for field orientations close to easy axis these become less pronounced as the field direction approaches the hard axis ($\theta = 90°$).

Although not so complicated as a structure, SAF is an important component of modern magnetic devices with a rather complicated magnetic behavior, as it is shown in the

appendices A.3 and A.4. In A.3 we present in detail the SAF technological applications and in A.4 we review the theoretical work done for the understanding of the magnetization switching in coupled thin films (in particular for SAF).

5.2. Synthetic Antiferromagnet (SAF) Critical Curve

5.2.1. SAF samples description

The SAF samples under study were thin film multilayer structures deposited on glass substrate. The samples were provided by Dr. Ganping Ju from Seagate Technology, Pittsburgh, PA. The first (bottom) ferromagnetic layer is FeCoB, the second layer is a non-magnetic metal, Ru, and the third, ferromagnetic layer is again FeCoB. On top of the third layer we have a C overcoat layer for surface protection. These samples were deposited at room temperature with DC magnetron sputtering with a base vacuum pressure below 3×10^{-9} Pa. The samples were cut in 5 mm diameter disk coupons.

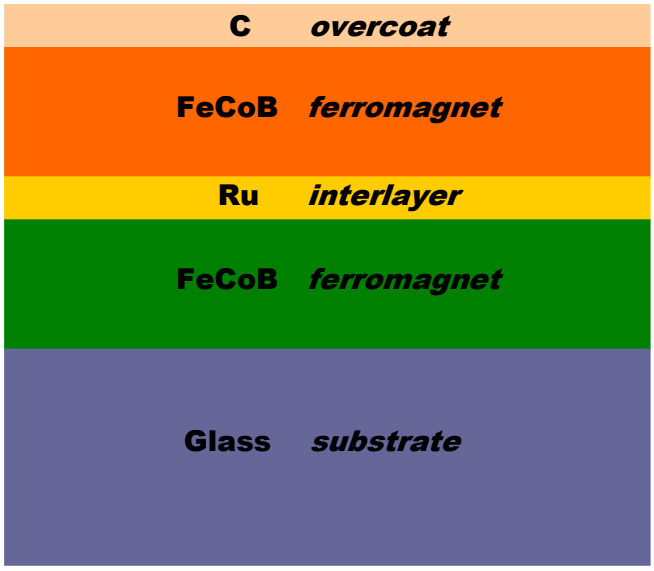

Figure 5.4. SAF samples structure (not at scale)

Three series of samples were produced; with the (t1, t2) thickness of the FeCoB layers (80 nm, 80 nm), (50 nm, 50 nm) and (80 nm, 20 nm) and with the Ru interlayer thickness ranging from 0 to 20 Å. It is important to mention that several series of samples was produced because the exact Ru thickness that will provide the antiferromagnetic coupling between the two ferromagnetic layers was not precisely known beforehand.

Therefore, only few of these samples were actually SAF structures; among the few selected we have chosen to discuss only the ones that better illustrates the use of our experimental method.

Hysteresis curves, along different directions in the plane of the samples, were measured by a vibrating sample magnetometer (VSM), as shown in Fig. 5.5.

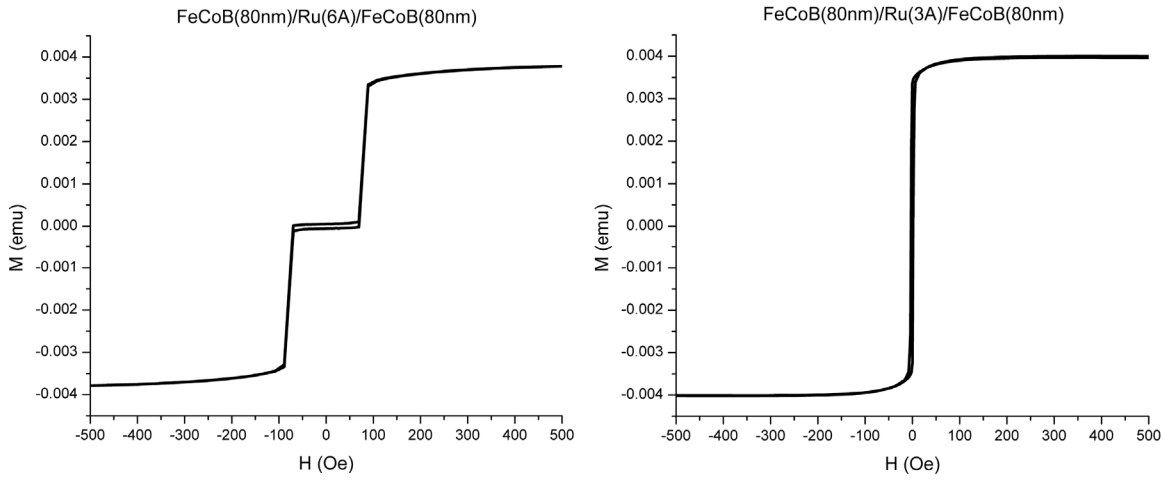

Figure 5.5. Example of $H_{dc} \,||\, EA$ hysteresis curves for a SAF structure (left) and for a multilayer structure without SAF characteristics (right)

As primary selection criteria, if the hysteresis curve, recorded when the H_{dc} is parallel to the easy axis, shows the antiferromagnetic coupling, then the samples is a SAF structure and we proceed to susceptibility experiments, in order to determine the switching characteristics.

5.2.2. The Reversible Susceptibility Tensor of a Synthetic Antiferromagnet

In this section we will present the study of the reversible susceptibility tensor, as being generalized from the transverse susceptibility components, in the case of a SAF structure. Knowing the magnetic anisotropy of a SAF structure is essential for the device functioning and the transverse susceptibility is one of the best methods to determine magnetic anisotropy and switching properties of magnetic systems.

First proposed by Aharoni [33], the theoretical study of transverse susceptibility model (TS) was improved by taking into account magnetic systems with different types of anisotropy [45] or studying the effect of interactions and thermal relaxation. In all the publication until that point, the transverse susceptibility for a specific free energy expression was evaluated employing a free energy minimization method. The disadvantage of this approach is the lack of generality and the difficulty of describing reversible transverse susceptibility (RTS) for magnetic systems with more complex free energy expressions. A new theoretic approach [47], based on magnetization vector dynamics, as described by the Landau–Lifshitz equation of motion, was capable of determining the susceptibility tensor for virtually any magnetic systems if an expression of its free energy was known. The core of this breakthrough was that the traditional TS experiment was proven to be, in fact, the zero-frequency limit of the ferromagnetic resonance (FMR). We will proceed now to see how this approach is applied to a SAF structure, as presented by Cimpoesu [93].

In a susceptibility experiment it is required to apply two magnetic fields: a *dc* field H_{dc} which can be varied in a large range, and a small perturbing *ac* field $H_{ac} = H_{ac,0}e^{i\omega t}$. The magnetization variation is then measured. In the absence of thermal agitations the dynamics

of the magnetization M of a single-domain particle is governed by the Gilbert equation that can be written in the Landau-Lifshitz form as:

$$\frac{dM}{dt} = -\gamma M \times H_{eff} - \frac{\alpha\gamma}{M_S} M \times (M \times H_{eff}) \tag{5.2}$$

where $\gamma = \frac{|\gamma_0|}{1+\alpha^2}$ is the gyromagnetic ratio, with $|\gamma_0| = 2.211 \times 10^5$ m/As and α is the phenomenological Gilbert damping constant. $H_{eff} = -\frac{\partial F}{\mu_0 V \partial M} + H_{ac}$ is the effective field and it incorporates the effects of different contributions in the free energy F (that contains the *dc* field) and the small, time-dependent, *ac* field, with V being the volume of the particle. In order to preserve the magnetization's magnitude the Landau-Lifshitz-Gilbert (LLG) equation can be expressed better in spherical coordinates (M_S, θ, φ). The singularities of the spherical coordinates along the polar axis can be avoided by an adequate choice of the Oz axis. Thus the time variation of the magnetization direction is given by:

$$\begin{aligned} \frac{d\theta}{dt} &= \gamma(H_\varphi + \alpha H_\theta) \\ \frac{d\varphi}{dt} &= \frac{\gamma(\alpha H_\varphi - H_\theta)}{\sin\theta} \end{aligned} \tag{5.3}$$

where $H_\theta = -\frac{F_\theta}{\mu_0 V M_S} + H_{ac,\theta}$ is the polar component of the effective field and $H_\varphi = -\frac{F_\varphi}{\mu_0 V M_S \sin\theta} + H_{ac,\varphi}$ is the azimuthal component of the effective field; $F_\theta = \frac{\partial F}{\partial \theta}$ and $F_\varphi = \frac{\partial F}{\partial \varphi}$. The time varying *ac* field will produce a dynamic component of the magnetization displaced with $\delta M = (0, M_S \delta\theta, M_S \sin\theta \delta\varphi)$ from the static equilibrium position.

SAF consists of two ferromagnetic layers 1 and 2 that have the thickness t_1 and t_2, and magnetizations M_1 and M_2, respectively, coupled through a nonmagnetic spacer. Assuming that the two magnetic layers behave like two single domain particles, the time evolution of the system is described by the coupled equations of motion for each magnetization. Similarly with the derivation presented in the ferromagnetic resonance (FMR) reference book [49], by solving the inhomogeneous system of linear equations on the deviations $\delta\theta_i$ and $\delta\varphi_i$ from the static equilibrium position, the susceptibility tensor χ in the laboratory reference system (x, y , z), defined by $\delta\widetilde{\mathrm{M}} = \chi \cdot H_{ac}$, with $\delta\widetilde{\mathrm{M}}$ the variation of the total magnetic moment, can be obtained as

$$\chi = \mu_0 M_1^2 V_1^2 \begin{bmatrix} \mathrm{T}_1 & \mathrm{T}_2 \end{bmatrix} \mathrm{D} \mathrm{A}^{-1} \Lambda \mathrm{D} \begin{bmatrix} \mathrm{T}_1^t \\ \mathrm{T}_2^t \end{bmatrix} \tag{5.4}$$

where:

$$\mathrm{A} = \Lambda \cdot \left(\Xi\right)_{ij} + \mathrm{i}\,\frac{\omega}{\gamma}\,\mu_0\,\mathrm{M}_1 V_1\,\mathrm{Diag}\left(1,-1,mt,-mt\right)$$

$$\Lambda = \mathrm{Diag}\left(\Lambda_0,\Lambda_0\right), \quad \Lambda_0 = \begin{bmatrix} \alpha & 1 \\ -1 & \alpha \end{bmatrix}$$

$$\mathrm{D} = \mathrm{Diag}\left(1,1,mt,mt\right)$$

$$\Xi_{ij} = \begin{bmatrix} F_{\theta_i\theta_j} & \dfrac{F_{\theta_i\varphi_j}}{\sin\theta_j^0} \\ \dfrac{F_{\theta_j\varphi_i}}{\sin\theta_i^0} & \dfrac{F_{\varphi_i\varphi_j}}{\sin\theta_i^0\sin\theta_j^0} \end{bmatrix}$$

$$\mathrm{T}_i = \begin{bmatrix} \cos\theta_i^0\cos\varphi_i^0 & -\sin\varphi_i^0 \\ \cos\theta_i^0\sin\varphi_i^0 & \cos\varphi_i^0 \\ -\sin\theta_i^0 & 0 \end{bmatrix}$$

and $m = M_2/M_1$, $t = t_2/t_1$, $V_1 = St_1$ is the volume of first layer, with S the area, $F_{\theta_i\theta_j}, F_{\theta_i\varphi_j}, F_{\varphi_i\varphi_j}$ are the second derivatives of free energy density at the static equilibrium position $\left(\theta_i^0, \varphi_i^0\right)$, and Diag is the diagonal matrix.

The element χ_{lp} of the tensor (5.4) is thus describing the response of the total magnetization in the *l*-th direction from an incremental change in the *p*-th direction of the applied field. If the *Oz* axis is parallel to the direction of the biasing *dc* field then the diagonal elements are the parallel susceptibility (PS) χ_{zz} measured in the field direction, and the two transverse susceptibilities (TS) χ_{xx} and χ_{yy}, measured perpendicular to the bias field direction. As it results from (5.3) the susceptibility is complex and depends on the *ac* field's frequency, ω, and on the damping constant, α.

For low values of the frequency of the *ac* field ($\omega \to 0$) it may be assumed that the magnetization lies in a minimum of the free energy at any moment, and the change of the applied field provides only reversible changes of magnetization (i.e. processes that involve no loss of energy), as is the case in Aharoni's model. In this case the reversible susceptibility tensor is given by:

$$\boldsymbol{\chi} = \mu_0 M_1^2 V_1^2 \begin{bmatrix} \mathrm{T}_1 & \mathrm{T}_2 \end{bmatrix} \cdot \mathrm{D} \cdot \left(\Xi\right)_{ij}^{-1} \cdot \mathrm{D} \cdot \begin{bmatrix} \mathrm{T}_1^{\mathrm{t}} \\ \mathrm{T}_2^{\mathrm{t}} \end{bmatrix} \tag{5.5}$$

In Eq. 5.5 the imaginary part and the dependence of damping constant, α, are eliminated.

The equations 5.4 and 5.5, due to their generality, are able to describe the susceptibility of a SAF coupled magnetic systems with virtually any type of anisotropy, any orientation of the anisotropy's axes and any type of interactions between the two layers.

Using this general approach it is possible to calculate not only TS and PS but all the susceptibility tensor's components and/or the susceptibility along any direction. This is very useful when the susceptibility along different directions, not only transverse to *dc* field, it is measured [32, 92].

If we assume that:

- the thin film sample and the *dc* field lie in the *xOz* plane,

- both ferromagnetic layers have uniaxial anisotropy with the easy axes in the sample's plane,

- the *ac* field is also applied in the sample's plane,

then, due to symmetry reasons the magnetizations $\mathbf{M}_i$ will lie in the *xOz* plane as well and the energy density [94] can be expressed by:

$$F = 2K_{u1}t_1\left\{-\left(h_x\cos\theta_1 + h_y\sin\theta_1\right) - mt\left(h_x\cos\theta_2 + h_y\sin\theta_2\right) - \frac{1}{2}\left[\cos^2\left(\theta_1-\theta_{K1}\right) + kt\cos^2\left(\theta_2-\theta_{K2}\right)\right] + h_J\cos\left(\theta_1-\theta_2\right)\right\} \tag{5.6}$$

where θ_{K1} and θ_{K2} denote the easy axes angle, K_{u1} and K_{u2} the anisotropy constants, $h_x = \frac{H_x}{H_{k1}}$ and $h_y = \frac{H_y}{H_{k1}}$ the applied field components, $H_{k1} = \frac{2K_{u1}}{\mu_0 M_1}$, $k = \frac{K_{u2}}{K_{u1}}$, and h_J the exchange coupling strength between the two layers (with $h_J < 0$ or $h_J > 0$ for ferromagnetic/antiferromagnetic coupling). The diagonal elements of the reversible susceptibility tensor can be written as:

$$\chi_{xx} = \mu_0 M_1^2 V_1^2 \frac{F_{\theta_2\theta_2}\cos^2\theta_1 - 2mt\,F_{\theta_1\theta_2}\cos\theta_1\cos\theta_2 + m^2t^2\,F_{\theta_1\theta_1}\cos^2\theta_2}{F_{\theta_1\theta_1}F_{\theta_2\theta_2} - F_{\theta_1\theta_2}^2}$$

$$\chi_{yy} = \mu_0 M_1^2 V_1^2 \frac{F_{\varphi_2\varphi_2}\sin^2\theta_1 - 2mt\,F_{\varphi_1\varphi_2}\sin\theta_1\sin\theta_2 + m^2t^2\,F_{\varphi_1\varphi_1}\sin^2\theta_2}{F_{\varphi_1\varphi_1}F_{\varphi_2\varphi_2} - F_{\varphi_1\varphi_2}^2} \qquad (5.7)$$

$$\chi_{zz} = \mu_0 M_1^2 V_1^2 \frac{F_{\theta_2\theta_2}\sin^2\theta_1 - 2mt\,F_{\theta_1\theta_2}\sin\theta_1\sin\theta_2 + m^2t^2\,F_{\theta_1\theta_1}\sin^2\theta_2}{F_{\theta_1\theta_1}F_{\theta_2\theta_2} - F_{\theta_1\theta_2}^2}$$

From Eqs. 5.6 and 5.7 we observe that for a SAF systems the diagonal elements of the reversible susceptibility will vary inverse proportionally with the discriminant of the free energy for the coupled magnetic thin films, and their singular points are zeros of the free energy discriminant, namely that the susceptibility is a measure of the "curvature" of free energy.

Next, in Fig. 5.6 are shown the field variation of the normalized total magnetic moment and the variation of the reversible susceptibility χ_{xx} for a symmetric SAF structure with the easy axes of the two layers parallel to each other and along *Ox* axis for two orientations of the *dc* field and for two coupling strengths.

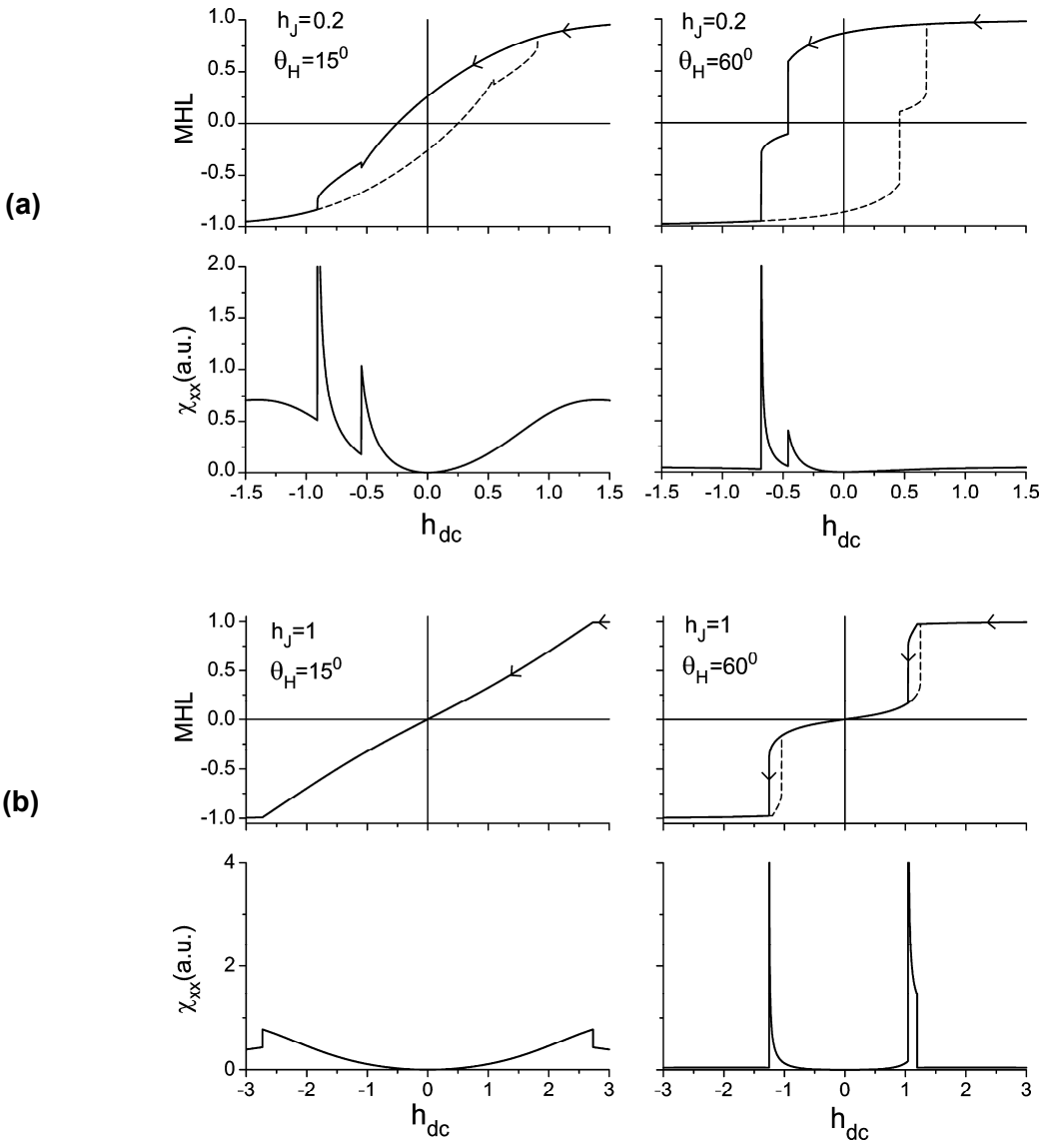

Figure 5.6. Major hysteresis loop and χ_{xx} for symmetric SAF structure for two orientations of the *dc* field $\theta_H = 15^\circ$ and $\theta_H = 60^\circ$, and for two coupling strength: (a) $h_J = 0.2$ and (b) $h_J = 1$.

Depending of coupling strength and applied field orientation, the magnetization switching of the two layers from the SAF structure can be more or less visible in the hysteresis loops. For example, as it is shown in Fig. 5.6a, for a field applied along a direction which makes an angle of $\theta_H = 60^\circ$ with the easy axis the switching is very well defined.

However, for $\theta_H = 15°$ the switching events are not very well visible, and experimentally this can be very difficult to be observed form regular hysteresis loops. On the other hand, one observes that the susceptibility vs. field curves present sharp peaks at the field values at which magnetization switches for entire angular domain of the applied field. Thus, plotting on a polar chart the switching field vs. the field orientation one can obtain the SAF critical curve [94], i.e. the equivalent of the astroid from the Stoner-Wohlfarth model. For larger coupling strengths switching events could become difficult to observe even in the susceptibility curves as can be observed in Fig. 5.6b. In this case the switching will determine only a shoulder (still more visible than in the hysteresis loops) and not a very well defined peak in the susceptibility vs. field curve.

For these particular "shoulder" situations, the susceptibility does have its denominator (and discriminant of the free energy) equaled to zero at the switching point, but also, the numerator is zero, and the reversible susceptibility has only a removable singularity. In these cases the zeroes of the free energy discriminant will not determine very sharp peak in susceptibility signal.

5.2.3. Reversible susceptibility studies of magnetization switching in SAF

In this subchapter we will present how the reversible susceptibility experiments that we perform in order to characterize the switching properties of the SAF structures, are useful in solving current problems in increasing the scalability and decreasing the error rate of MRAM devices. These problems can be overcome with a new MRAM writing scheme proposed by Savtchenko [89], the "toggle MRAM". This scheme greatly increases the operating margin of MRAM elements. In the toggle writing procedure the MRAM free layer has a SAF structure and word and bit fields are applied at 45° with respect to easy axis of the

magnetic anisotropy of the MRAM element. The toggle switching is achieved using a suitable time sequence for word and bit fields which rotate the effective magnetic moment vector of the MRAM cell, as described in Appendix A3.3. Recently, several studies were devoted to the use of the new writing scheme in order to optimize the magnetic parameters for toggle-MRAM [94-96]. The theoretical studies of the toggle writing mode in MRAM uses the concepts of SAF critical curve [94] which is a generalization of the well-known astroid from the coherent rotation model in the case of uniaxial anisotropy. The critical curve for a SAF structure is obtained as the envelope of the field trajectories giving a constant angle to the magnetization of one of the two layers, leaving the other as a variable in the field plane. Depending of the coupling strength between the two ferromagnetic layers in SAF structure the critical curve evolves from a simple astroid at zero coupling to a more complicated critical curves for larger coupling field values [94]. The SAF critical curve (see Figs. A4.6 and 5.7) is composed of two parts: the critical field curve for saturation which is the outermost envelope of the constant angle contours and the critical curves for switching which are the inner envelopes. Outside critical curve for saturation the magnetization directions in the two ferromagnetic layers becomes parallel.

The toggle switching mode is achieved only for specific field trajectories in the field plane with respect to the inner envelopes. Consequently, knowing the configuration of the SAF critical curve is of great importance in order to control its switching characteristics.

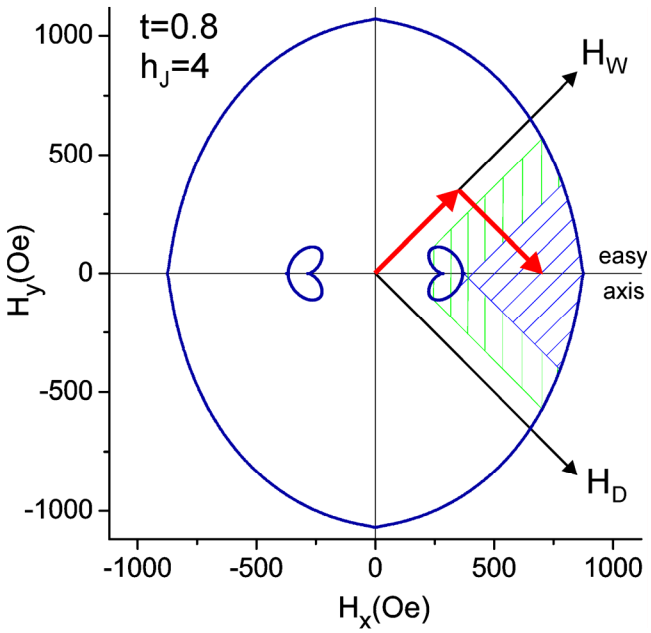

Figure 5.7. Critical Curve and the operating field margins for toggle mode (blue) and direct write mode (green); conditions for direct/toggle mode are shown on these theoretical critical field curves obtained by Fujiwara [94]. The toggle mode switching occurs for those field trajectories going around the interior part of the astroid.

Although several papers dealing with theoretical aspects of the critical curves for SAF systems [94, 96, 97] were published to date, due to the fact that switching critical curve is more complex in the case of SAF than in the case of a single magnetic layer, there are no other published experimental results in which the critical curves are determined for antiferromagnetically coupled magnetic layers.

In the case of the astroid, the general case of the critical curve for a single magnetic layer, the tangent to the astroid passing through the tip of the external applied field vector **h** in the $\left(h_x, h_y\right)$ plane gives the orientation of the magnetization at equilibrium for that particular field value and direction [24]. Moreover, the parameter value in the tangent point of the parametric critical curve has a value equal to the angle that gives the orientation of the magnetization with respect to the easy axis. For SAF the tangent at the critical curve passing

through the point representing the external applied field in the (h_x, h_y) plane gives the orientation of the first layer θ_1 while the orientation of the second layer θ_2 can be read from the position of the tangent point on the critical curve.

The relative low magnetic signal of the thin film layers in the SAF structure is another reason that makes difficult the experimental measurement of SAF critical curves. By applying same method that we use for another magnetic systems [31, 32], as presented in chapter 4, we will continue now with the experimental study of the switching characteristics of a series of SAF structures.

Hysteresis curves, along different directions in the plane of the samples, are measured by a vibrating sample magnetometer (VSM). The reversible susceptibility experiments are performed at room temperature using the TDO experimental setup. As in the other TDO-based experiments, the samples are placed in the sensing coil with both *ac* and *dc* field in the plane of the sample. The easy axis is oriented parallel to the direction of the *ac* field. The *dc* magnetic field is created by an electromagnet placed on a revolving stage with a protractor for measurement of the field direction.

The reversible susceptibility signal is recorded for different orientations of the applied *dc* field with respect to the sensing coil axis, and easy axis. For a given orientation of the applied *dc* field with respect to the sensing coil axis the measured susceptibility signal is a combination of transverse and longitudinal susceptibility. As it was shown previously in chapter 2, as in the case of a single thin film, this composite susceptibility signal still preserves the same singularities characterizing the switching fields from transverse susceptibility.

It was shown in the subchapter 5.2.2 that for the SAF systems the reversible

susceptibility signal varies inverse proportionally with the discriminate $D = F_{11}F_{22} - F_{12}^2$ of the free energy for the coupled magnetic thin films, $\chi_{xx} \propto \frac{1}{D(\theta_1, \theta_2)}$ where F_{11}, F_{22} and F_{12} are the second order derivative of the total free energy F of the SAF with respect to θ_1 and θ_2 which give the magnetization equilibrium orientations in the two magnetic layers. The singular points of χ_{xx} are zeros of the free energy discriminant which are points of the critical curve.

Shown in Fig. 5.8a and Fig. 5.9a are two typical examples of the hysteresis loops of the investigated SAF samples for two different magnetic field orientations. Figure 5.8a presents hysteresis loop of symmetric SAF sample with ferromagnetic layers thickness 80 nm separated with a 6 Å Ru interlayer and the Figure 5.9a presents hysteresis loop of an asymmetric SAF with the ferromagnetic layers thicknesses 80 nm and 20 nm separated with and a 10 Å layer of Ru. Both samples have very well defined anisotropy axes with sharp transitions of magnetization for the *dc* field applied along the easy axis $(\theta = 0^\circ)$.

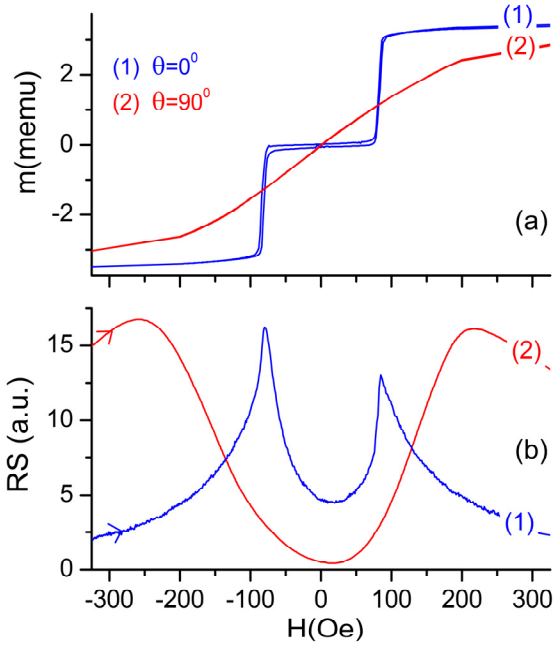

Figure 5.8. Hysteresis (a) and susceptibility (b) for a symmetric SAF sample with FeCoB ferromagnetic layers thickness of 80 nm separated by a 6 Å Ru interlayer

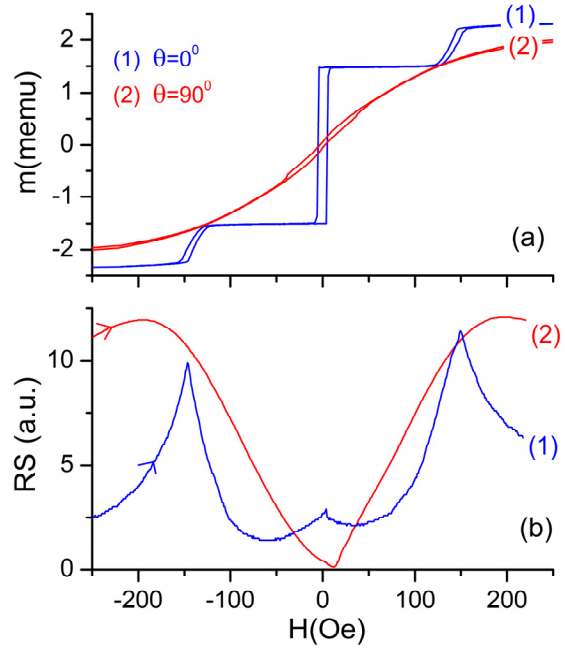

Figure 5.9. Hysteresis (a) and susceptibility (b) for a asymmetric SAF sample with FeCoB ferromagnetic layers thickness of 80 nm and 20 nm separated by a 10 Å Ru interlayer

At zero applied *dc* field, in the case of symmetric SAF, as shown in Fig. 5.8a, the

magnetization is perfectly compensated, while, a significant remanent magnetization is observed for the asymmetric SAF structure in Fig. 5.9a.

For the asymmetric sample and in the case of the applied field along the easy axis we identify a supplementary transition from a $(0,\pi)$ to a $(\pi,0)$ configuration with a direct write field value [98] of about 5 Oe. While clear magnetization transitions are observed for field orientations close to easy axis these become less pronounced as the field direction approaches the hard axis ($\theta = 90°$). However, the susceptibility vs. applied field curves present clear maxima at transition points in virtually entire angular domain.

The susceptibility curves at two field orientations ($\theta = 0^{\circ}$ and $\theta = 90°$) for symmetric and asymmetric SAF samples are presented in Fig. 5.8b and Fig. 5.9b, respectively. For clarity only the negative to positive saturation field sweep was shown (see arrow). In the case of symmetric SAF sample two peaks per field sweep are observed which correspond to the spin flop field H_{sf} and return field H_r [98]. The susceptibility curve along the easy axis for the asymmetric SAF sample has three peaks per sweep that besides the H_{sf} and H_r peaks also include the direct write field peak mentioned above.

After a set of the susceptibility vs. applied field experimental curves was performed along different directions in respect to the easy axis, the critical curve was obtained by plotting all the identified peaks as a function of field direction in a polar chart.

The critical curve for the symmetric SAF structure is shown in Fig. 5.10 (left). The right hand side inserts represent the magnetization (top) and susceptibility (bottom) curves at an intermediate field orientation ($\theta = 45°$).

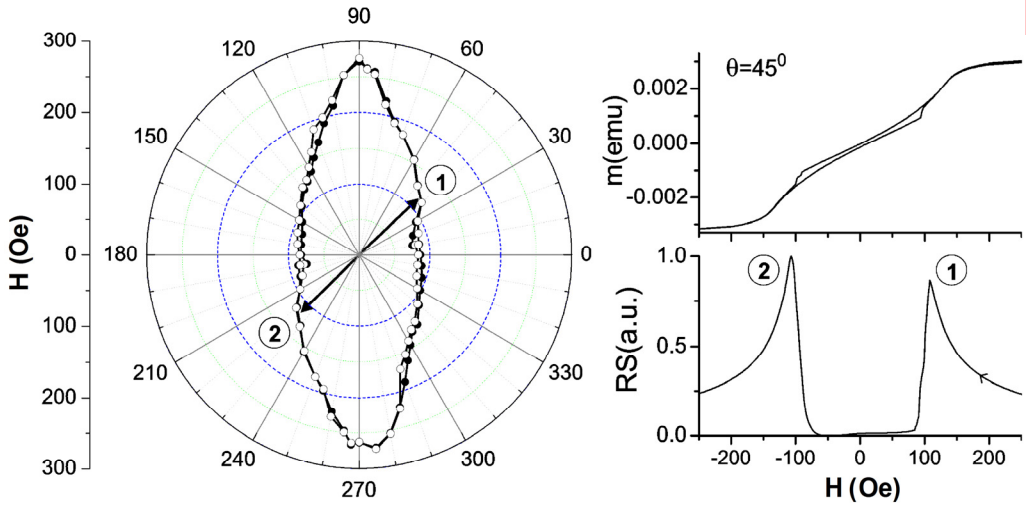

Figure 5.10. Critical curve (left) and hysteresis + susceptibility (right) for a symmetric SAF sample with FeCoB ferromagnetic layers thickness of 80 nm separated by a 6 Å Ru interlayer, for $\theta = 45°$ [92]

Full symbols (dots) correspond to the susceptibility signal peaks observed in the positive-to-negative field scan while the open symbols (circles) correspond to the peaks observed in the negative-to-positive field scan. The full and open symbols coincide for almost entire angular domain, a behavior that is due to very small differences between the return H_r and spin flop H_{sf} fields for this particular sample. The obtained critical curve is just the saturation curve of the SAF structure. The saturation critical curve has a switching field of 84 Oe along the easy axis and 275 Oe along the hard axis. As stated previously, as the coupling between layers increases, the inner critical curves become very small and cannot be easily observed experimentally with field scans along directions passing through the origin of the (h_x, h_y) plane. In this case a more elaborated, original, *dc* field scan procedure will be employed to reveal other features of the critical switching curve, as presented in the next subchapter.

5.2.4. Measurement of the critical curve of a synthetic antiferromagnet

As seen in the previous subchapter, the 2D-switching can be fully described using the concept of critical curve (CC), which is the locus of in-plane fields at which the irreversible magnetization reversal occurs [13, 14]. We know now that the critical curve is not only a theoretical concept to describe the magnetization reversal in magnetic systems, but also an important technological parameter for magnetic devices [26, 27, 42, 99] like MRAM. Several methods for CC determination were proposed and the obtained experimental critical curves were compared against the astroid corresponding to a magnetic uniaxial system [27, 100]. What make the SAF critical curve determination difficult are the inner features, the CC for switching. Next, we will propose a method capable of full determination of the SAF critical and to characterize its switching characteristics, but first we will shortly review the essential parts of CC theory.

The free energy, F landscape for every magnetic system at a given value of applied magnetic field presents a series of relative minima and maxima separated by energy barriers. At equilibrium the magnetic system will be found in one of its stable state corresponding to one of the free energy minima. As the field is changing, the configuration of maxima and minima will be altered and the stable states of magnetization will shift, and if precessional effects are neglected, the system will remain in its state of free energy minimum. However, for a critical field value the energy barrier adjacent to the system's energetic minimum will disappear and the stable state will switch to a neighboring minimum. The critical curve is in essence the locus of these critical field values. In the case of a single magnetic film, a sufficient condition for a critical state is to have $\frac{dF}{d\theta}=0$, $\frac{d^2F}{d\theta^2}=0$, and $\frac{d^3F}{d\theta^3}\neq 0$ simultaneously, where the angle θ describes the magnetization's orientation.

For coupled films as SAF the problem is more complicated because requires to find the critical states of magnetic free energy function of two variables , θ_1 and θ_2. In this case the critical states can be found as the solutions of the sufficient conditions: $\frac{\partial F}{\partial \theta_1} = \frac{\partial F}{\partial \theta_2} = 0$,

and $\delta(\theta_1, \theta_2) = \left(\frac{\partial^2 F}{\partial \theta_1 \partial \theta_2}\right)^2 - \left(\frac{\partial^2 F}{\partial \theta_1^2}\right)\left(\frac{\partial^2 F}{\partial \theta_2^2}\right) = 0$.

We use the susceptibility because this method is more sensitive over the magnetic and resistance hysteresis methods. For a SAF system, the in-plane diagonal elements of the reversible susceptibility tensor varies inversely proportional with the free energy discriminant, δ, (the determinant of free energy's Hessian) computed at the equilibrium position $\left(\theta_1^0, \theta_2^0\right)$, namely $\chi \propto \frac{1}{\delta\left(\theta_1^0, \theta_2^0\right)}$.

The tensor $\chi_{ij} = \frac{\partial M_i}{\partial H_j}$ is obtained as the derivative of components of magnetization M with respect to components of applied field H, and i and j refer to the directions. In this way, the problem of finding CC of coupled magnetic films is reduced to the determination of the singular points of susceptibility.

By probing the reversible susceptibility for different in-plane applied fields and identifying the susceptibility's peaks located at the switching fields, one can find experimentally the CC of coupled magnetic films.

The numerical simulation [101] of the reversible susceptibility's field variation with the in-plane *dc* field applied at different orientations θ_H, identifying the field values for which the susceptibility is singular, proves the suitability of this method. The critical curve obtained in this way is shown in Fig. 5.11.

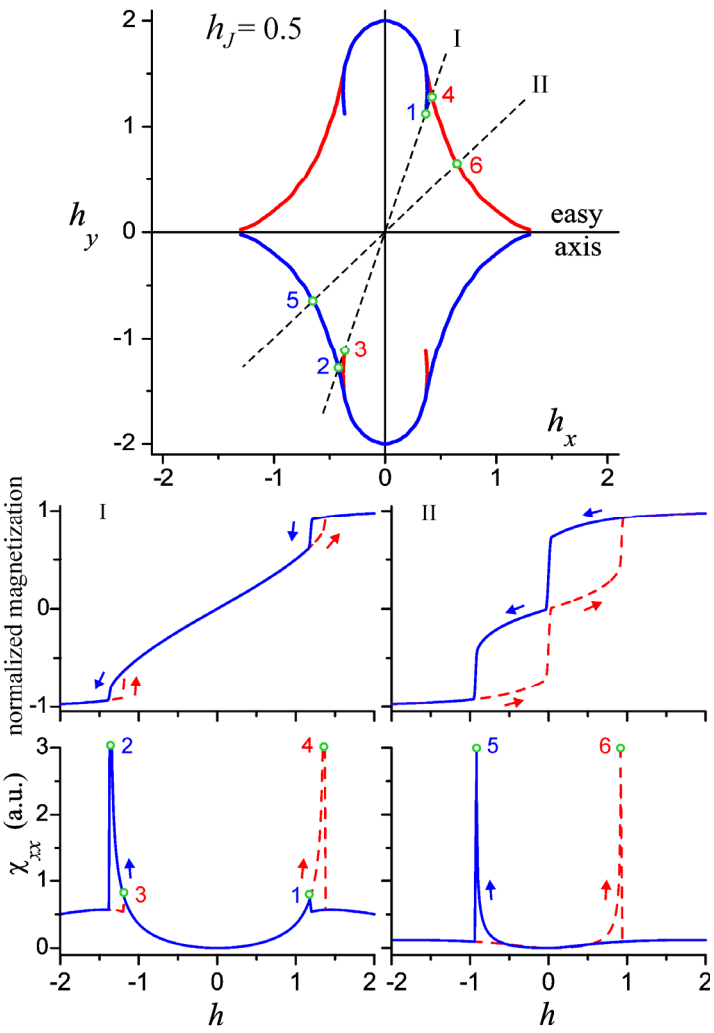

Figure 5.11. Top: CC for a symmetric SAF with a coupling $h_J = 0.5$, determined from susceptibility's curves. Middle: the projection of the normalized magnetization on the applied field's direction. Bottom: peaks locations, as the in-plane *dc* field is applied at different orientations. [101]

The susceptibility and hysteresis curves for two different orientations, for a symmetric SAF with the coupling $h_J = 0.5$, are presented in the middle and the bottom panels of Fig. 5.11, respectively, the magnetic field sweeping from positive saturation to negative saturation (continuous line) and then back to positive saturation (dotted line).

Depending on applied field orientation, the magnetizations' switching can be more or less visible in the hysteresis loops. For a field applied along the second direction (denoted

with II in Fig. 5.11), the switching is very well defined, while for the first orientation (denoted with I), the switching events are not very visible.

In contrast with the hysteresis loops, we observe that the susceptibility versus field curves presents well defined peaks. For the first orientation, the susceptibility curve has two peaks (denoted with 1 and 2 in Fig. 5.11) when the *dc* field sweeps from positive saturation, when the field crosses the interior CC (corresponding to saturation) and the exterior CC (corresponding to switching), and only one peak for the second orientation, because in this case the field trajectory crosses only the exterior CC. When the field trajectory crosses the CC for saturation, both reversible susceptibility's denominator and numerator are zero and the reversible susceptibility has only a removable singularity and will not determine always a very sharp peak in susceptibility. When the field trajectory crosses the CC for switching, only the denominator is zero and the reversible susceptibility has a pole or an essential singularity, which is very visible in susceptibility.

However, the method presented in Fig. 5.11 does not reveal the entire interior CC because there are portions where the field trajectory is "almost" tangent to it, and a very small increment of θ_H is required in order to build the entire CC. Nevertheless, in an experiment, the θ_H 's increment cannot be smaller than the protractor's angle division's unit, and a strategy to make these portions "visible" is to use field scans that do not pass through origin, applying a bias field perpendicular to easy axis and our initial sweeping field parallel to easy axis, as illustrated in Fig. 5.12.

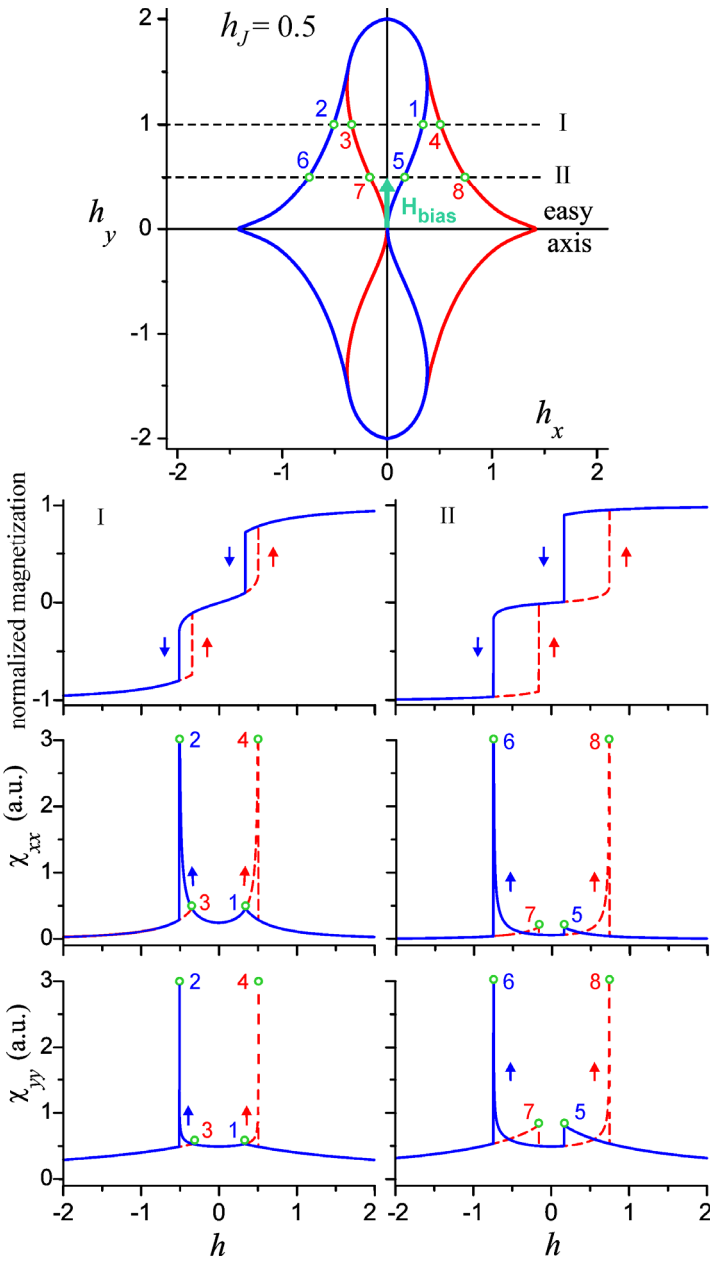

Figure 5.12. Top: CC for a symmetric SAF with coupling $h_J = 0.5$, as the in-plane *dc* field is swept along easy axis, and a hard axis *dc* bias field is also applied. Middle: the projection of the normalized magnetization on the sweeping field's direction. Bottom: parallel and perpendicular susceptibility peaks locations, as the hard axis *dc* bias field is applied at different amplitudes along hard axis. [101]

In order to better identify the susceptibility's peaks and to plot the saturation CC, both χ_{xx} and χ_{yy}, measured parallel and perpendicular to easy axis, respectively, can be used. For

example, in Fig. 5.12, the χ_{xx} 's peaks 1 and 3 are more visible in the case I, compared with χ_{yy} 's peaks 1 and 3, while in the case II, the χ_{yy} 's peaks 5 and 7 are more pronounced.

For applications such as MRAM, the exchange coupling between the two layers should be strong enough to make toggle writing method possible, and in Fig. 5.13 the simulated curves for $h_J = 2$ are presented. With the increase of h_J, the CC for saturation expands and becomes the outermost curve, the inner curves being the CC for switching.

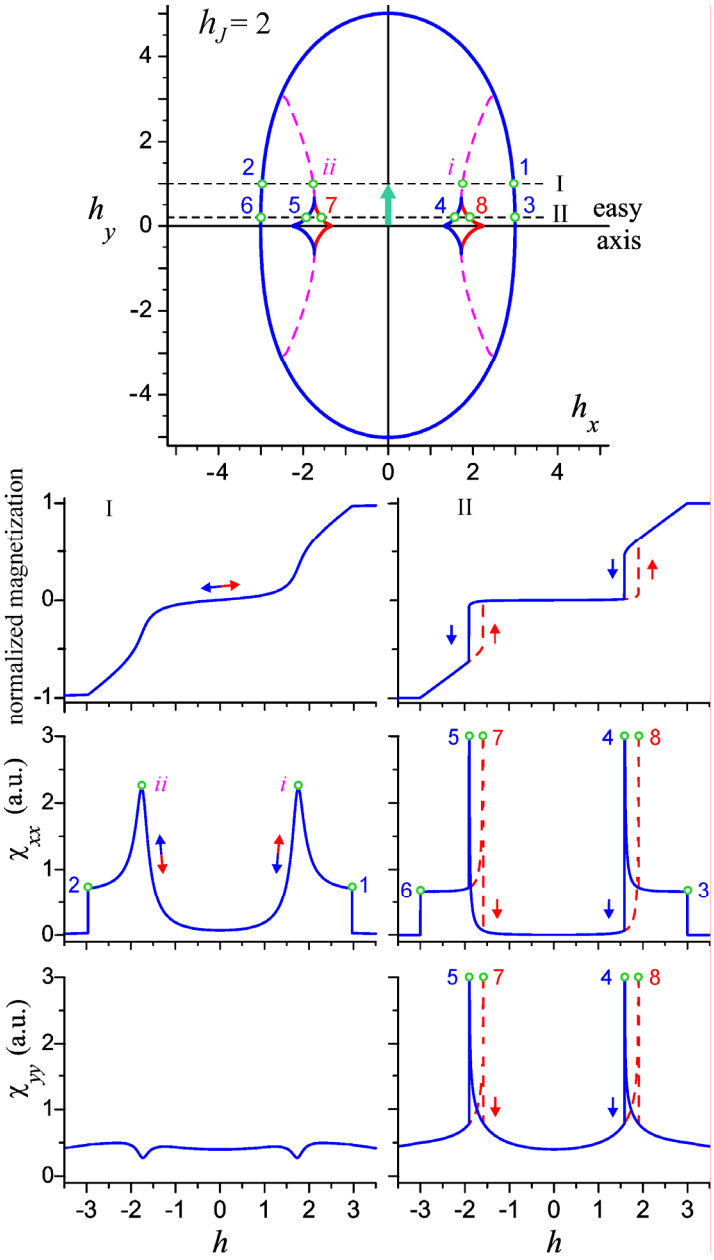

Figure 5.13. Top: CC for a symmetric SAF with coupling $h_J = 2$, as the in-plane *dc* field is swept along easy axis, and a hard axis *dc* bias field is also applied. Middle: the projection of the normalized magnetization on the sweeping field's direction. Bottom: parallel and perpendicular susceptibility peaks locations, as the hard axis *dc* bias field is applied at different amplitudes along hard axis. [101]

When the field crosses only the outermost CC, both the projection of the total magnetic moment on the sweeping field and susceptibility curves are reversible when the

field decreases and then increases. In this case, the intersection with the saturation CC determines only a shoulder (still more visible than in the hysteresis loops) and not a very well defined peak in the susceptibility curves. Moreover the susceptibility curve has two peaks (denoted with *i* and *ii* in Fig. 5.13) which are not determined by intersections with CC. These "false" peaks can be eliminated by looking only for the peaks of the curves which are not reversible, like in case II in Fig. 5.13.

To conclude our experiments, we proved that the reversible susceptibility singularities detection is one of the best methods that can reveal the entire CC for both low and high values of the exchange coupling in multilayer structures as SAF. Comparing the hysteresis and susceptibility curves, it was shown that susceptibility measurements are more appropriate for switching investigations of the SAF systems.

The method is general and can be applied for coupled films with asymmetrical layers. The use of an additional, bias, *dc* field is an original idea and it was put in practice on our experimental setup by adding an electromagnet on a perpendicular direction with respect to the field created by the initial one, as presented in chapter 3.

5.3 Summary

This chapter was dedicated to the experimental recording of critical curve for coupled thin films, in particular for the synthetic antiferromagnet (SAF) that has many technological applications, most interesting one being pinned and free layers for toggle MRAM.

The two ferromagnetic layers in a SAF type of structure are coupled together through a Ruderman-Kittel-Kasuya-Yosida (RKKY) type interaction. The first ferromagnetic layer is FeCoB, the second layer is a non-magnetic metal, Ru, and the third, ferromagnetic layer is again FeCoB. Depending of the coupling strength between the two ferromagnetic layers in

SAF structure the critical curve evolves from a simple astroid at zero coupling to a more complicated critical curves for larger coupling field values. There are no other published experimental results in which the critical curves are determined for antiferromagnetically coupled magnetic layers, so we propose a method capable of full determination of the SAF critical and to characterize its switching characteristics.

For a uniaxial system we have the sufficient conditions $\frac{\partial F}{\partial \theta}=0$ and $\frac{\partial^2 F}{\partial \theta^2}=0$ but for coupled films as SAF the problem is more complicated because requires to find the critical states of magnetic free energy function of two variables , θ_1 and θ_2. The critical states can be found as the solutions of the sufficient conditions $\frac{\partial F}{\partial \theta_1}=\frac{\partial F}{\partial \theta_2}=0$, and

$$\delta(\theta_1,\theta_2)=\left(\frac{\partial^2 F}{\partial\theta_1\partial\theta_2}\right)^2-\left(\frac{\partial^2 F}{\partial {\theta_1}^2}\right)\left(\frac{\partial^2 F}{\partial {\theta_2}^2}\right)=0$$

However, the initial TDO method did not reveal the entire interior CC because there are portions where the field trajectory is "almost" tangent to it. Therefore, the strategy proposed to make these portions "visible" is to use field scans that do not pass through origin, applying a bias field perpendicular to easy axis and our initial sweeping field parallel to easy axis. We proved that we can record the entire CC for the exchange coupled multilayers like SAF. Comparing the hysteresis and susceptibility curves, it was shown that susceptibility measurements are one of the best methods for switching investigations of the SAF systems. The method is general and can be applied for coupled films with asymmetrical layers. The use of an additional, bias, *dc* field is an original idea and it was put in practice on our experimental setup by adding an electromagnet on a perpendicular direction with respect to the field created by the initial one, as presented in chapter 3.

Conclusions

The subject of this dissertation, the magnetization dynamics, is a crucial technological parameter in designing devices using magnetic materials as non-volatile memories, reading heads, or sensors. Due to the geometric and electromagnetic constraints imposed by the specific device applications, modern magnetic devices have usually bi-dimensional geometries as thin films and multilayers, where the magnetization switching occurs in the plane of the device. Thus, controlling the two-dimensional magnetic switching is technologically valuable especially in devices using these new design ideas as in Magnetoresistive Random Access Memories (MRAM).

We presented at the beginning of this work the theoretical basis for a good understanding of magnetization dynamics including two essential models for critical curve and susceptibility studies: Stoner-Wohlfarth [15] and Aharoni [33]. In addition, the method of obtaining the critical curve from the susceptibility measurements was completely explained, in order to facilitate the understanding of the experimental TDO technique.

The 2D-switching can be fully described using the concept of critical curve, which is the locus of in-plane fields at which the irreversible magnetization reversal occurs. We focused our attention on critical curve determination for several magnetic systems with great emphasis on synthetic antiferromagnet (SAF) critical curve.

SAF has many technological applications as hard layer of exchange coupled composite media [87], soft underlayer for perpendicular recording [88], pinned and free layers for toggle MRAM cells [89], hard disk reading heads, or magnetic sensors [102]. The

performance of the devices using SAF structures relies heavily on their switching characteristics, which are governed by the individual reversal of the SAF composing ferromagnetic layers, and the interlayer-mediated interaction that exists between them. The simple critical curve theory of single films does not work for coupled films and an equivalent approach needed to be found.

In this work the experiment rely on the TDO susceptibility measurement method, based on the detection of singularities of reversible susceptibility experimental curves. This is a new, sensitive and simple method. The TDO experimental setup design was presented in detail underlining our original contribution to this measurement method, generally for thin film samples and particularly for the case of exploring SAF critical curve.

We improved the design of previously used TDO with a new way of increasing SNR as well as increasing the filling factor. All the trials and countless versions of the TDO design rewarded us with the capability of getting out the most of this technique in terms of sensitivity and stability. Both room temperature and low temperature measurements that were presented for several different samples demonstrated the reliability of this measurement technique.

An extensive programming effort was dedicated to the computer assisted operation of the TDO-based experiments and the result being a user friendly, versatile and error proof research instrumentation.

For SAF exploration a new way of recording the critical curve was proposed and supported with detailed analysis. It was shown that this method can reveal the entire critical curve for both low and high values of the exchange coupling [101]. Comparing the hysteresis

and susceptibility curves was shown that susceptibility measurements are more appropriate for switching investigations of the SAF systems [92].

One important conclusion that was made is that, in dealing with the problem of improving the density of data storage devices, like MRAM and toggle-MRAM, the magnetization switching is of crucial importance and therefore all efforts are justified for finding reliable ways of recording all the features appearing on the critical curve.

As suggested future research we would like to propose two main experimental directions: in terms of samples would be interesting to study SAF structures composed of different materials and with different coupling strength between the ferromagnetic layers and, in terms of instrumentation, we would like to integrate the TDO with a dilution refrigerator and use the susceptibility technique in exploring magnetic properties of new materials at mK temperatures.

References

[1] B. Hillebrands and K. Ounadjela, *Spin dynamics in confined magnetic structures I*. Berlin ; New York: Springer, 2002.

[2] B. Hillebrands and K. Ounadjela, *Spin dynamics in confined magnetic structures II*. Berlin ; New York: Springer, 2003.

[3] R. P. Cowburn, "The future of universal memory," *Materials Today,* vol. July/August, pp. 32-38, July/August 2003.

[4] M. Bauer, J. Fassbender, B. Hillebrands, and R. L. Stamps, "Switching behavior of a Stoner particle beyond the relaxation time limit," *Physical Review B,* vol. 61, pp. 3410-3416, Feb 1 2000.

[5] S. Kaka and S. E. Russek, "Precessional switching of submicrometer spin valves," *Applied Physics Letters,* vol. 80, pp. 2958-2960, Apr 22 2002.

[6] J. Miltat, G. Albuquerque, and A. Thiaville, "An introduction to micromagnetics in the dynamic regime," in *Spin Dynamics In Confined Magnetic Structures I*. vol. 83 Berlin: Springer-Verlag Berlin, 2002, pp. 1-33.

[7] L. Berger, "Emission of spin waves by a magnetic multilayer traversed by a current," *Physical Review B,* vol. 54, pp. 9353-9358, Oct 1 1996.

[8] L. Berger, "Multilayer configuration for experiments of spin precession induced by a *dc* current," *Journal Of Applied Physics,* vol. 93, pp. 7693-7695, May 15 2003.

[9] J. C. Slonczewski, "Current-driven excitation of magnetic multilayers," *Journal Of Magnetism And Magnetic Materials,* vol. 159, pp. L1-L7, Jun 1996.

[10] J. C. Slonczewski, "Excitation of spin waves by an electric current," *Journal Of Magnetism And Magnetic Materials,* vol. 195, pp. L261-L268, May 1999.

[11] T. Gerrits, H. A. M. van den Berg, J. Hohlfeld, L. Bar, and T. Rasing, "Ultrafast precessional magnetization reversal by picosecond magnetic field pulse shaping," *Nature,* vol. 418, pp. 509-512, Aug 1 2002.

[12] I. Tudosa, C. Stamm, A. B. Kashuba, F. King, H. C. Siegmann, J. Stohr, G. Ju, B. Lu, and D. Weller, "The ultimate speed of magnetic switching in granular recording media," *Nature,* vol. 428, pp. 831-833, Apr 22 2004.

[13] J. C. Slonczewski, IBM Research Center Poughkeepsie Research Memorandum R.M. 003.111.224, 1956.

[14] A. Thiaville, "Extensions of the geometric solution of the two dimensional coherent magnetization rotation model," *Journal Of Magnetism And Magnetic Materials,* vol. 182, pp. 5-18, Feb 1998.

[15] E. C. Stoner and E. P. Wohlfarth, "A mechanism of magnetic hysteresis in heterogeneous alloys," *Philosophical Transactions of the Royal Society of London,* vol. A240, pp. 599-644, 1948.

[16] B. D. Cullity, *Introduction to magnetic materials*. Reading, Mass.,: Addison-Wesley Pub. Co., 1972.

[17] S. Chikazumi and C. D. Graham, *Physics of ferromagnetism*, 2nd ed. Oxford, New York: Clarendon Press ; Oxford University Press, 1997.

[18] R. C. O'Handley, *Modern magnetic materials : principles and applications*. New York: Wiley, 2000.
[19] W. H. Meiklejohn and C. P. Bean, "New Magnetic Anisotropy," *Physical Review,* vol. 105, 1957.
[20] W. C. Cain, D. C. Markham, and M. H. Kryder, "Dual exchange biased NiFe-TbCo unshielded MR heads for high density recording," *IEEE Transactions on Magnetics,* vol. 25, 1989.
[21] J. L. Dormann, D. Fiorani, and E. Tronc, "Magnetic relaxation in fine-particle systems," in *Advances In Chemical Physics, Vol 98*. vol. 98 New York: John Wiley & Sons Inc, 1997, pp. 283-494.
[22] L. Néel, *Ann. Geophys.,* vol. 5, p. 99, 1949.
[23] W. F. Brown, "Thermal Fluctuations of a Single-Domain Particle," *Physical Review,* vol. 130, 1963.
[24] G. Bertotti, *Hysteresis in magnetism : for physicists, materials scientists, and engineers*. San Diego: Academic Press, 1998.
[25] H. Chang, "Analysis of static and quasidynamic behavior of magneostatically coupled thin magnetic films," *IBM Journal of Research and Development,* vol. 6, pp. 419-429, 1962.
[26] B. D. Schrag, A. Anguelouch, G. Xiao, P. Trouilloud, Y. Lu, W. J. Gallagher, and S. S. P. Parkin, "Magnetization reversal and interlayer coupling in magnetic tunneling junctions," *Journal Of Applied Physics,* vol. 87, pp. 4682-4684, May 1 2000.
[27] A. Anguelouch, B. D. Schrag, G. Xiao, Y. Lu, P. L. Trouilloud, R. A. Wanner, W. J. Gallagher, and S. S. P. Parkin, "Two-dimensional magnetic switching of micron-size films in magnetic tunnel junctions," *Applied Physics Letters,* vol. 76, pp. 622-624, Jan 31 2000.
[28] Y. Lu, P. L. Trouilloud, D. W. Abraham, R. Koch, J. Slonczewski, S. Brown, J. Bucchignano, E. O'Sullivan, R. A. Wanner, W. J. Gallagher, and S. S. P. Parkin, "Observation of magnetic switching in submicron magnetic-tunnel junctions at low frequency," *Journal Of Applied Physics,* vol. 85, pp. 5267-5269, Apr 15 1999.
[29] W. Wernsdorfer, "Classical and quantum magnetization reversal studied in nanometer-sized particles and clusters," in *Advances in Chemical Physics, Vol 118*. vol. 118 New York: John Wiley & Sons Inc, 2001, pp. 99-190.
[30] W. Wernsdorfer, D. Mailly, and A. Benoit, "Single nanoparticle measurement techniques," *Journal of Applied Physics,* vol. 87, pp. 5094-5096, May 2000.
[31] L. Spinu, A. Stancu, Y. Kubota, G. Ju, and D. Weller, "Vectorial mapping of exchange anisotropy in IrMn/FeCo multilayers using the reversible susceptibility tensor," *Physical Review B,* vol. 68, p. 220401(R), Dec 2003.
[32] L. Spinu, H. Pham, C. Radu, J. C. Denardin, I. Dumitru, M. Knobel, L. S. Dorneles, L. F. Schelp, and A. Stancu, "Probing two-dimensional magnetic switching in Co/SiO2 multilayers using reversible susceptibility experiments," *Applied Physics Letters,* vol. 86, p. 012506, Jan 3 2005.
[33] A. Aharoni, E. H. Frei, S. Shtrikman, and D. Treves, "The Reversible Susceptibility Tensor of the Stoner-Wohlfarth Model," *Bulletin of the Research Council of Israel,* vol. 6A, pp. 215-238, April-July 1957.
[34] R. Gans, "Zur Theorie des Ferromagnetismus: Die reversible longitudinale und transversale Permeabilitat," *Ann Phys,* vol. 29, pp. 301-315, 1909.

[35] L. Pareti and G. Turilli, "Detection Of Singularities In The Reversible Transverse Susceptibility Of An Uniaxial Ferromagnet," *Journal Of Applied Physics,* vol. 61, pp. 5098-5101, Jun 1 1987.
[36] A. Hoare, R. W. Chantrell, W. Schmitt, and A. Eiling, "The Reversible Transverse Susceptibility Of Particulate Recording Media," *Journal Of Physics D-Applied Physics,* vol. 26, pp. 461-468, Mar 14 1993.
[37] J. S. Yang, C. R. Chang, and I. Klik, "Thermomagnetics of Reversible Transverse Susceptibility," *Physical Review B,* vol. 51, pp. 15203-15210, Jun 1995.
[38] G. Zimmermann, "Transverse Susceptibility of Particulate Recording Media in Different Remanence States," *Journal of Applied Physics,* vol. 77, pp. 2097-2101, Mar 1995.
[39] L. Spinu, J. L. Dormann, M. Nogues, E. Tronc, and J. P. Jolivet, "Relaxation under field of the zero-field-cooled magnetisation of gamma-Fe2O3 nanoparticle assemblies," *Journal Of Magnetism And Magnetic Materials,* vol. 197, pp. 64-66, May 1999.
[40] D. Cimpoesu, Spinu, L., Stancu, A., "Transverse Susceptibility Method in Nanoparticulate Magnetic Media," *Journal of Nanosience and Nanotechnology,* vol. 8, pp. 1-14, 2008 2008.
[41] J. D. Lawrence, *A Catalog of Special Plane Curves*: Dover Publications, 1972.
[42] C. C. Shir and Y. S. Lin, "Critical curves for determining magnetization directions in implanted garnet-films," *Journal of Applied Physics,* vol. 50, pp. 4246-4258, 1979.
[43] L. Spinu, H. Srikanth, C. J. O'Conner, A. Gupta, X. W. Li, and G. Xiao, "Switching behavior and its strain dependence in epitaxial CrO2 thin films," *Ieee Transactions On Magnetics,* vol. 37, pp. 2596-2598, Jul 2001.
[44] L. Spinu, H. Srikanth, A. Gupta, X. W. Li, and G. Xiao, "Probing magnetic anisotropy effects in epitaxial CrO2 thin films," *Physical Review B,* vol. 62, pp. 8931-8934, Oct 1 2000.
[45] L. Spinu, A. Stancu, C. J. O'Connor, and H. Srikanth, "Effect of the second-order anistropy constant on the transverse susceptibility of uniaxial ferromagnets," *Applied Physics Letters,* vol. 80, pp. 276-278, Jan 14 2002.
[46] A. Stancu and L. Spinu, "Transverse susceptibility for single-domain particle with cubic anisotropy," *Journal Of Magnetism And Magnetic Materials,* vol. 266, pp. 200-206, Oct 2003.
[47] L. Spinu, I. Dumitru, A. Stancu, and D. Cimpoesu, "Transverse susceptibility as the low-frequency limit of ferromagnetic resonance," *Journal Of Magnetism And Magnetic Materials,* vol. 296, pp. 1-8, Jan 1 2006.
[48] S. G. Gevorgyan, T. Kiss, A. A. Movsisyan, H. G. Shirinyan, Y. Hanayama, H. Katsube, T. Ohyama, M. Takeo, T. Matsushita, and K. Funaki, "Highly sensitive open-flat coil magnetometer for the lambda(H,T) measurements in plate-like high-T-c cuprates," *Review of Scientific Instruments,* vol. 71, pp. 1488-1494, Mar 2000.
[49] S. V. Vonsovskii, *Ferromagnetic resonance; the phenomenon of resonant absorption of a high-frequency magnetic field in ferromagnetic substances*, [1st English ed. Oxford, New York,: Pergamon Press, 1966.
[50] R. Meservey and P. M. Tedrow, "Measurements of the Kinetic Inductance of Superconducting Linear Structures," *Journal of Applied Physics,* vol. 40, pp. 2028-2034, 1969.

[51] R. B. Clover and W. P. Wolf, "Magnetic Susceptibility Measurements With A Tunnel Diode Oscillator," *Review Of Scientific Instruments,* vol. 41, pp. 617-&, 1970.
[52] Y. J. Kingma and V. Dvorak, "A negative resistance oscillator with two modes," *International Journal Of Electronics,* vol. 30, pp. 1 - 17, 1971.
[53] J. Aslam and W. Weyhmann, "A Tunnel Diode NMR Spectrometer," *Review of Scientific Instruments,* vol. 44, pp. 71-72, 1973.
[54] C. T. VanDegrift, "Tunnel-Diode Oscillator For 0.001 Ppm Measurements At Low-Temperatures," *Review Of Scientific Instruments,* vol. 46, pp. 599-607, 1975.
[55] J. G. Brisson and I. F. Silvera, "Transmission-Line Tunnel-Diode Oscillator - A Sensitive, Fast, And Flexible Low-Temperature Detection System," *Review Of Scientific Instruments,* vol. 57, pp. 2842-2847, Nov 1986.
[56] R. Meservey and J. S. Moodera, "Performance of a magnetic susceptometer for thin films and surfaces," *Journal of Applied Physics,* vol. 60, pp. 3007-3014, 1986.
[57] H. Srikanth, J. Wiggins, and H. Rees, "Radio-frequency impedance measurements using a tunnel-diode oscillator technique," *Review Of Scientific Instruments,* vol. 70, pp. 3097-3101, Jul 1999.
[58] T. Coffey, Z. Bayindir, J. F. DeCarolis, M. Bennett, G. Esper, and C. C. Agosta, "Measuring radio frequency properties of materials in pulsed magnetic fields with a tunnel diode oscillator," *Review Of Scientific Instruments,* vol. 71, pp. 4600-4606, Dec 2000.
[59] S. Gevorgyan, T. Kiss, H. Shirinyan, A. Movsisyan, V. Gevorgyan, S. Egashira, Y. Eltsev, T. Matsushita, T. Mito, and M. Takeo, "Complicated shape of the superconductive transition curve revealed by a sensitive OFC-magnetometer," *Ieee Transactions on Applied Superconductivity,* vol. 13, pp. 3574-3577, Jun 2003.
[60] S. Gevorgyan, H. Shirinyan, A. Manukyan, E. Sharoyan, M. Takeo, A. Polyanskii, A. Sarkisyan, and T. Matsushita, "Flat coil-based tunnel diode oscillator enabling to detect the real shape of the superconductive transition curve and capable of imaging the properties of HTSC films with high spatial resolution," *Nuclear Instruments & Methods In Physics Research Section A-Accelerators Spectrometers Detectors And Associated Equipment,* vol. 520, pp. 314-319, Mar 11 2004.
[61] S. G. Gevorgyan, T. Kiss, M. Inoue, A. A. Movsisyan, H. G. Shirinyan, V. S. Gevorgyan, T. Matsushita, and M. Takeo, "Weakly expressed "paramagnetic" peculiarity of the superconductive transition detected in YBaCuO film by highly sensitive OFC-magnetometer," *Physica C-Superconductivity And Its Applications,* vol. 378, pp. 404-408, Oct 1 2002.
[62] S. G. Gevorgyan, T. Kiss, M. Inoue, A. A. Movsisyan, H. G. Shirinyan, T. Harayama, T. Matsushita, T. Nishizaki, N. Kobayashi, and M. Takeo, "Peculiarities of the magnetic phase diagram in small-size untwinned YBa2Cu3Oy crystal constructed by highly sensitive OFC-magnetometer," *Physica C-Superconductivity and Its Applications,* vol. 378, pp. 531-536, Oct 2002.
[63] S. G. Gevorgyan, T. Kiss, T. Ohyama, M. Inoue, A. A. Movsisyan, H. G. Shirinyan, V. S. Gevorgyan, T. Matsushita, and M. Takeo, "New paramagnetic peculiarity of the superconductive transition detected by a highly sensitive OFC magnetometer," *Superconductor Science & Technology,* vol. 14, pp. 1009-1013, Dec 2001.
[64] S. G. Gevorgyan, T. Kiss, T. Ohyama, A. A. Movsisyan, H. G. Shirinyan, V. S. Gevorgyan, T. Matsushita, M. Takeo, and K. Funaki, "Calibration of the open-flat

coil-based tunnel diode oscillator technique (OFC magnetometer) for quantitative extraction of physical characteristics of superconductive state," *Physica C,* vol. 366, pp. 6-12, Dec 15 2001.

[65] S. G. Gevorgyan, T. Kiss, H. G. Shirinyan, A. A. Movsisyan, T. Ohyama, M. Inoue, T. Matsushita, and M. Takeo, "The possibility of detection of small absorption in HTS thin films by means of the highly sensitive OFC magnetometer," *Physica C,* vol. 363, pp. 113-118, Nov 1 2001.

[66] S. G. Gevorgyan, G. D. Movsesyan, A. A. Movsisyan, V. T. Tatoyan, and H. G. Shirinyan, "Modeling of tunnel diode oscillators and their use for some low temperature investigations," *Review of Scientific Instruments,* vol. 69, pp. 2550-2560, Jun 1998.

[67] L. Spinu, C. J. O'Connor, and H. Srikanth, "Radio frequency probe studies of magnetic nanostructures," *Ieee Transactions On Magnetics,* vol. 37, pp. 2188-2193, Jul 2001.

[68] C. C. Agosta, "Resistivity and penetration depth measurements of organic superconductors in high magnetic fields using a tunnel diode oscillator," *International Journal of Modern Physics B (IJMPB),* vol. 16, pp. 3227-3232, 2002.

[69] E. Ohmichi, E. Komatsu, and T. Osada, "Application of a tunnel diode oscillator to noncontact resistivity measurement in pulsed magnetic fields," *Review Of Scientific Instruments,* vol. 75, pp. 2094-2097, Jun 2004.

[70] G. T. Woods, P. Poddar, H. Srikanth, and M. M. Ya, "Observation of charge ordering and the ferromagnetic phase transition in single crystal LSMO using rf transverse susceptibility," *Journal of Applied Physics,* vol. 97, p. 10C104, 2005.

[71] Aeroflex-Metelics, "MBD Series Planar Back Tunnel Diodes A17077 " 2005.

[72] K. P. Kämper, W. Schmitt, G. Güntherodt, R. J. Gambino, and R. Ruf, "CrO2-A New Half-Metallic Ferromagnet?," *Physical Review Letters,* vol. 59, p. 2788, 1987.

[73] X. W. Li, A. Gupta, and G. Xiao, "Influence of strain on the magnetic properties of epitaxial (100) chromium dioxide (CrO2) films," *Applied Physics Letters,* vol. 75, pp. 713-715, 1999.

[74] M. Rabe, J. Dreßen, D. Dahmen, J. Pommer, H. Stahl, U. Rüdiger, G. Güntherodt, S. Senz, and D. Hesse, "Preparation and characterization of thin ferromagnetic CrO2 films for applications in magnetoelectronics," *Journal of Magnetism and Magnetic Materials,* vol. 211, pp. 314-319, 2000.

[75] B. H. Miller and E. D. Dahlberg, "Use of the anisotropic magnetoresistance to measure exchange anisotropy in Co/CoO bilayers," *Applied Physics Letters,* vol. 69, pp. 3932-3934, Dec 16 1996.

[76] V. Strom, B. J. Jonsson, K. V. Rao, and D. Dahlberg, "Determination of exchange anisotropy by means of *ac* susceptometry in Co/CoO bilayers," *Journal Of Applied Physics,* vol. 81, pp. 5003-5005, Apr 15 1997.

[77] R. D. McMichael, M. D. Stiles, P. J. Chen, and W. F. Egelhoff, "Ferromagnetic resonance studies of NiO-coupled thin films of Ni80Fe20," *Physical Review B,* vol. 58, pp. 8605-8612, Oct 1 1998.

[78] P. Miltenyi, M. Gruyters, G. Guntherodt, J. Nogues, and I. K. Schuller, "Spin waves in exchange-biased Fe/FeF2," *Physical Review B,* vol. 59, pp. 3333-3336, Feb 1 1999.

[79] M. R. Fitzsimmons, P. Yashar, C. Leighton, I. K. Schuller, J. Nogues, C. F. Majkrzak, and J. A. Dura, "Asymmetric magnetization reversal in exchange-biased hysteresis loops," *Physical Review Letters,* vol. 84, pp. 3986-3989, Apr 24 2000.
[80] H. S. Jung and W. D. Doyle, "High-moment FeCo-IrMn exchange-coupled soft underlayers for perpendicular media," *Ieee Transactions On Magnetics,* vol. 39, pp. 679-684, Mar 2003.
[81] H. W. Xi, M. H. Kryder, and R. M. White, "Study of the angular-dependent exchange coupling between a ferromagnetic and an antiferromagnetic layer," *Applied Physics Letters,* vol. 74, pp. 2687-2689, May 3 1999.
[82] H. Xi, R. M. White, and S. M. Rezende, "Irreversible and reversible measurements of exchange anisotropy," *Physical Review B,* vol. 60, pp. 14837–14840, 1 December 1999 1999.
[83] A. Gerber, A. Milner, B. Groisman, M. Karpovsky, A. Gladkikh, and A. Sulpice, "Magnetoresistance of granular ferromagnets," *Physical Review B,* vol. 55, p. 6446, 1997.
[84] I. Beardsley, "Modeling the record process," *Magnetics, IEEE Transactions on,* vol. 22, pp. 454-459, 1986.
[85] I. S. Jacobs and C. P. Bean, "An Approach to Elongated Fine-Particle Magnets," *Physical Review,* vol. 100, p. 1060, 1955.
[86] N. C. Emley, F. J. Albert, E. M. Ryan, I. N. Krivorotov, D. C. Ralph, R. A. Buhrman, J. M. Daughton, and A. Jander, "Reduction of spin transfer by synthetic antiferromagnets," *Applied Physics Letters,* vol. 84, pp. 4257-4259, May 2004.
[87] S. Hernandez, M. Kapoor, and R. H. Victora, "Synthetic antiferromagnet for hard layer of exchange coupled composite media," *Applied Physics Letters,* vol. 90, p. 132505, Mar 26 2007.
[88] S. C. Byeon, A. Misra, and W. D. Doyle, "Synthetic antiferromagnetic soft underlayers for perpendicular recording media," *IEEE Transactions on Magnetics,* vol. 40, pp. 2386-2388, Jul 2004.
[89] L. Savtchenko, B. N. Engel, N. D. Rizzo, M. F. Deherrera, and J. A. Janesky, "Method of writing to scalable magnetoresistance random access memory element " US Patent 6,545,906 B1: Motorola, Inc. (Schaumburg, IL) 2003.
[90] A. Veloso and P. P. Freitas, "Spin valve sensors with synthetic free and pinned layers," *Journal of Applied Physics,* vol. 87, pp. 5744-5746, May 2000.
[91] M. A. Ruderman and C. Kittel, "Indirect Exchange Coupling of Nuclear Magnetic Moments by Conduction Electrons," *Physical Review,* vol. 96, p. 99, 1954.
[92] C. Radu, D. Cimpoesu, E. Girt, G. P. Ju, A. Stancu, and L. Spinu, "Reversible susceptibility studies of magnetization switching in FeCoB synthetic antiferromagnets," *Journal of Applied Physics,* vol. 101, p. 09D109, May 2007.
[93] D. Cimpoesu, A. Stancu, and L. Spinu, "The reversible susceptibility tensor of synthetic antiferromagnets," *Journal of Applied Physics,* vol. 101, p. 09D112, May 2007.
[94] H. Fujiwara, S. Y. Wang, and M. Sun, "Magnetization Behavior of Synthetic Antiferromagnet and Toggle-Magnetoresistance Random Access Memory," *Transactions of the Magnetics Society of Japan,* vol. 4, pp. 121-129, 2004.
[95] Y. Fukumoto, T. Suzuki, and S. Tahara, "Low writing field with large writing margin in toggle magnetic random access memories using synthetic antiferromagnet

ferromagnetically coupled with soft magnetic layers," *Applied Physics Letters,* vol. 89, p. 3, Aug 2006.
[96] S. Y. Wang and H. Fujiwara, "Optimization of magnetic parameters for toggle magnetoresistance random access memory," *Journal Of Magnetism And Magnetic Materials,* vol. 286, pp. 27-30, Feb 1 2005.
[97] H. Fujiwara, S. Y. Wang, and M. Sun, "Critical-field curves for switching toggle mode magnetoresistance random access memory devices (invited)," *Journal of Applied Physics,* vol. 97, pp. 10P507-10P507-5, 2005.
[98] D. C. Worledge, "Spin flop switching for magnetic random access memory," *Applied Physics Letters,* vol. 84, pp. 4559-4561, May 31 2004.
[99] J. S. Best, "Critical curves for implanted garnet-films in the presence of a demagnetizing field," *Journal of Applied Physics,* vol. 52, pp. 2367-2369, 1981.
[100] J. Z. Sun, J. C. Slonczewski, P. L. Trouilloud, D. Abraham, I. Bacchus, S. S. P. Parkin, and R. H. Koch, "Thermal activation-induced sweep-rate dependence of magnetic switching astroid," *Applied Physics Letters,* vol. 78, pp. 4004-4006, Jun 18 2001.
[101] C. Radu, D. Cimpoesu, A. Stancu, and L. Spinu, "Measurement of the critical curve of a synthetic antiferromagnet," *Applied Physics Letters,* vol. 93, p. 022506, 2008.
[102] A. Veloso, P. P. Freitas, and L. V. Melo, "Spin valves with synthetic ferrimagnet and antiferromagnet free and pinned layers," *Ieee Transactions on Magnetics,* vol. 35, pp. 2568-2570, Sep 1999.
[103] P. Grünberg, R. Schreiber, Y. Pang, M. B. Brodsky, and H. Sowers, "Layered Magnetic Structures: Evidence for Antiferromagnetic Coupling of Fe Layers across Cr Interlayers," *Physical Review Letters,* vol. 57, p. 2442, 1986.
[104] E. N. Abarra, A. Inomata, H. Sato, I. Okamoto, and Y. Mizoshita, "Longitudinal magnetic recording media with thermal stabilization layers," *Applied Physics Letters,* vol. 77, pp. 2581-2583, Oct 2000.
[105] E. E. Fullerton, D. T. Margulies, M. E. Schabes, M. Carey, B. Gurney, A. Moser, M. Best, G. Zeltzer, K. Rubin, H. Rosen, and M. Doerner, "Antiferromagnetically coupled magnetic media layers for thermally stable high-density recording," *Applied Physics Letters,* vol. 77, pp. 3806-3808, Dec 2000.
[106] A. Inomata, E. N. Abarra, B. R. Acharya, H. Akimoto, and I. Okamoto, "Exchange coupling strength in synthetic ferrimagnetic media," *Ieee Transactions on Magnetics,* vol. 37, pp. 1449-1451, Jul 2001.
[107] T. M. Maffitt, J. K. DeBrosse, J. A. Gabric, E. T. Gow, M. C. Lamorey, J. S. Parenteau, D. R. Willmott, M. A. Wood, and W. J. Gallagher, "Design considerations for MRAM," *IBM Journal of Research and Development,* vol. 50, pp. 25-39, Jan 2006.
[108] T. Suzuki, Y. Fukumoto, and N. Ishiwata, "Analysis for toggling magnetic random access memories with low writing field using four ferromagnetic layers for free layer stack," *Journal of Applied Physics,* vol. 101, p. 5, Jan 2007.
[109] M. Prutton, "Transverse susceptibility of single-crystal ferromagnetic films," *Journal of Applied Physics,* vol. 39, pp. 1153-1154, 1968.
[110] E. Goto, N. Hayashi, T. Miyashita, and K. Nakagawa, "Magnetization and Switching Characteristics of Composite Thin Magnetic Films," *Journal of Applied Physics,* vol. 36, pp. 2951-2958, September 1965.

[111] N. Hayashi and E. Goto, "Effective biaxial anisotropy in double-layered thin magnetic films," *Journal of Applied Physics,* vol. 37, pp. 3715-3718, 1966.
[112] S. Y. Wang and H. Fujiwara, "Orthogonal shape/intrinsic anisotropy toggle-mode magnetoresistance random access memory," *Journal Of Applied Physics,* vol. 98, Jul 15 2005.
[113] A. N. Bogdanov and U. K. Rossler, "Instabilities of switching processes in synthetic antiferromagnets," *Applied Physics Letters,* vol. 89, p. 3, Oct 2006.
[114] A. N. Bogdanov, A. V. Zhuravlev, and U. K. Rossler, "Spin-flop transition in uniaxial antiferromagnets: Magnetic phases, reorientation effects, and multidomain states," *Physical Review B,* vol. 75, p. 13, Mar 2007.

Appendices

A.1. Derivation of the parametric equations that describes the critical curve

The dimensionless form (see chapter 1) of the free energy density for a uniaxial particle is:

$$g(\theta,\mathbf{h}) = \frac{1}{2}\sin^2\theta - h_{\perp}\sin\theta - h_{\parallel}\cos\theta \tag{A1.1}$$

By taking the first and second derivative of the energy function (A1.1) and by imposing the condition $\frac{\partial g}{\partial \theta} = 0$; $\frac{\partial^2 g}{\partial \theta^2} = 0$ we obtain the equations that describe the energy in this plane:

$$\begin{cases} \frac{\partial g}{\partial \theta} = \frac{1}{2}2\sin\theta\cos\theta + h\sin\left(\theta - \theta_K\right) = \frac{1}{2}\sin 2\theta + h\sin\left(\theta - \theta_K\right) \\ \frac{\partial^2 g}{\partial \theta^2} = \frac{1}{\cancel{2}}\cancel{2}\cos 2\theta + h\cos\left(\theta - \theta_K\right) \end{cases} \tag{A1.2}$$

$$\begin{cases} \frac{1}{2}\sin 2\theta + h\sin\left(\theta - \theta_K\right) = 0 \\ \cos 2\theta + h\cos\left(\theta - \theta_K\right) = 0 \end{cases} \tag{A1.3}$$

$$\begin{cases} \frac{1}{2}\sin 2\theta + h\sin\theta\cos\theta_K - h\cos\theta\sin\theta_K = 0 \\ \cos 2\theta + h\cos\theta\cos\theta_K + h\sin\theta\sin\theta_K = 0 \end{cases} \tag{A1.4}$$

$$\begin{cases} \frac{1}{2}\sin 2\theta + h_{\parallel}\sin\theta - h_{\perp}\cos\theta = 0 \\ \cos 2\theta + h_{\parallel}\cos\theta + h_{\perp}\sin\theta = 0 \end{cases} \tag{A1.5}$$

Next we divide both eq. in the system (A1.5) by $\sin\theta$ (first eq.) and by $\cos\theta$ (second eq.), and after that we add both eq. in order to solve for $h_{\parallel}$:

$$\frac{1}{2}\sin 2\theta\sin\theta + \cos 2\theta\cos\theta + h_{\parallel}\underbrace{\left(\sin^2\theta + \cos^2\theta\right)}_{1} + h_{\perp}\underbrace{\left(-\cos\theta\sin\theta + \sin\theta\cos\theta\right)}_{0} = 0$$

$$-h_{\parallel} = \frac{1}{2}\sin 2\theta\sin\theta + \cos 2\theta\cos\theta$$

$$-h_{\parallel} = \frac{1}{2}2\sin\theta\cos\theta\sin\theta + \left(\cos^2\theta - \sin^2\theta\right)\cos\theta$$

$$-h_{\parallel} = \sin^2\theta\cos\theta + \cos^3\theta - \sin^2\theta\cos\theta$$

$$h_{\parallel} = -\cos^3\theta \tag{A1.6}$$

Similarly, we divide both eq. in the system (A1.5) by $\cos\theta$ (first eq.) and by $-\sin\theta$ (second eq.), and after that we add both eq. in order to solve for $h_{\perp}$:

$$\frac{1}{2}\sin 2\theta\cos\theta - \cos 2\theta\sin\theta + h_{\parallel}\sin\theta\cos\theta - h_{\parallel}\cos\theta\sin\theta - h_{\perp}\cos^2\theta - h_{\perp}\sin^2\theta = 0$$

$$\frac{1}{\cancel{2}}\cancel{2}\sin\theta\cos\theta\cos\theta - \left(\cos^2\theta - \sin^2\theta\right)\sin\theta - h_{\perp}\underbrace{\left(\cos^2\theta + \sin^2\theta\right)}_{1} = 0$$

$$h_{\perp} = \underbrace{\sin\theta\cos^2\theta - \sin\theta\cos^2\theta}_{0} + \sin^3\theta$$

$$h_{\perp} = \sin^3\theta \tag{A1.7}$$

Eq. (A1.6) and (A1.7) are the parametric equations that describes the critical curve - the astroid - when θ varies in the interval $(0,\ 2\pi)$.

A.2. Transverse Susceptibility expression in Aharoni's Model

The free energy density is:

$$F = K\left[-2h_{dc}\cos\theta - 2h_{ac}\sin\theta\cos\varphi + 1 - \left(\sin\theta\sin\theta_K\cos(\varphi-\varphi_K) + \cos\theta\cos\theta_K\right)^2\right] \quad \text{(A2.1)}$$

where $h_{dc} = \frac{H_{dc}}{H_K}$. In order for magnetization of the particle to be in an extreme of the free energy, there are 2 necessary conditions that need to be satisfied:

$$\begin{cases} \frac{\partial F}{\partial \theta} = 0 \\ \frac{\partial F}{\partial \varphi} = 0 \end{cases} \quad \text{(A2.2)}$$

For $h_{ac} = 0$ we find that the extreme points satisfy:

$$\begin{cases} \sin(\varphi - \varphi_K) = 0 \\ 2h_{dc}\sin\theta + \sin 2(\theta \mp \theta_K) = 0 \end{cases} \quad \text{(A2.3)}$$

where '−' sign correspond to $\varphi = \varphi_K$ and '+' to $\varphi = \varphi_K + \pi$. It can be shown that there are two minima with $\varphi^0 = \varphi_K$ and $\varphi^0 = \varphi_K + \pi$ separated one from another by a saddle point by $\varphi_K + \pi$. The corresponding values of the polar angle are θ_1^0 and θ_2^0. The extremes points in the presence of a small *ac* field could be approximated by their Taylor's series, truncated at the h_{ac} terms, the first sign corresponding to $i = 1$ and the second to $i = 2$:

$$\begin{cases} \theta_i(h_{ac}) \approx \theta_i^0 + h_{ac}\delta\theta_i \\ \varphi_i(h_{ac}) \approx \varphi_i^0 + h_{ac}\delta\varphi_i \end{cases} \quad \text{(A2.4)}$$

where:

$$\delta\theta_i = \lim_{h_{ac}\to 0}\frac{d\theta_i}{dh_{ac}} = \pm\frac{\cos\theta_i^0\cos\varphi_K}{\cos 2(\theta_i^0 \mp \theta_K) + h_{dc}\cos\theta_i^0} \quad \text{(A2.5)}$$

and

$$\delta\varphi_i = \lim_{h_{ac}\to 0}\frac{d\varphi_i}{dh_{ac}} = -\frac{\sin\varphi_K}{\cos(\theta_i^0 \mp \theta_K)\sin\theta_K} \qquad \text{(A2.6)}$$

The variations $\delta\theta_i$ and $\delta\varphi_i$ are obtained by differentiating the relations (A2.2) with respect to h_{ac}.Using (A2.5) and (A2.6) the transverse susceptibility from Eq. 2.8, chapter 2, can be written:

$$\frac{\chi_t}{\chi_0} = \frac{3}{2}\left(\cos^2\varphi_K\frac{\cos^2\theta_i^0}{\cos 2(\theta_i^0 \mp \theta_K) + h_{dc}\cos\theta_i^0} + \sin^2\varphi_K\frac{\sin(\theta_K \mp \theta_i^0)}{h_{dc}\sin\theta_K}\right) \qquad \text{(A2.7)}$$

A3. Synthetic Antiferromagnet Applications

Indirect coupling between two ferromagnetic layers through a nonmagnetic metallic spacer has been the subject of intense investigation for more than 20 years since its discovery in 1986 [103] and, although its general features are well defined and understood, the characterization methods are often difficult. In what follows we will discus several SAF uses.

A3.1. Soft Under-Layer

SAF advantages as soft under-layers compared to exchange-biased structures are the absence of edge demagnetization fields, improved flux carrying efficiency because of the thinner spacing layers required and improved thermal stability. In order to obtain higher areal density and to overcome the thermal stability barrier at low $M_r t$ (M_r is the remanence magnetization and t is the thickness) SAF media have proven to be a useful structure [104], [105]. In this structure, the bottom (stabilizing) magnetic layer couples antiferromagnetically with the top (recording) magnetic layer through a thin Ru layer.

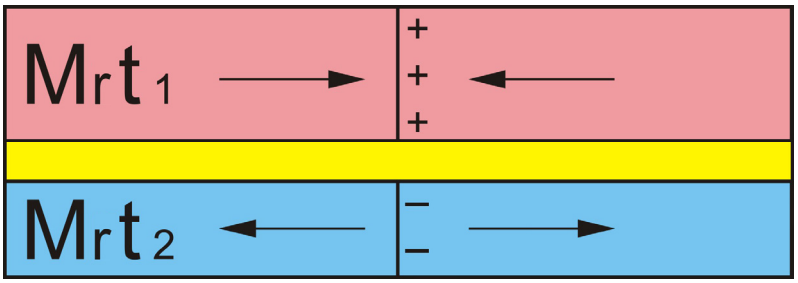

Figure A3.1. Schematic representation of the AFC media showing the two magnetic layers coupled antiparallel with a single transition. The + and - symbols represent the magnetic poles arising from the transition.

The recording media is made up of two ferromagnetic layers (# 1 and # 2 with $M_r t$ values of $M_r t_1$ and $M_r t_2$, respectively) separated by a nonmagnetic layer whose thickness is tuned to couple the layers antiferromagnetically. For such a structure, the effective Mrt of the composite structure is given by $M_r t = M_r t_1 - M_r t_2$.

If one compares the AFC media depicted in Fig. A3.1 to a single-layer media consisting of only layer # 1, the addition of an AF-coupled magnetic layer # 2 reduces the effective $M_r t$ of the composite structure while maintaining or enhancing its thermal stability as compared to the single-layer media. An enhancement of stability arises from the exchange coupling between layers # 1 and # 2.

The exchange field strength (Hex) or the exchange coupling constant, J , ($J = HexM_B t_B$ where M_B and t_B are the magnetization and thickness of the bottom layer) plays a critical role in the enhancement of thermal stability at low $M_r t$ for the SAF media. It has been reported that the exchange coupling strength can be increased by either increasing M_S the or the thickness of the bottom layer [106]. The methods to increase the exchange coupling constant and to improve thermal stability for the SAF media are trying to optimize

the K_u (anisotropy constant), M_S (saturation magnetization), t_B (magnetic layer thickness) and V_B^* (magnetic switching volume) for the stabilizing layer.

A3.2. Magnetic Tunnel Junctions

SAF is also used in magnetic tunnel junctions (MTJs). The MTJs are suitable for high areal density read head and magnetic random access memory (MRAM) applications because they exhibit large tunneling magneto-resistance (TMR) ratios. A subsequent special subsection will address MRAM construction. MTJs generally consist of hard magnet (reference-pinned layer)/insulator (non-magnetic spacer)/soft magnet (sensing-free) structure, so the interactions between the two ferromagnetic (FM) layers are very important. The interaction between the hard and the soft magnet has great influence on the reversal (switching) of the FM layers.

These characteristics are especially important for a high density MRAM with sub-micrometer sized MTJ cells. As the cell size becomes smaller, larger switching field H_{SW} is required, because of the larger demagnetizing field arising from the poles of the submicrometer-sized cell edges.

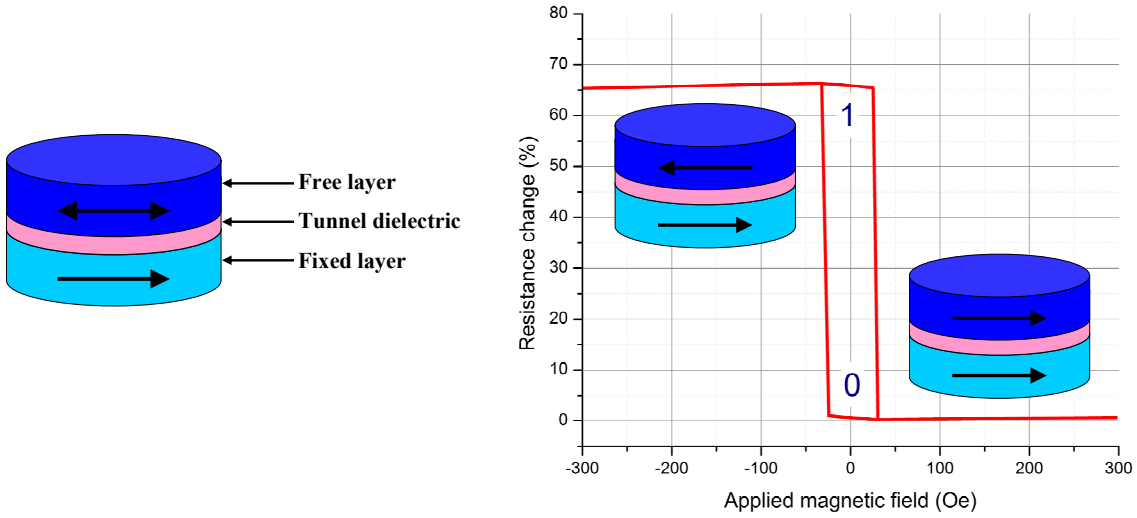

Figure A3.2. (left) Fundamental MTJ device structure, with indicated direction of layer magnetization; (right) MTJ switching typical characteristic

To reduce the H_{SW}, a synthetic antiferromagnet (SAF) free layer structure has been used. According to the Stoner–Wohlfarth's single domain model, H_{SW} depends on the saturation magnetization and shape anisotropy [15]. To get low H_{SW}, the M_S and the shape anisotropy must be small.

A3.3. MRAM and toggle-MRAM

By far until now the most important application of SAF is as a part of magnetic memory elements in MRAM and toggle-MRAM. To illustrate the significance of SAF for this magnetic device we will dedicate the following sub-section to the MRAM design and operation, focusing our attention on SAF role.

MRAM will be a cost-effective solution for long-term data retention and rapid on/off applications such as mobile handheld and general consumer electronic systems. In such cases MRAM may effectively replace a battery and SRAM (static random access memory) and/or flash memory to provide fast, low-power, nonvolatile storage. In large-system applications

requiring a reduction in system start-up time (boot time) and the protection of memory contents in the event of sudden unexpected power-down events, MRAM may serve as a replacement for various combinations of SRAM, DRAM (dynamic random access memory), and flash memory components [107].

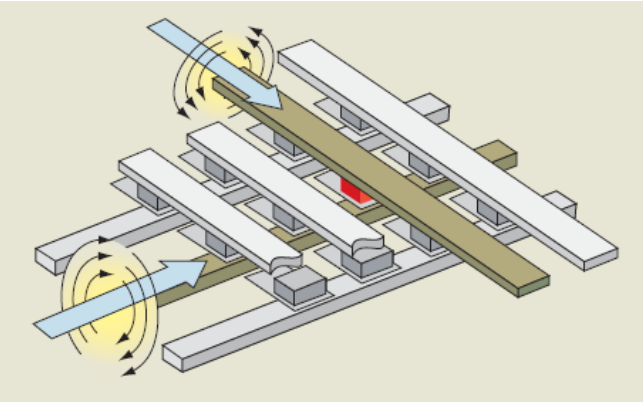

Figure A3.3. MRAM write operation [107]

Figure A3.3 illustrates the MRAM write operation. The selected MTJ, shown in red, is situated between the selected word line (WL) and the selected bit line (BL), both shown in green, which are orthogonal to each other. During the write process, currents (blue arrows) are applied along the selected WL and the selected BL, creating magnetic fields in the vicinity of these wires. The vector sum of the fields at the selected MTJ must be sufficient to switch its state. However, the field generated by the WL or BL alone must be small enough that it never switches the state of the so-called half-selected MTJs that lie along the selected WL and BL. The process is designed so that the word lines and bit lines are as close as possible to the MTJs for good magnetic coupling to the MTJs. Nonetheless, currents of the order of 5 mA are typically required to switch the state of an MTJ. These currents are considered large by integrated circuit standards and create a variety of challenges for write circuit design. Further, the associated voltage drops along the lines limit their allowable

lengths, limiting the maximum number of cells in a memory array. The pulse widths of the WL and BL current pulses are typically approximately equal to or less than 10 ns. However, the two pulses are typically offset by a few ns, with the WL pulse beginning first, so that the free layer can be switched to its new state in a controlled manner. The magnetic field experienced by WL or BL half-selected MTJs is perpendicular to the wire that generates the field. Further, the field applied to the fully selected MTJ points in a third, diagonal direction. The hysteresis loop shown in Fig. A3.2 (right) is insufficient to fully describe these situations, since it is limited to fields in one direction only (along the long axis). The critical curve plot, the astroid, as illustrated in Fig. A3.4, describes the switching of the free layer in response to both field strength and direction.

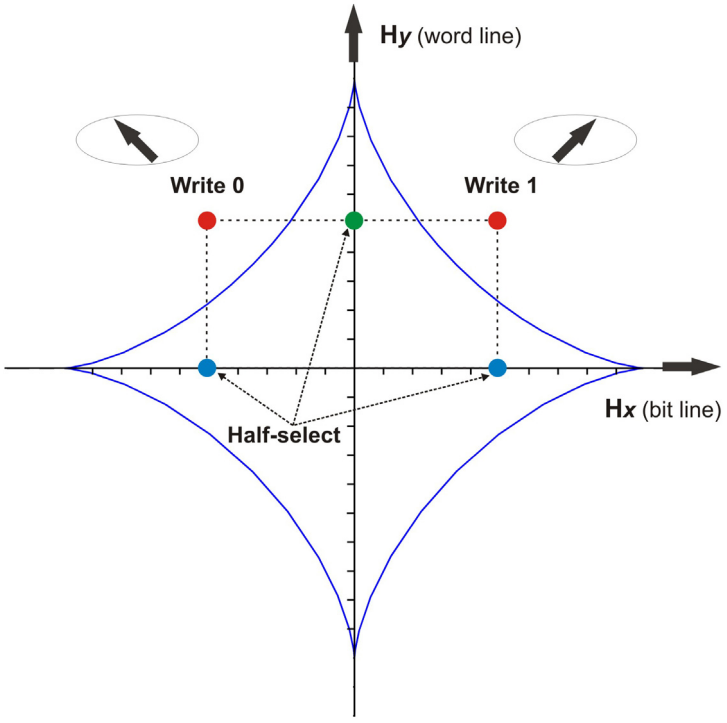

Figure A3.4. Ideal critical curve plot describing the switching of the free layer of an MTJ

The *x* and *y*-axes represent the *x* and *y* components of the magnetic field applied to the MTJ. In this figure, the long axis of the MTJ and the WL are assumed to be horizontal

and the BL to be vertical. Since the WL field applied to the MTJ is perpendicular to and proportional to the WL current, the *y* component of the field is proportional to the WL current. Similarly, the *x* component of the field is proportional to the BL current. The astroid plot is interpreted in the following manner: If the applied field begins at the origin (no applied field), moves to a point to the right of the *y*-axis and astroid, and returns to the origin, the free layer will point to the right (data state 1). Similarly, if the applied field begins at the origin, moves to a point to the left of the *y*-axis and the astroid, and returns to the origin, the free layer will point to the left (data state 0). If the applied field remains inside the astroid, the state of the MTJ remains unchanged.

The fully selected MTJ experiences both *x* and *y* field components, placing it in the first or second quadrant of the figure depending on the data state to be written. Since the polarity of the *x* field component or BL current determines the written data state, the BL write circuitry must support a bidirectional current. The *y* field component is independent of the data state to be written, simplifying the design of the WL write circuitry because bidirectional currents are not required. In order to write successfully, the fully selected field points must always lie outside the astroid. As indicated in Fig. A3.4, WL half-selected MTJs experience a *y* field component only, whereas BL half-selected MTJs experience an *x* field component only. The polarity of the field experienced by a BL half-selected MTJ depends on the state being written to the fully selected MTJ. To avoid half-select disturbs (data loss between an MTJ being written and read), the half-select field points must always lie inside the astroid. To explain this process we will introduce the term “write margin”[107].

Write margin is the ability to reliably write the selected MTJ without disturbing other bits. Write margin requires that the fully selected fields always lie outside the astroid, while

the half-selected fields lie within the astroid. Several additional mechanisms degrade the write margin, as described below.

In addition to the half-select field described above, the two WL half-selected MTJs immediately adjacent to the fully selected MTJ experience a small *x* component field because of the adjacent BL current. Similarly, the two BL half-selected MTJs immediately adjacent to the fully selected MTJ experience a small *y* component field because of the adjacent WL current. The magnitude of these stray fields depends on the design of the memory cell and is typically less than 10% of the corresponding BL or WL field. Nonetheless, these stray fields further degrade the write margin. The stray field problem becomes more significant as the cell size and hence the distance to the adjacent WL and BL are reduced.

The astroid shown in Fig. A3.4 is ideal, as in SW model. The real shape and size of the astroid are dependent upon the shape, size, and other properties of the MTJ. Correspondingly, the shape and size of each MTJ within a chip vary because of local variations in shape, size, and other properties. The resulting statistical spread of the astroid further degrades the write margin. The write margin challenge is further exacerbated by the finite chance that MTJs operated close to the astroid boundary may undergo undesired thermally activated switching over a vanishingly small potential barrier from one data state to the other [100]. In addition, the applied field varies with variations in circuit parameters (transistor, wiring resistance, and supply voltage). The resulting variations in the position of the full and half-select field points on the astroid plot degrade the write margin still further. It is the goal of the write circuit design to limit these variations and to compensate for the temperature dependence of the astroid. In response to the write margin difficulties associated with the conventional MTJ device, a more advanced, "toggle-mode" MTJ device and

switching method have been developed [89]. Fig. A3.5 illustrates the toggle-mode MTJ device structure. The structure is similar to that of the conventional MTJ except that the free layer consists of two weakly anti-parallel coupled ferromagnetic layers. Therefore, the free layer in a toggle cell is a synthetic antiferromagnet SAF trilayer stack.

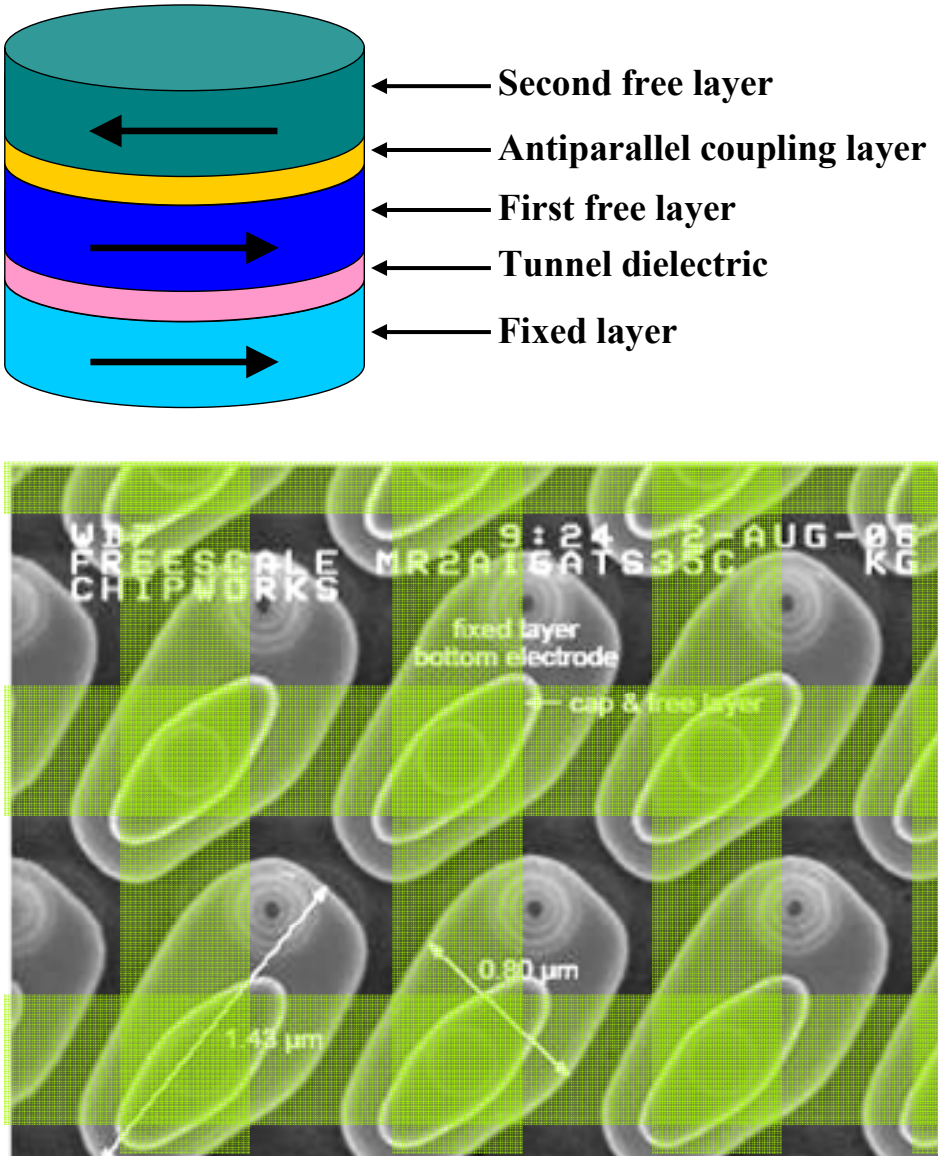

Figure A3.5. Example of toggle-mode MTJ device structure. Top – layers schematics, bottom – electron microscope image of the MTJ structure within a Freescale's MRAM chip

In addition, the long axis of the structure lies at 45° with respect to the WL as opposed to being parallel to the WL, in the conventional MRAM.

The read operation is essentially unchanged, with the magnetic orientation of the lower free layer determining the effective resistance of the structure. In the writing process, magnetic fields from bit and word lines are applied in sequence.

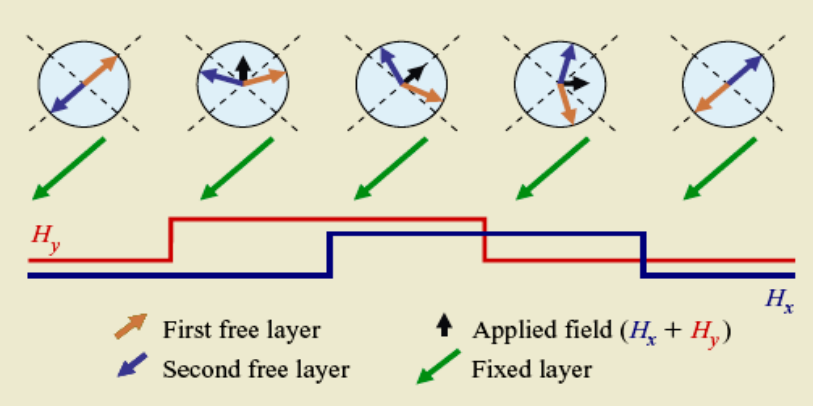

Figure A3.6. Toggle-mode switching [107]

The magnetization direction of the two magnetic layers rotates along the effective field maintaining an open scissors state, as shown in Fig. A3.6 and A3.7. The writing field is set between the spin flop field and the saturation field, considering their distribution.

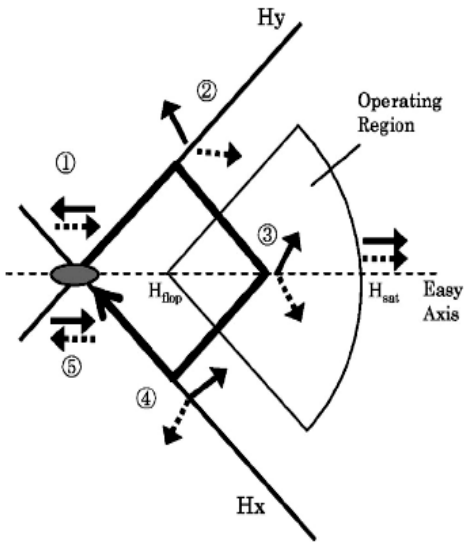

Figure A3.7. Write operating region for toggle MRAM [108]. Arrows indicate magnetization. During operation, the magnetization of the two free layers rotates like scissors, in a step by step process from (1) to (5).

Whereas the conventional MTJ is written directly into one state or the other depending on the polarity of the BL current, the toggle-mode MTJ toggles its state when exposed to a similar WL and BL current pulse sequence. As illustrated in Fig. A3.2 and A3.3, the dipoles of the free layer rotate slightly in the direction of the applied field, and essentially follow the applied field as it rotates during the WL and BL current pulse sequence. At the end of the sequence, the free-layer dipoles have rotated 180° from the initial state, regardless of the initial state. The criterion for a successful toggle is that the applied field must trace a path in the applied field plane that encloses a particular point in the plane, referred to as the "spin-flop" point.

Unlike a conventional MTJ, a toggle-mode MTJ is largely insensitive to half-select disturbs, regardless of WL and BL field strength, since such disturbs do not trace a path that encloses the spin-flop point. In addition, since the free layer has no net magnetic moment, the field experienced by a particular device is insensitive to the state of adjacent devices. This advantage is of particular importance as cell size and hence the distances to the adjacent devices are reduced.

A final advantage of the toggle-mode MTJ is that only one BL write current direction must be supported, simplifying the design of the write circuits. Because of the toggle nature of the device, the device must be read at the start of the write cycle. The device is then toggled if its current state does not match that of the incoming write data. Although the read can be performed concurrently with preparations for the WL and BL write pulse sequence, the required read represents a write-performance disadvantage compared with that of a conventional MTJ.

To conclude this review on SAF increasing importance for MRAM we use Fig. A3.8.

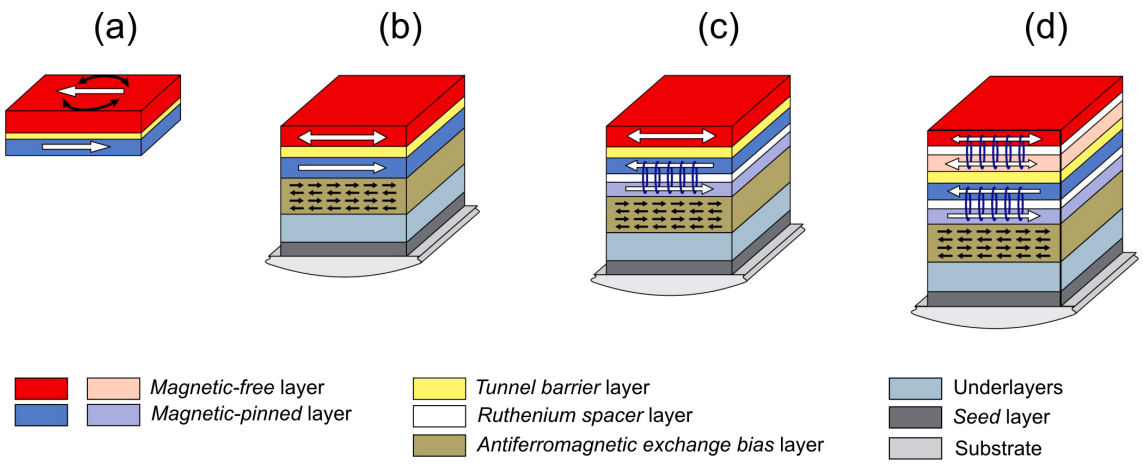

Figure A3.8. Evolution of MTJs engineered for MRAM applications

In Fig. A3.8 (a) it is shown a basic magnetic tunnel junction structure consisting of two ferromagnetic metals separated by a thin insulating layer. Both magnetic film layers have same anisotropy direction. (b) By exchange-coupling one of the magnetic layers to an antiferromagnetic layer (by "pinning" the layer) the TMR response reflects the hysteresis of the other so-called "free" layer and has a response more suitable for memory. (c) The magnetic offset caused by fields emanating from the pinned layer can be avoided by replacing the simple pinned layer with a SAF pinned layer, which consists of a pair of ferromagnetic layers antiferromagnetically coupled through a ruthenium (Ru) spacer layer. The lower layer in this artificial antiferromagnet is pinned via exchange bias, as shown in (b). This flux closure increases the magnetic stability of the pinned layer and reduces coupling to the free layer. (d) Structure in which both the pinned and free elements consist of antiferromagnetically coupled pairs; used in the modern toggle-MRAM.

A.4. Literature survey on SAF critical curve

In the previous appendix we demonstrated the importance of synthetic antiferromagnet (SAF) structures in designing modern spintronic devices due to their reduced shape anisotropy and reduced switching fields and for application as soft underlayer (SUL) in perpendicular magnetic recording media due to suppressed noise [88]. Current problems in improving the MRAM devices are closely connected to the switching properties of the SAF structures. Some of these problems can be overcome with a new MRAM writing scheme, toggle MRAM[89] that increases the operating margin of the MRAM elements. In the toggle writing procedure the MRAM free layer has a SAF structure.

Recently, several studies were devoted to the use of the new writing scheme in order to optimize the magnetic parameters for toggle-MRAM [94-96]. The theoretical studies of the toggle writing mode in MRAM use the concepts of SAF critical curve [94] which is a generalization of the well-known astroid from the coherent rotation model in the case of uniaxial anisotropy, presented in detail in the first two chapters. The critical curve for a SAF structure is obtained as the envelope of the field trajectories giving a constant angle to the magnetization of one of the two layers, leaving the other as a variable in the field plane.

Depending on the coupling strength between the two ferromagnetic layers, in a SAF structure the critical curve evolves from a simple astroid at zero coupling to a more complicated critical curves for larger coupling field values [94]. On the SAF critical curve one distinguishes two parts: the critical field curve for saturation which is the outermost envelope of the constant angle contours and outside of which the magnetizations in two layers become parallel one to each other and the critical curves for switching which are the inner envelopes.

The toggle switching mode is achieved only for specific field trajectories in the field plane with respect to the inner envelopes. Consequently, knowing the configuration of the SAF critical curve is of great importance in order to control its switching characteristics.

Several papers dealing with theoretical aspects of the critical curves for SAF systems [94, 96, 97] were recently published but only few are presenting experimental methods and results in which the critical curves are determined for antiferromagnetically coupled magnetic layers [92]. One of the reasons is that switching critical curve is more complex in the case of SAF than in the case of a single magnetic layer. It is well known that in the case of the astroid (or in the general case of the critical curve for a single magnetic layer) the tangent to the astroid passing through the tip of the external applied field vector **h** in the $\left(h_x, h_y\right)$ plane gives the orientation of the magnetization at equilibrium for that particular field value and direction [24]. Moreover, the parameter value in the tangent point of the parametric critical curve has a value equal to the angle that gives the orientation of the magnetization with respect to the easy axis. For SAF the tangent at the critical curve passing through the point representing the external applied field in the $\left(h_x, h_y\right)$ plane gives the orientation of the first layer θ_1 while the orientation of the second layer θ_2 can be read from the position of the tangent point on the critical curve.

In what follows in this appendix, we will review the main contributions to the exploration of the SAF critical curve. This is intended to set the scene for our new method of recording the SAF critical curve presented in chapter 5.

A4.1. Magnetostatically coupled thin magnetic films

In a paper published by Chang [25] is presented a direct derivation from SW model and from Slonczewski and Pruton early studies [13, 109] toward the understanding of magnetization switching in one dimensional thin film. The two ferromagnetic films under investigation are far enough to prevent atomic interaction between them but close enough to allow the magnetostatic interaction. The strength of interaction is shown to depend on the thickness to diameter ratio (anisotropy) and on the magnetization of the films in the specimen.

From the beginning of this early work the author is introducing the idea of the potential memory application for such structures.

Coherent rotational flux reversal for single films is described by critical curves and hysteresis loops which predict multiple stable states, switching threshold and hysteresis. In the two-film structures, similar information is desired. However, as the orientations of the two magnetization vectors have to be represented by two dependent variables, the mathematical formulation of the problem and the presentation of the results are very much different from those for the single-film theory.

In order to facilitate this analysis, the following assumptions are made:

- Each film behaves as a single domain with uniform magnetization and can therefore be represented by a single magnetization vector.

- The flux change is done by the rotation of the magnetization vector. This can be realized under either of the two following situations: The threshold field for wall motion is much higher than that required for rotation; or the wall motion is much slower than the

rotation, such that for an applied pulse of short duration only the rotation movement can take place.

- The magnetization vector of each film is confined to the plane of the film; otherwise excessive magnetization energy would result from a magnetization component perpendicular to the film plane.

- The magnetization of each film produces an internal demagnetizing field. Moreover, the two superposed films are in such proximity that each is exerting a planar uniform field throughout the other.

$$H \simeq \left(\frac{\pi}{4}\right)\left(\frac{t}{d}\right)M \qquad \text{(A4.1)}$$

where: H is the uniform planar magnetic field inside or outside of the film due to its magnetization; t is the film thickness; d is the film diameter; M is the uniform magnetization of the film.

- The anisotropy energy of each film is assumed to be of the form $K_n \sin^2 n\theta$, where K_n is the anisotropy constant, n is the number of axes of symmetry, and θ is the angle between the magnetization vector and the major axis of symmetry.

The total free energy of a uniaxial film is given by

$$F = -\mu_0 M \cdot H + K \sin^2 \theta \qquad \text{(A4.2)}$$

where: θ is the orientation of M as measured from easy axis, F is the total free energy per unit volume, $-\mu_0 M \cdot H$ is the mutual magnetization energy per unit volume between the film and the applied field, K is the anisotropy constant.

In the Fig. A4.1 is represented the critical curve for an uniaxial thin film. When the field varies to a value that lowers the energy barrier such that the minimum state will vanish, the stable state will suddenly switch into a neighboring minimum point.

Such a field value is a critical one. The loci of critical field values in the (h_x, h_y) coordinates constitute a critical curve or rotational switching threshold curve.

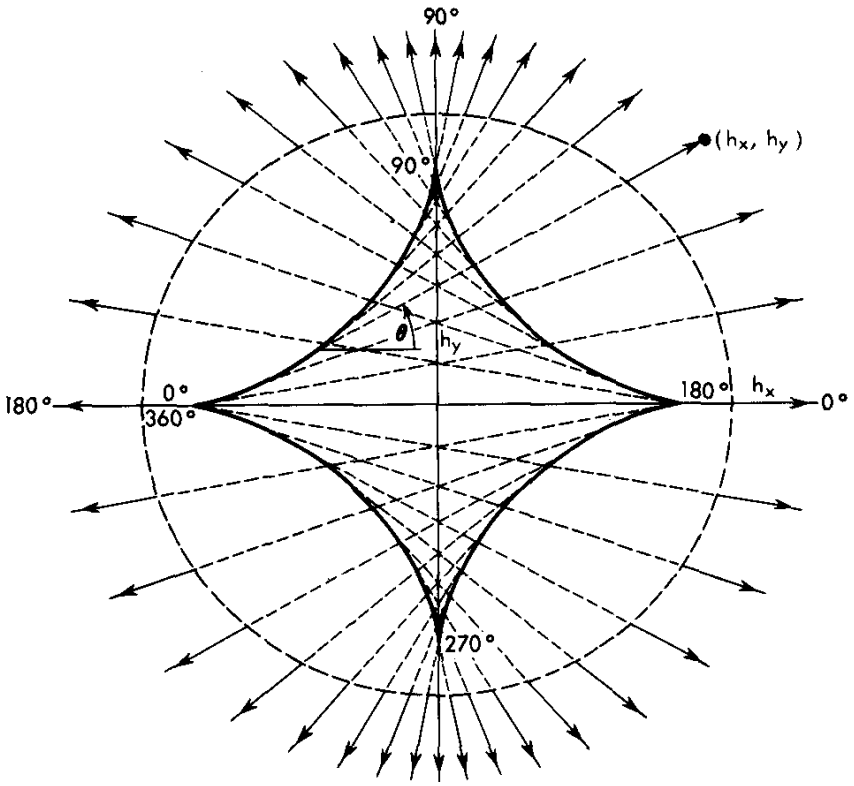

Figure A4.1. Critical curve and stable state lines for an uniaxial ferromagnetic film [25]

When the field varies to a value that lowers the energy barrier such that the minimum state will vanish, the stable state will suddenly switch into a neighboring minimum point. Such a field value is a critical one. The loci of critical field values in the (h_x, h_y) coordinates constitute a critical curve or rotational switching threshold curve.

In the theory for a single film, the critical state is mathematically identified as a point of inflection as well as an extremum point, and can be found by solving $\frac{\partial F}{\partial \theta} = 0$ and $\frac{\partial^2 F}{\partial \theta^2} = 0$ simultaneously.

Further on, it is proved that the stable states can be represented by families of straight lines in the (h_x, h_y) plane. The orientation of each line is the stable magnetization vector orientation, and the points on the line indicate all possible field values to maintain the magnetization orientation. The envelope of the family of equilibrium lines is the well-known astroid-shaped critical curve. All equilibrium lines are tangent to and terminate on the critical curve. These geometrical relationships make the critical curve a uniquely convenient and concise method of presenting both stable states and critical states in the Fig. A4.1.

The next step is to investigate the switching for a multilayer system. The physical structure under consideration in this paper is made of two superposed films with their major easy axes at an angle α, as in Fig. A4.2. The purpose of this analysis is to find stable orientations of the films for a given applied field as well as the threshold for rotational switching. A stripline wraps both or just one film, to provide the same or different fields to the films. More than one stripline are used to provide fields in different directions or to sense various components of flux changes.

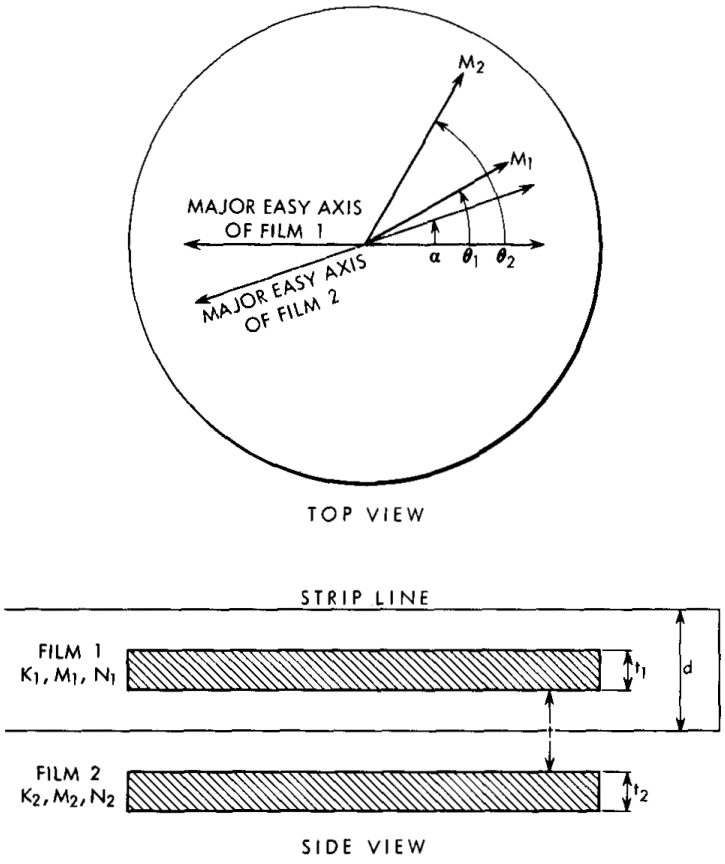

Figure A4.2. Superposed ferromagnetic films [25]

The physical principle utilized for the analysis is that a system tends toward minimum energy for its stable state. The total free energy of the two-film structure consists of the individual anisotropy energies, the individual magnetization energies, and the interaction magnetization energy. In the normalized form, the total free energy is:

$$g = -\left[\cos\theta_1 + sm_2\cos\theta_2\right]h_x - \left[\sin\theta_1 + sm_2\sin\theta_2\right]h_y + h_i\cos\left(\theta_1 - \theta_2\right) + \\ + \sin^2 p\theta_1 + k_{2q}\sin^2 q\left(\theta_2 - \alpha\right) \tag{A4.3}$$

where: g is the total free energy of the coupled films, (θ_1, θ_2) are the orientations of the magnetization vectors, (h_x, h_y) are the x and y components of the applied field, h_y is the

interaction field, α is the angle between the easy axes of the films, (m_2, k_{2q}) are the ratios of magnetization and anisotropy constants of the films, (p,q) are the degrees of symmetry in the anisotropy energies of the films, s is a constant determined by the layout of the strip lines. A systematic characterization of the energy landscape is given in the Table A4.1.

Conditions at (θ_1, θ_2)			Then $g(\theta_1, \theta_2)$ is	Physical meaning
$g(\theta_1, \theta_2)\varepsilon c^2$	$\frac{\partial^2 g}{\partial\theta_1\partial\theta_2} - \frac{\partial^2 g}{\partial\theta_1^2}\frac{\partial^2 g}{\partial\theta_2^2} < 0$	$\frac{\partial^2 g}{\partial\theta_1^2}$ or $\frac{\partial^2 g}{\partial\theta_2^2} < 0$	relative maximum	unstable
		$\frac{\partial^2 g}{\partial\theta_1^2}$ or $\frac{\partial^2 g}{\partial\theta_2^2} > 0$	relative minimum	stable
$\frac{\partial g}{\partial\theta_1} = \frac{\partial g}{\partial\theta_2} = 0$	$\frac{\partial^2 g}{\partial\theta_1\partial\theta_2} - \frac{\partial^2 g}{\partial\theta_1^2}\frac{\partial^2 g}{\partial\theta_2^2} > 0$		saddle point	unstable

Table A4.1. Superposed ferromagnetic films [25]

The total free energy for a system of coupled films it is a sum of anisotropy energies, magnetization energy due to applied field and (different from the one dimensional case) the magnetization energy due to interacting field.

The author presents next the derivation of a different graphical representation of both stable states and critical states. Because the rotational threshold curve (or critical curve) constructed in the (h_x, h_y) plane based on the previous definitions does not relate to the stable states in any sense other than being their limiting values, a constant-field contours in (θ_1, θ_2) plane is used for the prediction of switching behavior.

To conclude the review of this paper, we will focus on its main contributions. The analysis reveals properties such as multiple stable states, switching, threshold and hysteresis

for the coupled films. These suggest possible applications for memory and logic. There are three distinctive features of the coupled films:

(a) The films form a closed magnetic path which allows the use of thick films with high demagnetizing field when not coupled.

(b) Each film acts as a rotatable bias on the other. This may allow "novel" memory and logic operations.

(c) The two films constitute a system of two elements with coupling which is a sine function of the angular displacement between the magnetizations.

A4.2. Switching characteristics and biaxial anisotropy for composite thin films

In this publication [110], Goto et al. presents a study of the composite magnetic thin films properties. These films are composed of layers of different magnetic materials in close molecular contact with one another. In the previous studies on multiple layers of magnetic thin film [25], the coupling mechanism between magnetic films has been almost exclusively restricted to couplings caused by demagnetizing or fringe magnetic fields, which have the tendency of making the magnetization of two films antiparallel to each other. Also it has been discovered at that time a new coupling mechanism which takes place when two metallic ferromagnetic films are separated by a very thin layer of nonmagnetic metals.

Nevertheless, this study, on the other hand, was focused on the effects of ferromagnetic exchange coupling between magnetic thin films, which are believed to be different from any of the coupling mechanisms mentioned above.

It is considered, as example, the behavior of two magnetic films made of different magnetic material in close molecular contact with each other. Let an external magnetic field be applied on the films and let’s assume that the effects of demagnetizing fields are

negligibly small. If there were no magnetic coupling between the films, the magnetizations of the films would point, independently of each other, to different stable directions. Ferromagnetic exchange coupling between spins in the neighborhood of the interface of the two films, however, will impart a tendency of aligning the direction of spins in parallel and thus, the magnetizations of the two films become not only interdependent but also dependent upon the depth along the thickness of the films. Under such circumstances, the spins exhibit a continuous rotation as in Bloch walls.

The authors are discussing several cases for the continuous rotation model: first an extremely soft magnetic film placed on an extremely hard substrate, next the model is generalized to the case of dual uniaxial films, in close molecular contact with each other.

The critical switching curve of dual uniaxial films is found to be drastically deformed from the classic SW model's astroid. In some cases, the theoretical switching curve has an elongated shape in the hard direction.

The energy of a dual uniaxial system is given in a simplified expression:

$$F = \frac{1}{2} H_{k1} \sin^2 \theta_1 - H_x \cos \theta_1 - H_y \sin \theta_1 + \frac{1}{2} H_2 \sin^2 \theta_2 + \frac{1}{2} H_a (\theta_1 - \theta_2)^2 \qquad \text{(A4.4)}$$

where: H_x and H_y are the external fields, H_{k1} is the uniaxial anisotropy of the first film, H_2 is the uniaxial anisotropy of the second film, H_a is the exchange coupling between the two films.

Under given external fields H_x and H_y the magnetization angles θ_1 and θ_2 will set themselves up in such a way as to minimize the energy F. The switching curve for H_{k1}=1, H_a=0.5, H_2=1 is shown in Fig. A4.3.

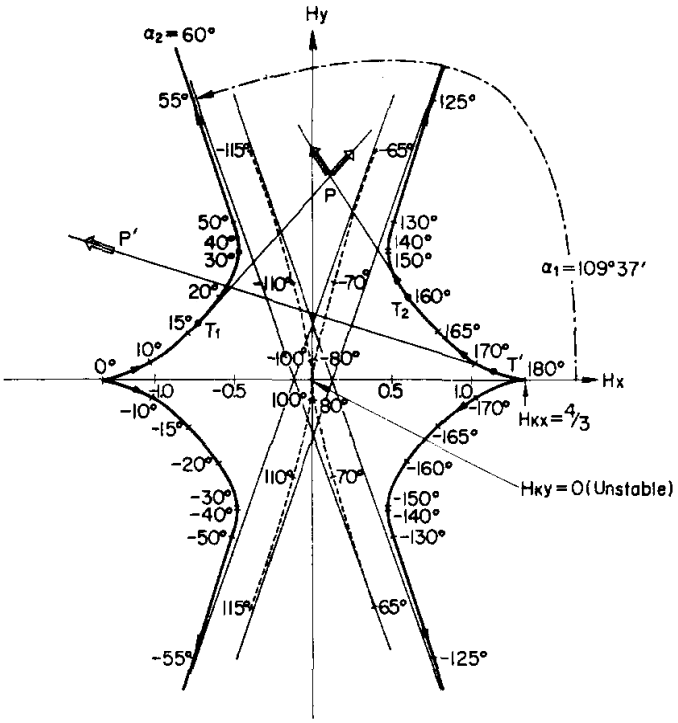

Figure A4.3. Switching curve for dual uniaxial films. Arrows at P and P' shows the stable directions of the first film [110].

This study of exchange-coupled composite thin magnetic films was based on a continuous rotation model of spins along the depth of films.

Next, in support of the previous results, same authors are presenting quantitative experimental results [111] which prove the deformation of the critical curve of multilayer magnetic films in terms of effective multiaxial anisotropies. The structure of the double layer films is shown in Fig. A4.4, being constructed from two layers of NiFeCo alloy (70/19/11 weight %), with $H_k = 20\,Oe$, with their easy axes perpendicular one to each other.

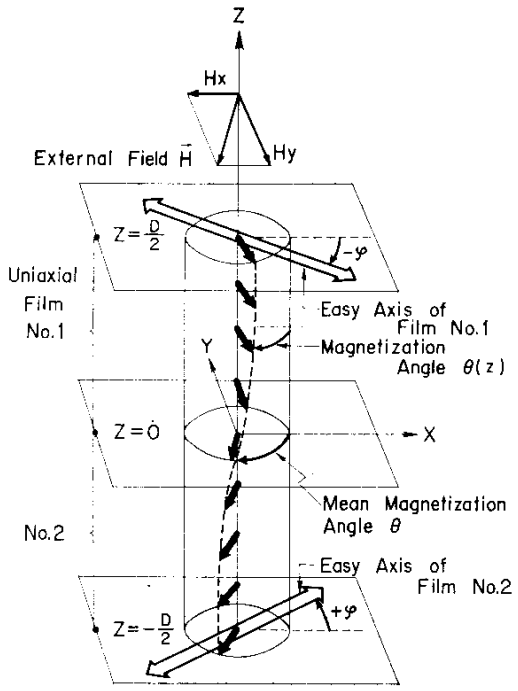

Figure A4.4. Structure of crossed dual films [111]

From their experiments, the authors were able to conclude that the effective biaxial anisotropy is proportional to the square of film thickness. From this dependence, the value of the exchange constant of the studied NiFeCo alloy is found to be $A \approx 1.6 \times 10^{-6}\ erg/cm$, which is in good agreement with the value $A \approx 0.86 \times 10^{-6}\ erg/cm$ obtained from a spin-wave resonance measurement.

A4.3. Magnetic parameters, critical curves, shape and intrinsic anisotropy in toggle magnetoresistance RAM

This work was published in papers by Wang [96, 112] and Fujiwara [97]. The review of the next three papers starts with the section on the optimization of magnetic parameters for toggle-MRAM [96]. The magnetic parameters of the synthetic antiferromagnetic (SAF)

elements for toggle-mode magnetoresistance random access memories (toggle-MRAMs) have been optimized using the critical field curves obtained by analytical method with the aid of numerical calculations, to maximize the operating field margin taking into account the required memory density, storage lifetime, half-select disturb robustness, and the available strength of operating field.

The two ferromagnetic (FM) layers of the SAF are assumed to have the same thickness t, magnetization M_s, and uniaxial anisotropy constant K_u. The easy axes of the FM layers are assumed to be parallel to each other and the antiferromagnetic exchange coupling is strong enough to make the antiparallel magnetization configuration when no external field is applied.

Critical field curves for switching and saturation are obtained from the equilibrium conditions of the following energy density expression:

$$\begin{aligned} F = 0.5H_k M_s t[\sin^2\theta_1 + \sin^2\theta_2] - M_s t[H_x\cos\theta_1 + H_y\sin\theta_1] \\ - M_s t[H_x\cos\theta_2 + H_y\sin\theta_2] + J\cos(\theta_1 - \theta_2) \end{aligned} \quad \text{(A4.5)}$$

where $\mathrm{K_u} = \dfrac{\mathrm{H_k M_s}}{2}$, θ_1 and θ_2 the magnetization angles of the first and second FM layers with respect to the positive easy axis, J the exchange coupling strength, and H_x and H_y the external fields in the easy and hard direction, respectively. The energy density in Eq. (A4.5) includes the anisotropy, Zeeman and exchange coupling energy densities, and can be normalized by $\mathrm{H_k M_s} t$:

$$g = 0.5[\sin^2\theta_1 + \sin^2\theta_2] - [h_x\cos\theta_1 + h_y\sin\theta_1] - [h_x\cos\theta_2 + h_y\sin\theta_2] + h_J\cos(\theta_1 - \theta_2) \quad \text{(A4.6)}$$

where: $g = \dfrac{F}{H_k M_s t}$, $h_x = \dfrac{H_x}{H_k}$, $h_y = \dfrac{H_y}{H_k}$ and $h_J = \dfrac{J}{H_k M_s t}$.

Two examples of the critical field curves are shown in Fig. A4.5 (a) and (b); (a) for h_J=2 and (b) h_J=5, respectively.

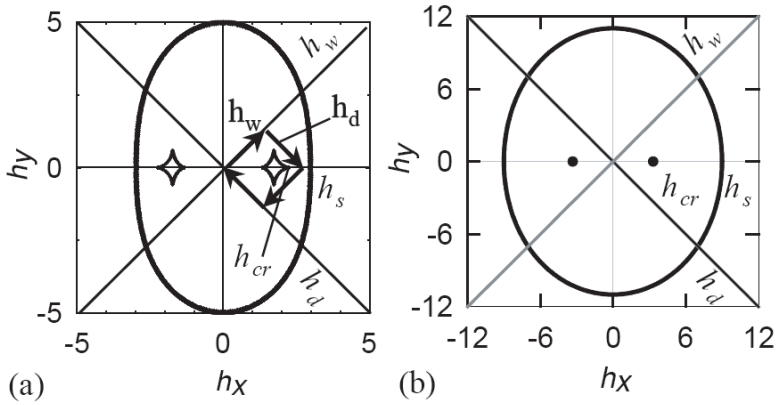

Figure A4.5. Critical curves for (a) h_J=2 and (b) h_J=5; the critical points h_{cr} and h_s are marked on the positive h_y axis. The trajectory for toggle switching is shown by the vectors: h_w, h_d, $-h_w$ and $-h_d$ [96].

In Fig. A4.5(a), the critical curve is composed of an oval-like outermost curve and two small astroid-like curves, which are called astroids. With the increase of h_J the outermost curve expands, but the astroid reduces its size and eventually shrinks into a spot (Fig. A4.5(b)). The outermost curve is the critical curve for saturation and the astroid is the critical curve for switching which corresponds to the astroid known for the single uniaxial anisotropy layers. The two critical points h_{cr} and h_s in h_y-axis marked in Fig. A4.5 can be found analytically as $h_{cr} = \sqrt{2h_j + 1}$ and $h_s = 2h_j - 1$.

In the memory operation, the operating field must be restricted within the saturation curve. A smooth toggle mode switching occurs only when the operating field trajectory goes around the astroid within the saturation curve, as is shown in Fig. A4.5(a).

The control of especially low-exchange coupling strength in the SAF in addition to the increase of the operating field has been found to be essential for the development of toggle-MRAM.

On a next publication [97], same authors, are performing an analytical study with the aid of numerical calculation and found that the field contours in the in-plane field coordinate which keep the angle of the magnetization of one layer constant leaving the other variable give a good insight into the response of the magnetization of each layer constituting the coupled bilayers. In the previous paper, however, the magnetostatic coupling between the two layers were neglected for simplicity. Worledge [98] has made a similar analysis, assuming the coupling field is equal to the demagnetizing field. This paper [97] gives a comprehensive description of the magnetization behavior in the coupled bilayers taking into account the fact that the actual effective magnetostatic coupling field in one of the two layers is smaller than the demagnetizing field in the other. It also gives a type of expression for the magnetization response to the in-plane field, in which the field trajectories giving a constant value to the average angle of the magnetizations of the two layers or to the angle between the two leaving the average angle variable, which makes it easier to visualize the magnetization behavior. The necessary conditions for obtaining toggle-mode switching are also given. Throughout the analysis the Stoner–Wohlfarth model is applied.

The results obtained will be valid when applied to real 100-nm features, and it applies for the toggle-mode operation, in which switching occurs through rotational mechanism rather than wall-propagation-like switching.

Choosing as a variable parameter the thickness ratio of the two ferromagnetic layers, $t = t_2 / t_1$, in Fig. A4.6 are plotted the critical-field curves obtained keeping all other parameters constant: (a) t=1, (b) t=0.8, and (c) t=0.6.

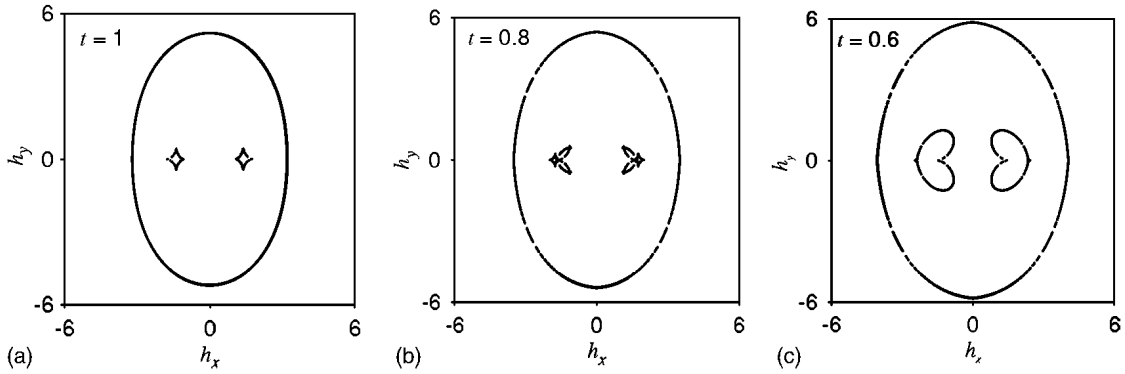

Figure A4.6. Critical curves for: (a) t=1, (b) t=0.8, and (c) t=0.6 [97]

One noticeable feature in the critical curve evolution is that with increasing the imbalance, that is, with decreasing the thickness ratio *t* in the case of the present examples, the "heart" portion becomes larger.

In a standard toggle MRAM, we apply the word field h_w and the digit field h_d, sequentially, in the ±45° directions with respect to the easy axis.

Figure A4.7 shows the magnetization configuration response to the sequentially applied field in the ±45° directions with respect to the easy axis (*x* axis).

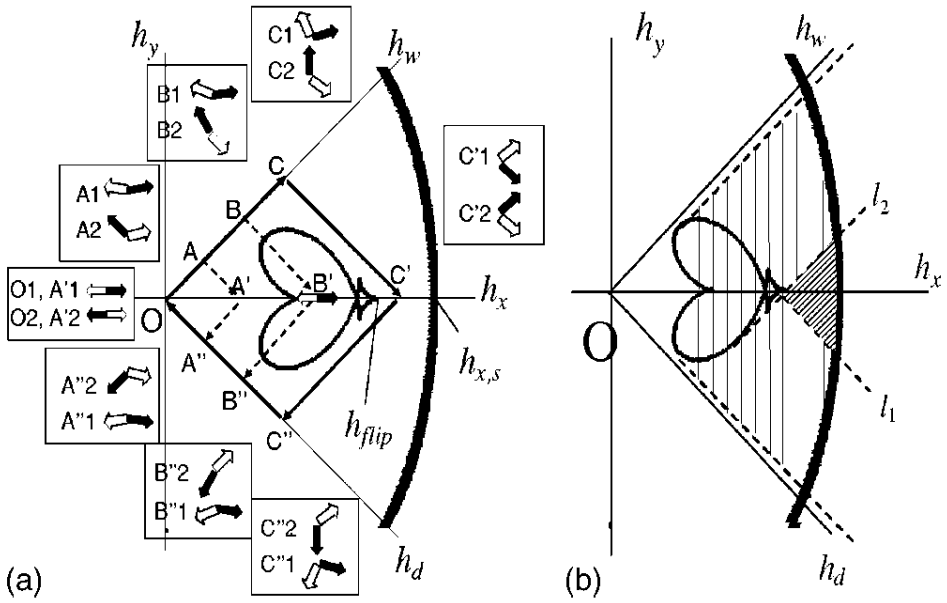

Figure A4.7. Magnetization configuration response to the sequentially applied field in the ±45° directions with respect to the easy axis (*x* axis) [97]

Three different field trajectories, *a*: OAA'A"O, *b*: OBB'B"O, and *c*: OCC'C"O, are shown with respect to typical critical-field curves. For each point, a rough sketch of stable magnetization configurations are shown by pairs of black (M_1) and white (M_2) arrows. The two pairs of arrows in a rectangle represent the two stable configurations at the same point. For each trajectory the following configuration changes were confirmed: for *a*, O1-A1-A'1-A"1-O1 and O2-A2-A'2-A"2-O2; for *b*, O1-B1-B'-B"1-O1 and O2-B2-B'-B"1-O1; and for *c*, O1-C1-C'1-C"2-O2 and O2-C2-C'2-C"1-O1.Note that there is only one stable configuration at B'. It is seen that trajectory *c* only results in the toggle switching: O1 switches through C1, C'1, C"2 to O2, and O2 through C2, C'2, C"1 to O1; trajectory *a* does not change to either O1 or O2; trajectory *b* switches O1 into O2 but not O2 into O1. This kind of switching mode is called "direct-mode" switching. Note that at B' the examination of the contour maps has revealed that when we allow asymmetry to h_w and h_d with respect to the *x* axis, the operating field margin is represented by the part hatched with inclined lines in Fig. A4.7 (b) surrounded

by the two tangents, l_1 (−45° tangent to the astroid) and l_2 (+45° tangent to the heart), and the outermost critical curve. The region shaded with the vertical lines is the margin for the direct-mode operation.

Another publication by same authors is concerned with the shape/intrinsic anisotropy of toggle MRAM elements [112]. Magnetization response to in-plane applied fields has been studied, using SW model, on the bilayer systems of synthetic antiferromagnet having an anisotropy configuration in which the induced intrinsic uniaxial anisotropy is set either parallel or orthogonal to the shape anisotropy, like in Fig. A4.8.

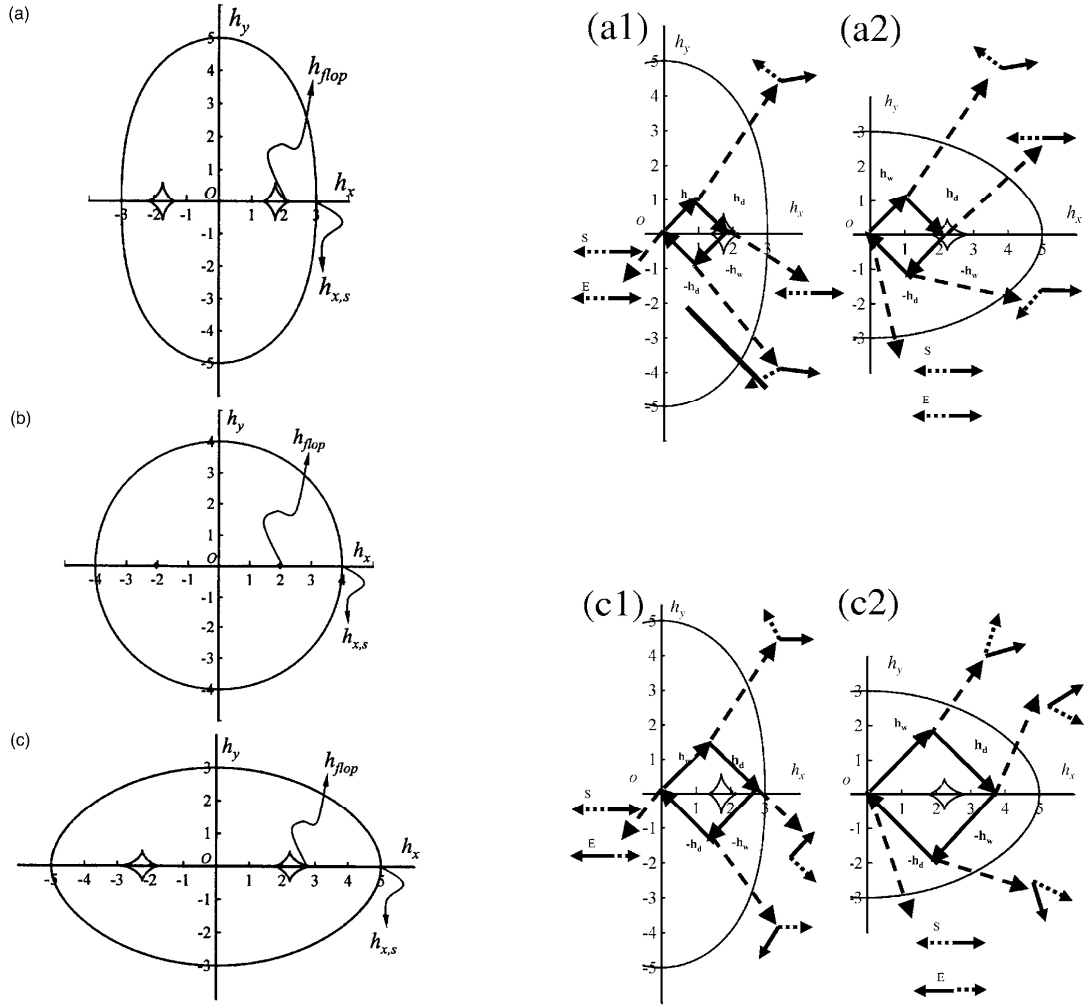

Figure A4.8. Critical curves with $h_{k,t}$=1 (a), 0 (b) and -1 (c) [112]

The element can be switched when h_w+h_d falls between h_{flop} and $h_{x,s}$.

Therefore, the operating field margin for the toggle switching can be obtained as the gray-filled area shown in Fig. A4.9.

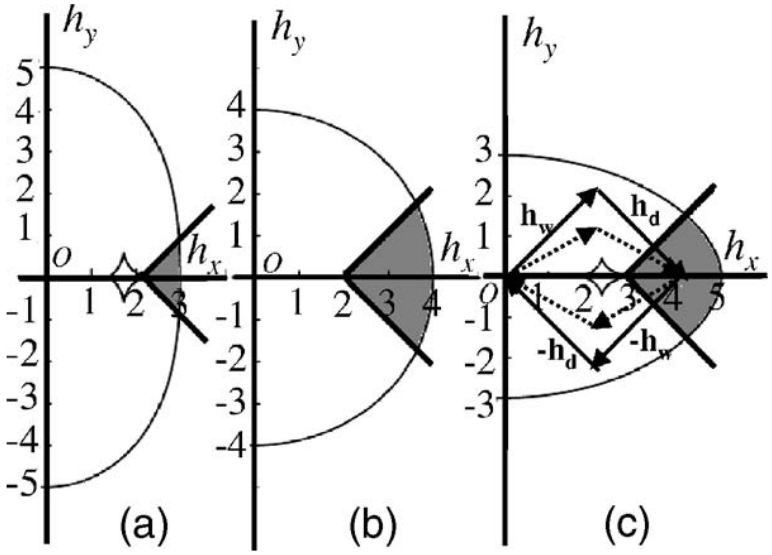

Figure A4.9. The operating field margin for different cases shown in Fig. A4.8 [112]

It has been found that the toggle-mode MRAM operation is possible even when the shape anisotropy exceeds the intrinsic anisotropy to some extent due to the anisotropic effect of the magnetostatic coupling and that the minimum operating field and maximum relative operating field margin are attained when the two anisotropy compensate each other. The optimal operating fields increase with the increase of the absolute value of the total anisotropy constant. However, the tolerance of total anisotropy constant in the positive direction is greater than in the negative direction if zero total anisotropy is chosen to be optimal.

A4.4. Instabilities of switching processes in SAF

The effort of understanding the switching behavior of SAF as a main constituent part of MRAM was accompanied by the prediction regarding the switching instabilities in papers by Bogdanov [113, 114]. The work on this subject shows that magnetic states and field-

driven reorientation transitions in synthetic antiferromagnets crucially depend on contributions of higher-order anisotropies. A phenomenological macrospin model is derived to describe the magnetic states of two antiferromagnetically coupled magnetic thin-film elements.

The field-driven reorientation transition in a synthetic two-layer antiferromagnet with a common uniaxial anisotropy is akin to the spin-flop transition in a two-sublattice antiferromagnet. At the spin-flop field, the uniaxial anisotropy and the Zeeman energy balance each other. Hence, near the spin-flop field, the magnetic state is subject to weaker higher-order anisotropies. This causes magnetic instabilities. The authors analyze the instability mechanism for an elementary macrospin model with competing uniaxial and cubic anisotropies. This model is relevant for magnetic layer systems with intrinsic cubic magnetocrystalline anisotropy and an in-plane easy axis, e.g., induced by substrate-film interactions (see Fig. A4.10). However, instabilities of the spin-flop phase in an antiferromagnet are a general phenomenon related to higher-order magnetic anisotropies.

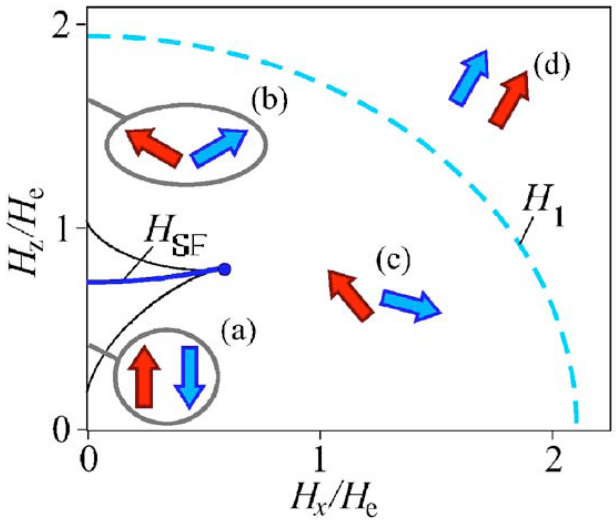

Figure A4.10. The magnetic phase diagram for small cubic anisotropies [113]

The magnetic phase diagram for small cubic anisotropies $K_c < K$ holds only planar stable phases. Antiferromagnetic (a) and spin-flop (b) states exist in a magnetic field H_z along the easy axis n. The first-order spin-flop transition occurs in the critical field H_{SF}. In oblique magnetic fields, $H_x \neq 0$, the transition occurs between canted (c) phases that are distorted antiferromagnetic and spin-flop states. Thin lines give stability limits of metastable states, and dashed line H_1 is the continuous transition into the saturated spin-flip phase (d).

In layered synthetic antiferromagnets, such a biaxial anisotropy can be induced by perpendicular surface anisotropy of the single ferromagnetic layers. These effects are expected even in soft polycrystalline or amorphous magnetic films because they generally locally own perpendicular anisotropies with random distribution due to the unavoidable surface effects.

The results for the model with a competition of uniaxial and cubic anisotropies exemplify the more general phenomenon of escaped magnetic configurations in antiferromagnetic layer systems. These escaped phases are metastable in wide regions of the field even for weak cubic anisotropies and for secondary uniaxial anisotropies. The higher-order anisotropies also lead to wide extension of the first-order line H_{SF} in the phase diagram in Fig. A4.10, while toggle switching requires staying away from this exact region. Therefore, switching processes in toggle mode MRAM devices may fail because the field-driven system can escape into metastable states with perpendicular magnetization components.

As we have notice from this literature review, there are many aspects of SAF operation, as an important part of MRAM, that underline the importance of critical curve and the magnetization switching processes described by it.

List of Publications

1. C. Radu, D. Cimpoesu, A. Stancu and L. Spinu – "Measurement of the critical curve of a synthetic antiferromagnet", Appl. Phys. Lett., 93, 022506, July 2008.

2. C. Radu, D. Cimpoesu, E. Girt, G. Ju, A. Stancu, L. Spinu – "Reversible Susceptibility Studies of Magnetization Switching in FeCoB Synthetic Antiferromagnets", J. Appl. Phys., 101, 09D109, May 2007.

3. J.W. Eslick, H.N. Pham, **C. Radu**, A. Puri – "Quantum entanglement in an oscillating macroscopic mirror" European Physical Journal, D 38 (3), 553-562, June 2006.

4. J. Chen, **C. Radu**, A. Puri - ''Aberration-free negative-refractive-index lens" , Appl. Phys. Lett., 88 (7), 071119, February 2006.

5. Z. Wang, Y. Hong, J. Tang, **C. Radu**, Y. Chen, L. Spinu, W. Zhou, L. Tung - "Giant negative magnetoresistance of spin polarons in magnetic semiconductors-chromium-doped Ti2O3 thin films", Appl. Phys. Lett., 86 (8), 082509, February 2005.

6. L. Spinu, H. Pham, **C. Radu**, J. C. Denardin, I. Dumitru, M. Knobel, L. S. Dorneles, L. F. Schelp, A. Stancu – "Probing two-dimensional magnetic switching in Co/SiO_2 multilayers using reversible susceptibility experiments", Appl. Phys. Lett., 86, 012506, January 2005.

7. L. Spinu, A. Stancu, **C. Radu**, F. Li, J. Wiley – "Method for characterization of nanowire structures", IEEE Trans. Mag., 40, 2116 – 2118, July 2004.

8. F. M. Tufescu, **C. Radu** – "Mobile phones and human health; power measurements for mobile telephone handsets" Scientific Annuals, Iasi University, 2002.

Vita

Cosmin Radu was born in Tecuci, Romania and received his B.S. and M.S. from Al. I. Cuza University of Iasi, Romania.